The Coupled Cluster Method in the Hamiltonian Lattice Gauge Theory: SU(3) Glueballs in Two Dimensions

Dissertation

zur

Erlangung des Doktorgrades (Dr. rer. nat.)

der

Mathematisch-Naturwissenschaftlichen Fakultät

der

Rheinischen Friedrich-Wilhelms-Universität Bonn

vorgelegt von

Vera Wethkamp

aus

Münster

Bonn 2003

Anfertigung mit Genehmigung der Mathematisch-Naturwissenschaftlichen Fakultät
der Rheinischen Friedrich-Wilhelms-Universität Bonn.

1. Referent: Prof. Dr. D. Schütte
2. Referent: Prof. Dr. H. Monien
Tag der Promotion: 20. März 2003

Contents

Introduction

Symmetries play an important role for the description of physics. They help classifying solutions of physical theories and they lead to conservation laws for physical quantities.

The Standard Model of Particle Physics is based on a symmetry principle, the principle of gauge invariance. It describes three of the four fundamental forces of nature with the help of gauge field theories: The theory of the electromagnetic interaction is associated with the Abelian symmetry of the gauge group U(1), the theory of the unified electromagnetic and weak interaction with a brocken symmetry group SU(2)×U(1) and the theory of the strong interaction, called Quantum Chromodynamics (QCD), with the non-Abelian symmetry group SU(3).

The fundamental forces can be characterised by the strength of their interaction. The weakest force, gravitation, is not incorporated in the Standard Model. The strength of the weak and electromagnetic interaction is described by a small value of the coupling constant. Thus here perturbation theory is a powerful and very successful calculational technique. For the case of the strong interaction, where the coupling constant is of an order $\alpha_s \simeq O(1)$, we want to inspect the properties of the describing theory, the QCD, in more detail.

QCD introduces as fundamental degrees of freedom quarks and gluons to describe hadronic systems with strong interactions. As it is a gauge theory based on the non-Abelian gauge group SU($N_c = 3$), the quarks should come in $N_c = 3$ "colours" and there are $N_c^2 - 1 = 8$ gluons mediating the interaction between the quarks.

QCD is asymptotically free, i.e. the effective coupling of the theory decreases for short distances or for increasing momenta. Therefore processes with an energy scale large compared to the natural scale of the strong interaction are often amenable to techniques of perturbation theory.

For long distances the coupling increases – possibly leading to quark confinement – and perturbation theory fails. In this low energy regime there are different possibilities of treating hadronic systems. One way is employing quark models based on the SU($N_f = 3$) "flavour" symmetry (see e.g. refs. [33, 50] for mesons and refs. [38, 39, 40] for baryons). Alternatively one uses the techniques of effective field theories (see e.g. ref. [8]) at small energies and low momenta.

The only approach we have for performing *ab initio* calculations is lattice QCD. It provides a natural gauge invariant regularisation scheme in order to treat divergences which occur in interacting theories, like QCD.

Wilson (see ref. [67]) introduced the concept of a lattice gauge field theory in which the continuous space-time is replaced by a space-time lattice. This discretisation regularises the theory as the lattice spacing provides a natural cut-off which restricts the domain of momenta. In the continuum limit, i.e. the limit of vanishing lattice spacing, the physics of

a renormalisable field theory should be independent of the details of the cut-off. Renormalisation group arguments predict a typical scaling for the behaviour of observables for small lattice spacing. For an overview on lattice QCD see refs. [13, 44, 52].

There are two standard formulations of lattice gauge field theories: the Lagrangian and the Hamiltonian formulation.

Most work has been carried out in the Lagrangian formulation. Here the Euclidean spacetime is replaced by a lattice. It is an approach based on numerical calculations of path integrals with Monte Carlo techniques. For a review in this field see ref. [46].

The Hamiltonian formulation developed by Kogut and Susskind (see ref. [32]) involves the discretisation of space only, the time variable remains continuous. In this approach the Monte Carlo techniques are replaced by many body methods. The advantage is that physical quantities, especially the mass spectrum and the wave functions are more directly accessible.

The aim of the present thesis is to calculate the pure SU($N_c = 3$) glueball spectrum in two spatial dimensions in the Hamiltonian lattice gauge field theory.

Glueballs are bound states of mainly gluons. The non-Abelian structure of QCD implies that a self-coupling of the gluons exists and consequently suggests the existence of glueballs, as well as their mixing with quark-antiquark states.

The experimental search for glueballs is mainly concentrated on the scalar meson sector. Here the number of states seems to exceed the number expected from quark models. Scalar mesons are produced in processes like J/Ψ decays, central hadronic production and proton-antiproton annihilation in which one supposes to find also signatures for glueballs (see e.g. refs. [2, 54]). The interpretation of the experimental data is highly controversial. The examination of branching ratios of decays and the classification of states concerning the SU($N_f = 3$) flavour symmetry of the quarks lead to various statements: In ref. [3], for example, the scalar $f_0(1500)$ state is interpreted as a glueball candidate and the $f_0(1710)$ is dominantly a quark-antiquark state. In ref. [43] the $f_0(1500)$ state is member of a quark-antiquark nonet and the broad object formed by $f_0(400-1200)$ and $f_0(1370)$ is a glueball candidate. Scalar states being mesons with a gluish admixture is discussed for example in ref. [12] and in refs. [30, 31] the existence of pure glueballs in the scalar sector is called into question.

Thus theoretical considerations on the glueball spectrum may help clarifying the experimental situation. Additionally, they play an important role for the testing and understanding of non-perturbative aspects of QCD.

Currently lattice calculations provide the best possibility of studying glueballs.

Because of numerical limitations the most reliable lattice computations were up to now performed in the pure SU($N_c = 3$) gauge theory, neglecting the effects of quarks. This is a necessary and useful first step, since it provides an inside in the theory and helps focusing the experimental searches for pure glueball candidates. To explain mixing effects of glueballs with quarkonia, quarks have to be included.

The largest progress was made in the Lagrangian lattice formulation. There exist very reliable standard Monte Carlo calculations by Morningstar and Peardon [45] on the pure glueball spectrum. Investigations including the effect of quarks were also performed: Results of calculations in the quenched approximation are presented in ref. [34] and in refs. [25, 26] data of $N_f = 2$ lattice computations are reported. Refs. [6, 41, 42] review the status of lattice calculations of the glueball spectrum and discuss the mixing effects between glueballs

and quarkonia. In addition we want to mention the work of Teper [60] on pure SU(N_c) glueballs in two space dimensions.

Specialisations to lower space dimensions and calculations with varying number of colours N_c are useful. They yield a first insight in the structures of full QCD and are numerically less expensive.

Also within the Hamiltonian lattice formulation various investigations were carried out, not only with numerical but also with analytic techniques. In addition to the glueball spectrum discussions of the vacuum and glueball wave functions are possible. Examples are the coupled cluster expansion and the Greens function Monte Carlo calculations of Hamer *et al.* [22, 23, 24], the light front approach of Dalley and van de Sande [14], the maximal tree approach of Ligterink *et al.* [36] and the variational studies of Arrisue *et al.* [4, 5] and Carlsson *et al.* [9].

In this thesis the coupled cluster method in the Hamiltonian lattice gauge field theory will be used to calculate the SU($N_c = 3$) glueball spectrum in two spatial dimensions.

The theory in $D = 2$ space dimensions shares important features with the one in $D = 3$ dimensions. In both theories the dimensionless coupling becomes weak for short distances. In $D = 2$ dimensions the square of the coupling has the dimension of length and vanishes linearly with distance – the theory is super-renormalisable. In the $D = 3$ case the coupling vanishes logarithmically with distance – the theory is asymptotically free. Additionally, both theories share the effect, that an overall mass scale is determined by the value of the coupling. For $D = 2$ dimensions the coupling itself has the dimension of a mass and in the $D = 3$ dimensions the running of the coupling provides the mass scale (see ref. [60]). This supports the assumption that by considering $D = 2$ space dimensions we already learn about characteristics of the $D = 3$ theory.

Results for SU($N_c = 2$) glueballs using the coupled cluster method are given in ref. [64] - the preceding work to the present thesis. The SU($N_c = 2$) gauge theory has the same non-Abelian structure as the SU($N_c = 3$) theory and we will see that the extension to SU($N_c = 3$), i.e. the implementation of the correct SU($N_c = 3$) quantum numbers and of charge parity, provides some features we already known from the SU($N_c = 2$) case, like the structure of the wave functions. For the SU($N_c = 3$) calculations the numerical effort increases. However, compared to the Monte Carlo simulations in the Lagrangian lattice formalism, the amount of computer capacity needed in the Hamiltonian lattice formulation is very small.

Calculations similar to ours, i.e. performed within the same framework, were reported in refs. [11, 18, 20, 27]. First attempts to include quarks using the coupled cluster method exist, but only in the Schwinger model, i.e. the $1 + 1$ dimensional U(1) case (see ref. [17]).

Within the Hamiltonian formulation the quantum states are gauge invariant functions $\Psi(U) = \Psi(U_{l_1}, \ldots, U_{N_l})$ of N_l link variables $U_l \in SU(3)$ representing the lattice gauge field. All calculations presented here have been performed in the infinite volume limit, where $N_l \to \infty$. For the coupled cluster method the ground state (vacuum state) $\psi_0(U)$ is written as $\psi_0 = e^S$ and the eigenvalue problem $H_{KS}\Psi(U) = E\Psi(U)$ of the Kogut-Susskind Hamiltonian H_{KS} is reformulated as a non-linear equation for the ground state correlation function $S(U)$. Excited states (glueball states) are written in terms of an excitation operator $F(U)$ as $\psi = Fe^S$, leading to a linear eigenvalue problem for F.

In order to expand S and F a large but finite gauge invariant basis is constructed. This basis is built by plaquette products, as the plaquette is the simplest gauge invariant

quantity on the lattice. It is truncated to the order δ by taking all states created by up to δ-fold products. This truncation scheme was proposed by Guo *et al.* [20]. Within this work we will be able to extend the calculations of the basis up to the order $\delta = 6$ and solve the ground state and excited state equations up to the order $\delta = 5$.

Lattice translation and rotation symmetries and the operation of charge conjugation are used to project onto states with definite lattice angular momentum, parity and charge parity: J^{PC}. Since we will specialise to a two-dimensional lattice we will be able to compute glueballs with $J^{PC} = 0^{++}$, 0^{--}, 0^{-+}, 0^{+-}, 2^{++}, 2^{-+}, 2^{--}, 2^{+-}, $1^{\pm+}$, $1^{\pm-}$.

To correct the discretisation errors arising in a lattice formulation and to reduce the numerical effort one may implement a so-called improvement. How to improve the Lagrangian lattice is discussed in ref. [35]. For the Hamiltonian lattice theory one can construct improved Hamiltonians in an analogous way. In our context improvement essentially provides an alternative regularisation scheme with the same continuum limit as for the unimproved case. By comparing unimproved and improved results their consistency will be checked.

It will be shown that for the vacuum state satisfactory convergence and a good agreement with the coupled cluster results of ref. [27] and the analytic variational approach of ref. [9] is obtained. At higher inverse coupling β, where the calculations of ref. [9] are still valid, the iteration procedure to solve our vacuum equation breaks down. This problem we already know from the SU($N_c = 2$) calculations in ref. [64]. It has a larger effect in the SU($N_c = 3$) case, because here it occurs at smaller β.

For the glueball states mass ratios will be calculated. These should be independent of the inverse coupling $\beta = \frac{2N_c}{g^2 a}$ for small lattice spacing a, i.e. for large β, in order to reflect scaling. Because of the truncation of the basis our method breaks down for large β, analogous to the occurrence of finite volume effects in Standard lattice Monte Carlo calculations. Therefore only a scaling window occurs. The analytic method of Carlsson *et al.* [9], can avoid this effect, a very good scaling behaviour is to be seen. Unfortunately the Ansatz of ref. [9] is too restricted to give very reliable results. We will see that in our context an approximate scaling window occurs at $\beta \approx 6$ for the calculations without improvement and at $\beta \approx 3$ with improvement. Our results will be tested by comparing the calculations in different orders, with and without improvement. The corresponding wave functions will also be examined. We will show that the mass values for glueballs which we are able to estimate reliably, e.g. the 0^{++}, the 0^{--} and the 2^{++} glueball, agree with the results of refs. [9, 11, 18, 60] and with the analytic study of ref. [53].

This thesis is organised as follows:

- In chapter 1 the basic concepts of a lattice gauge theory in the Lagrangian and the Hamiltonian formulation will be introduced. We will briefly outline the discretisation procedure to compare the important quantities on the lattice and in the continuum theory and give a recipe for the implementation of improvement. The coupled cluster Ansatz for the vacuum and the glueball wave functions will be given and the coupled cluster equations for the corresponding states will be derived.

- The ground (vacuum) state correlation function and the excitation (glueball) operator will be expanded in a gauge invariant basis. In chapter 2 we will first construct this basis using SU(3) coupling rules and then we will discuss its properties.

- In chapter 3 the symmetries of the lattice will be introduced. They determine the operators we need to project onto states with good momentum, angular momentum-parity and charge parity. In this thesis only zero momentum states will be considered.

- The computational details and results will be given in chapter 4. We will present the method to solve the coupled cluster equations and the truncation scheme. The results for the vacuum state and the glueball states will be given. To summarise a final estimate for our glueball spectrum on the basis of the calculation in different orders, with and without improvement will be shown at the end of this chapter.

Finally we will give an outlook on the next possible steps to be done in our context.

The appendices contain more detailed calculations, special notations and definitions, as well as numerous tables and listings.

Chapter 1 Hamiltonian lattice gauge theory

For the calculation of the glueball spectrum we rely on the concepts of a pure gauge theory on the lattice, the lattice Yang-Mills theory. Within the Hamiltonian formulation the Kogut-Susskind theory gives the computational framework of any such gauge theory.

In this chapter we first introduce the basics of the Hamiltonian lattice formulation and then we will derive the coupled cluster equations to be solved to obtain the spectrum of the Kogut-Susskind Hamiltonian in a truncated basis.

1.1 Hamiltonian lattice regularisation

As we have mentioned in the introduction the discretisation of space and time implementing a lattice provides one way to regularise the quantum field theory and to cure the problems it suffers from singularities. A lattice regularisation has the particular advantage that it preserves gauge invariance.

To illustrate this we start by describing the basic quantities of the continuum gauge theory, the Yang-Mills theory. Following its geometrical interpretation we will present the corresponding lattice quantities, especially the Kogut-Susskind Hamiltonian (see ref. [32]), and discuss their behaviour under gauge transformations. Additionally, we will check the continuum limit of the lattice introduced.

1.1.1 Continuum gauge theory

Yang-Mills theories are gauge invariant theories. Here we concentrate on the gauge group given by the special unitary group $\mathrm{SU}(N_c)$, which has $N_c^2 - 1$ elements and is non-Abelian for $N_c \geq 2$. In this thesis we will consider especially $\mathrm{SU}(3)$, which corresponds to 3 colour degrees of freedom.

The Yang-Mills action

The quantities describing this theory are the Yang-Mills action S_{YM} or the corresponding Lagrangian L_{YM}:

$$S_{\mathrm{YM}} = \frac{1}{2g^2} \int \mathrm{d}^{D+1}x \sum_{\mu,\nu} \mathrm{Tr}(F_{\mu\nu})^2 \tag{1.1}$$

$$L_{\mathrm{YM}} = \frac{1}{2g^2} \int \mathrm{d}^{D}x \sum_{\mu,\nu} \mathrm{Tr}(F_{\mu\nu})^2 \,. \tag{1.2}$$

Here g is the coupling constant of the theory and $F_{\mu\nu}$ is the field strength tensor

$$F_{\mu\nu} = \partial_\mu A_\nu - \partial_\nu A_\mu + [A_\mu, A_\nu] \ ,$$

with the gauge fields A_μ which are elements of the Lie algebra of $\mathrm{SU}(N_c)$ and can therefore be parametrised by

$$A_\mu = -\mathrm{i}\, g \frac{1}{2} A_\mu^a \lambda^a \, .$$

The indices μ and ν run over the values $0, 1, \ldots, D$, where D is the number of space dimensions; the temporal axis has the index 0. The matrices λ^a, $a = 1, \ldots, (N_c^2 - 1)$, which are called the generators of the gauge group, are traceless, Hermitian and normalised:

$$\mathrm{Tr}(\lambda^a \lambda^b) = 2\delta_{ab} \, .$$

They fulfil the commutation relations

$$\left[\lambda^a, \lambda^b\right] \quad = \quad \mathrm{i}\, 2 f^{abc} \lambda^c,$$

where the structure constants f^{abc} are completely antisymmetric and real. For SU(3) the generators $\lambda^a, a = 1, \ldots, 8$ are the Gell-Mann matrices.

A local gauge transformation $\Lambda(x)$ for space-time points x is an element of $\mathrm{SU}(N_c)$ and it acts on the gauge fields and the field strength tensor as follows:

$$\begin{aligned} A_\mu(x) \to A'_\mu(x) &= \Lambda^{-1}(x)(A_\mu(x) + \partial_\mu)\Lambda(x) \\ F_{\mu\nu}(x) \to F'_{\mu\nu}(x) &= \Lambda^{-1}(x) F_{\mu\nu}(x) \Lambda(x) \, . \end{aligned}$$

Then the Lagrangian and consequently the action are gauge invariant.

Canonical quantisation

As we are interested in the Hamiltonian formulation we perform the standard equal-time quantisation of the Yang-Mills theory. The quantisation procedure for gauge theories is quite involved as it imposes gauge fixing via constraints (see as well ref. [48]).

Here we will choose the temporal gauge fixing $A_0 = 0$, leaving open the time-independent gauge transformations and the constraint that is given by the non-Abelian analogue of the Gauss law (see as well ref. [36]).

We reformulate the theory in terms of generalised (colour) electric and magnetic fields, $E_i = F_{i0}$ and $B_i = -\frac{1}{2}\epsilon_{ijk} F_{jk}$, with $i, j, k = 1, \ldots, 3$ for $D = 3$ and an analogous form for $D = 2$. Then we obtain the following Yang-Mills Hamiltonian

$$H_{\mathrm{YM}} = \frac{1}{2g^2} \int \mathrm{d}^D x \mathrm{Tr}(\mathbf{E}^2 + \mathbf{B}^2) \, ,$$

where the canonical momenta $\Pi_j^a(\mathbf{x})$ of the gauge field $\mathbf{A}$ are given by

$$E_j^a = \Pi_j^a(\mathbf{x}) \, .$$

In the theory A_0 is not dynamical and therefore has no corresponding conjugate momentum.

As already said we now choose the temporal gauge $A_0 = 0$. It is a partial gauge fixing and implies that we have to implement the Gauss law by hand. The Gauss law itself states that the physical Hilbert space is spanned by gauge invariant states

$$\Psi(\mathbf{A}) = \Psi(\mathbf{A}')\,, \tag{1.3}$$

where $A_i' = \Lambda^{-1}(\mathbf{x})(A_i(\mathbf{x}) + \partial_i)\Lambda(\mathbf{x})$ is the gauge transformed field. In the temporal gauge the remaining gauge transformations are time-independent. Under these the Hamiltonian is invariant.

The quantisation of the theory is reflected by the following commutation relation

$$[E_i^a(\mathbf{x}), A_j^b(\mathbf{x}')] = -\mathrm{i}\delta^{ab}\delta_{ij}\delta(\mathbf{x} - \mathbf{x}')$$

between the canonical conjugate field operators $\mathbf{A}(\mathbf{x})$ and $\mathbf{E}(\mathbf{x})$. The canonical momentum is given by:

$$E_j^a = -\mathrm{i}\frac{\partial}{\partial A_j^a(\mathbf{x})}\,.$$

1.1.2 Discretisation

Introducing a lattice to regularise the theory, we have to redefine the quantities described above. At first we consider a $D+1$ dimensional lattice with D space dimensions and one time dimension. The lattice spacing is a (see fig. 1.1).

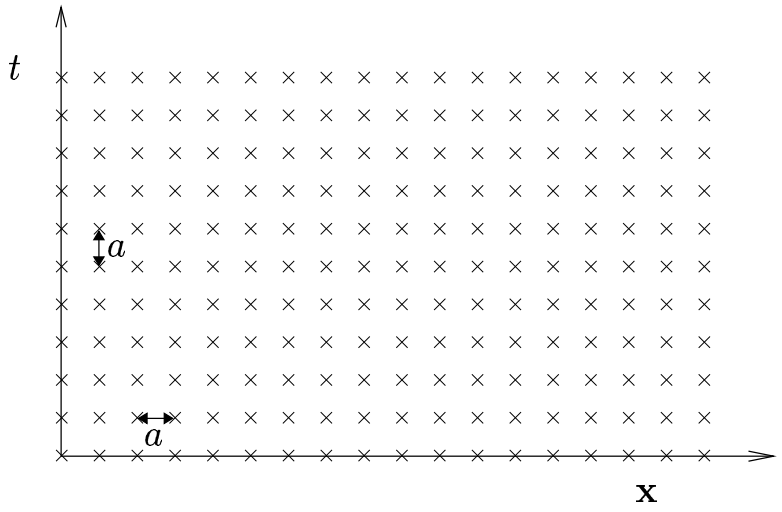

Figure 1.1: Illustration of a lattice which is symmetric in the time and space direction.

Taking the geometrical interpretation of the Yang-Mills theory into account we can illustrate the properties of the lattice quantities.

Parallel transporters and link variables

The gauge fields A_μ in the continuum theory generate parallel transporters along an infinitesimal curve κ in space-time from x to $x + \mathrm{d}x$:

$$U_{x+\mathrm{d}x,x} = \mathbb{1} - A_\mu(x)\mathrm{d}x^\mu\,.$$

A general parallel transporter along a curve κ from x to y is then given by

$$U_{yx} = \mathrm{P}\ \exp\left(-\int_\kappa A_\mu \mathrm{d}x^\mu\right) .$$

The symbol P denotes path ordering. Thus every curve κ is associated with an $\mathrm{SU}(N_c)$ matrix U. It has the following properties for the composition and reversion of curves:

$$\begin{aligned} U_{xx} &= \mathbb{1} \\ U_{yx} &= U_{xy}^{-1} \\ U_{zx} &= U_{zy}U_{yx} . \end{aligned}$$

Here x, y and z are starting– and endpoints of curves. Under gauge transformation we get:

$$U_{yx} \to U'_{yx} = \Lambda^{-1}(y) U_{yx} \Lambda(x) . \tag{1.4}$$

As the shortest non-zero distance on a lattice is the lattice spacing a, the corresponding parallel transporter is along a link l of the lattice. Let x be a point on the lattice and $x + a\hat{\mu}$ the neighbouring point in the direction of the lattice axis $\mu = 0, 1, \ldots, D$. The corresponding link l is the straight path from x to $x + a\hat{\mu}$ and for the parallel transporter along that link we can write:

$$U_l = U_{x+a\hat{\mu},x} = \exp(-aA^L_\mu(x)) .$$

A^L_μ are now the gauge fields on the lattice. The lattice parallel transporter is called link variable. It has the same properties under composition and reversion of (now) links and under gauge transformations (now on lattice points) as the continuum parallel transporters.

Having introduced an infinitesimal parallel transporter in the continuum we obtain a connection between two different space-time points. For a matter function on space-time points $\phi(x) \in \mathrm{SU}(N_c)$ we define a covariant differential by

$$D\phi(x) = U^{-1}_{x+\mathrm{d}x,x}\phi(x + \mathrm{d}x) - \phi(x) .$$

Then we obtain

$$D\phi(x) = (D_\mu\phi)(x)\mathrm{d}x^\mu$$

with the covariant derivative

$$(D_\mu\phi)(x) = (\partial_\mu + A_\mu(x))\phi(x) .$$

Then the field strength $F_{\mu\nu}$ corresponds to the curvature tensor via

$$F_{\mu\nu}(x) = [D_\mu, D_\nu] . \tag{1.5}$$

It can be interpreted geometrically as a parallel transporter along a closed infinitesimal path (see fig. 1.2, left part).

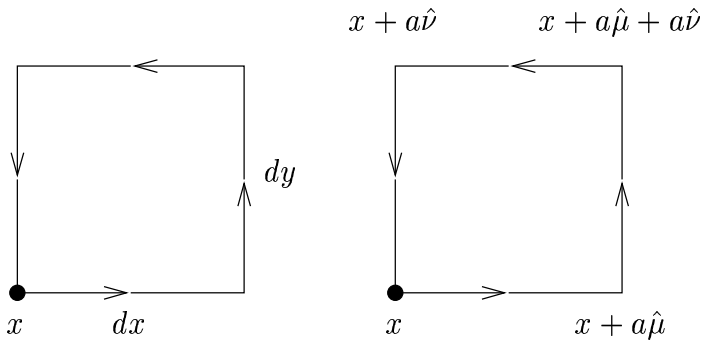

Figure 1.2: Illustration of the smallest closed path in the continuum (left figure) and on the lattice (right figure).

The plaquette variable and the Wilson action

To find the corresponding field strength on the lattice one has to look for the smallest closed lattice path, the plaquette (see fig. 1.2, right part). A parallel transporter along a plaquette containing the points

$$x, \qquad x + a\hat{\mu}, \qquad x + a\hat{\mu} + a\hat{\nu}, \qquad x + a\hat{\nu}$$

is given by

$$\begin{aligned} U_{p_{st}}(x) &= U^{-1}_{x+a\hat{\nu},x} U^{-1}_{x+a\hat{\mu}+a\hat{\nu},x+a\hat{\nu}} U_{x+a\hat{\mu}+a\hat{\nu},x+a\hat{\mu}} U_{x+a\hat{\mu},x} \\ &= \square_{st} \,. \end{aligned} \tag{1.6}$$

The index st denotes that here we have the plaquette function in space-time.

Wilson (see ref. [67]) proposed the following action for the Yang-Mills theory on the lattice:

$$S_W = \sum_{p_{st}} \frac{1}{g'^2} \mathrm{Tr} \left(2 - \square_{st} - \square_{st} \right) . \tag{1.7}$$

Here $\sum_{p_{st}} = \sum_x \sum_{\mu<\nu}$. The connection of the lattice coupling constant g' and the continuum coupling g will be shown below. The behaviour of the link variables under gauge transformation (see eq. (1.4)) ensures that $\mathrm{Tr} U'_{p_{st}} = \mathrm{Tr} U_{p_{st}}$. Thus the Wilson action is gauge invariant.

1.1.3 The continuum limit

Now we investigate in which sense the Wilson action (eq. (1.7)) on the lattice is related to the Yang-Mills action (see eq. (1.1)) for gauge fields in the continuum. Indeed, considering the covariant derivative on matter functions ϕ on the lattice

$$D^L_\mu \phi(x) = \frac{1}{a} \left(U^{-1}_{x+a\hat{\mu},x} \phi(x + a\hat{\mu}) - \phi(x) \right)$$

one can show that (see ref. [63])

$$\mathrm{Tr}(\square_{st} + \square_{st}) = \mathrm{Tr} \left(2 - a^4 \left([D^L_\mu, D^L_\nu]^\dagger [D^L_\mu, D^L_\nu] \right) \right) .$$

With $\frac{1}{2}\sum_{\mu,\nu} = \sum_{\mu<\nu}$, we have

$$S_W = \frac{a^4}{g'^2}\sum_{p_{st}} \mathrm{Tr}\left([D^L_\mu, D^L_\nu]^\dagger [D^L_\mu, D^L_\nu]\right) = \frac{a^4}{2g'^2}\sum_x \sum_{\mu,\nu} \mathrm{Tr}\left(F^L_{\mu\nu}\right)^2 ,$$

where we have defined a field strength $F^L_{\mu\nu}$ on the lattice analogous to eq. (1.5) in the continuum. Note that $F^L_{\mu\nu}$ still depends on the link variables U_l and is therefore nonlinear in the gauge fields A_μ. Performing the continuum limit, $a \to 0$ and replacing $a^{D+1}\sum_x \to \int \mathrm{d}x^{D+1}$, we get

$$S_W = \frac{a^4}{2g'^2 a^{D+1}} \int \mathrm{d}^{D+1}x \sum_{\mu,\nu} \mathrm{Tr}(F_{\mu\nu})^2 + O(a^2) .$$

Thus the leading term for small a of the Wilson action coincides with the Yang-Mills action, if we set

$$g'^2 \frac{a^{D+1}}{a^4} = g^2$$

and identify g with the bare coupling constant of the theory. Since in this thesis we specialise to $D = 2$ space dimensions, we have

$$\frac{g'^2}{a} = g^2 . \tag{1.8}$$

On the lattice the natural length scale is given by the lattice spacing a and consequently in the 2-dimensional case the bare coupling has the dimension of $(\text{length})^{-\frac{1}{2}}$.

Improvement

Classical improvement

By performing the continuum limit we see that the Wilson action leads to a discretisation error of $O(a^2)$. Symanzik (see ref. [59]) proposed to use so-called improved actions, that give a discretisation error of only $O(a^4)$. The aim was to reduce the numerical effort by working with coarser lattices, i.e. with larger lattice spacing.

If we change the plaquette term in the Wilson action

$\mathrm{Tr}\left(\square_{st} + \square_{st}\right) \quad \to \quad c_1 \mathrm{Tr}\left(\square_{st} + \square_{st}\right)$

$+c_2 \mathrm{Tr}\left(\square\!\square_{st} + \square\!\square_{st} + \square\!\!\square_{st} + \square\!\!\square_{st}\right)$ (1.9)

the new action S_{improved} has an improved continuum limit:

$$S_{\text{improved}} = \frac{a^4}{2g'^2 a^{D+1}} \int \mathrm{d}^{D+1}x \sum_{\mu,\nu} \mathrm{Tr}(F_{\mu\nu})^2 + O(a^4) .$$

As is illustrated in fig. 1.3, the rectangular term in eq. (1.9) corresponds to a parallel transporter along a rectangle containing the points

$$x, \qquad x + 2a\hat{\mu}, \qquad x + 2a\hat{\mu} + a\hat{\nu}, \qquad x + a\hat{\nu}$$

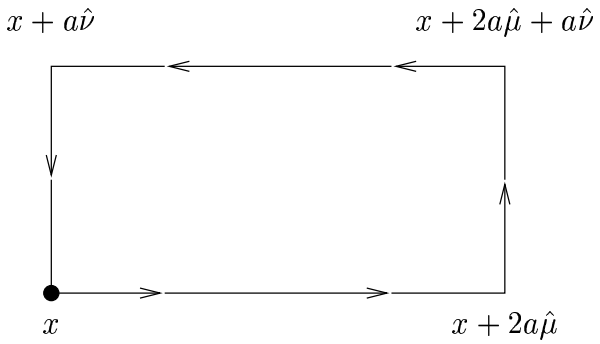

Figure 1.3: Illustration of a closed rectangular path on the lattice.

and we can write:

$$\square_{st} = U^{-1}_{x+a\hat{\nu},x} U^{-1}_{x+2a\hat{\mu}+a\hat{\nu},x+a\hat{\nu}} U_{x+2a\hat{\mu}+a\hat{\nu},x+2a\hat{\mu}} U_{x+2a\hat{\mu},x}$$

The correct coefficients for this classical improvement are $c_1 = \frac{5}{3}$ and $c_2 = -\frac{1}{12}$ (see ref. [35]).

Tadpole improvement

In addition to the classical improvement one can largely cancel lattice artifacts by dividing every link variable (with link index l) by the mean link u_0 (see again ref. [35]):

$$U_l \to \frac{U_l}{u_0}\,.$$

The division by the mean value

$$u_0 = \frac{1}{N_c}\mathrm{ReTr}U_l$$

avoids tadpole contributions caused by the (nonlinear) gluon link operator U_l of the lattice regularisation and it can be calculated via the plaquette variable

$$u_0 = \langle 0|\frac{1}{2N_c}\mathrm{Tr}\left(\square_{st} + \square_{st}\right)|0\rangle^{\frac{1}{4}}. \tag{1.10}$$

To consider the tadpole improvement we have to change the coefficients c_1 and c_2 from above according to

$$c_1 \to \frac{c_1}{u_0^4}, \quad c_2 \to \frac{c_2}{u_0^6}\,.$$

1.1.4 Hamiltonian formulation

We want to calculate the glueball spectrum within the Hamiltonian formulation of lattice gauge theory. Therefore we have to change the lattice introduced before. The time coordinate has to remain continuous (see fig. 1.4). In analogy to the Hamiltonian formulation in the continuum we restrict the gauge fields by imposing the temporal gauge $A_0 = 0$. The link variables in the pure temporal direction are now the identity. The local gauge transformations on the lattice points are time independent.

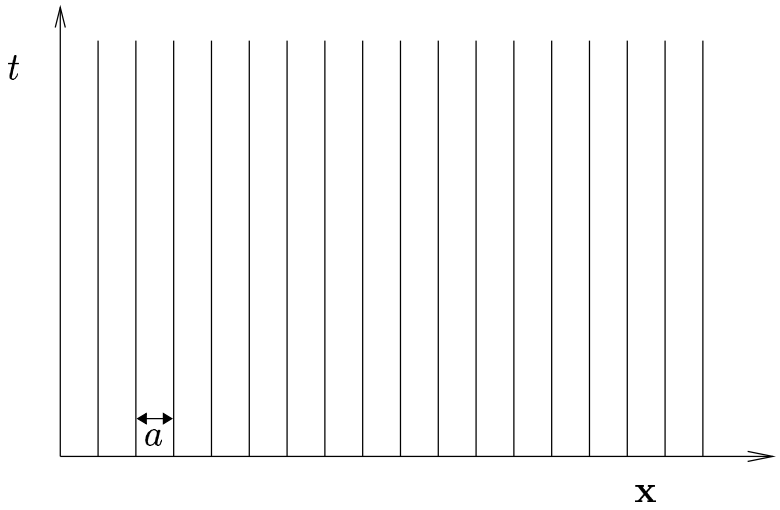

Figure 1.4: Illustration of a lattice in space with continuous time.

To deduce the Hamiltonian from the Wilson action one has to set up the Lagrangian L for the lattice Yang-Mills theory for continuous time

$$S_W = \sum_{x_0} a_t L \stackrel{a_t \to 0}{=} \int \mathrm{d}t L \,,$$

where $a_t = a$ is the lattice spacing in the time direction.

The Kogut-Susskind Hamiltonian

After a Legendre transformation (see ref. [57]) of the Lagrangian we get the Kogut-Susskind Hamiltonian for $D = 2$ space dimensions and for $SU(3)$:

$$H_{KS} = \frac{g^2}{2}\left(\sum_{l,a} E_l^a E_l^a + \sum_p \frac{2}{g^4 a^2}\mathrm{Tr}\left(2 - \square - \square\right)\right) = \frac{g^2}{2} H \,. \qquad (1.11)$$

Here we denote $\sum_p = \sum_{\mathbf{x}} \sum_{i<j}$, where $i, j = 1, \ldots, D$.

The magnetic term which is illustrated in fig. 1.5 now consists of the spatial plaquette function:

$$\square = U^{-1}_{\mathbf{x}+a\hat{j},\mathbf{x}} U^{-1}_{\mathbf{x}+a\hat{i}+a\hat{j},\mathbf{x}+a\hat{j}} U_{\mathbf{x}+a\hat{i}+a\hat{j},\mathbf{x}+a\hat{i}} U_{\mathbf{x}+a\hat{i},\mathbf{x}} \,.$$

For the electric part we have defined the canonical momenta E_l^a of the gauge fields, which are represented on the lattice via the link variables U_l:

$$[E_l^a, U_l] = \frac{\lambda^a}{2} U_l \delta_{lm} \,. \qquad (1.12)$$

Here l, m are link indices. $E_l^a E_l^a$ corresponds to the quadratic Casimir operator of SU(3). Its eigenvalues will be discussed in the appendix B.

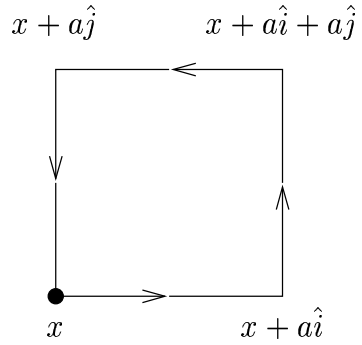

Figure 1.5: Illustration of the spatial plaquette on the lattice.

H is the dimensionless Hamiltonian, since g^2 has the dimension of an inverse length (see eq. (1.8)) in $D = 2$ space dimensions. Because of this we can define a new dimensionless coupling β by

$$\frac{2N_c}{\beta} = g^2 a \quad \text{for} \quad D = 2$$

and the dimensionless Hamiltonian in eq. (1.11) then takes the form:

$$H = \sum_{l,a} E_l^a E_l^a - \sum_p \frac{\beta^2}{2N_c^2} \mathrm{Tr}(\square + \square) \,. \tag{1.13}$$

The constant term in the Hamiltonian does not contribute to the solutions and is therefore omitted.

The Hilbert space

Accounting for the Gauss law the Hilbert space consists of gauge invariant functions $\Psi(U)$ of the link variables $U = (U_{l_1}, \ldots, U_{l_{N_l}})$, where N_l is the number of the lattice links:

$$\Psi\left(\Lambda^{-1}(\mathbf{y}_1) U_{l_1} \Lambda(\mathbf{x}_1), \ldots, \Lambda^{-1}(\mathbf{y}_{N_l}) U_{l_{N_l}} \Lambda(\mathbf{x}_{N_l})\right) = \Psi(U_{l_1}, \ldots, U_{l_{N_l}}) \,.$$

We have the gauge transformation $\Lambda \in \mathrm{SU}(N_c)^{N_p}$, where N_p is the number of lattice points and l_i is the link from $\mathbf{x}_i$ to $\mathbf{y}_i$. With respect to the Haar-measure $\mathrm{D}U$ the wave functions are square-integrable and accordingly the norm is given by:

$$||\Psi(U)||^2 = \int \mathrm{D}U \Psi^*(U_{l_1}, \ldots, U_{l_{N_l}}) \Psi(U_{l_1}, \ldots, U_{l_{N_l}}) < \infty \,.$$

The Haar-measure is a measure on a compact group G, here $\mathrm{SU}(N_c)^{N_l}$ on the lattice links, and has the following properties:

- gauge invariance:

$$\int_G DU f(U) = \int_G DU f(\Lambda U) = \int_G DU f(U\Lambda) \,, \, \Lambda \in G \,. \tag{1.14}$$

- normalisation:

$$\int_G DU = 1\,.$$

To construct the gauge invariant functions we rely on a method from differential geometry. We choose Ψ in the loop space, which is built of functions consisting of parallel transporters along loops, i.e. along closed paths. We have seen that the plaquette function, for example, is gauge invariant $\mathrm{Tr}U_p = \mathrm{Tr}U_p'$ and therefore it will be an important building block for the construction of the basis of the Hilbert space (see chapter 2).

1.2 The coupled cluster method

1.2.1 Wave functions

The idea of the coupled cluster method is to reformulate the eigenvalue problem of the Kogut-Susskind Hamiltonian $H\Psi = E\Psi$ as equations for the ground state correlation function S and for the excitation operator F. Here S and F are given by the following Ansätze:

$$\begin{aligned} \Psi_0(U) &= \exp(S(U))\,, \\ \Psi(U) &= F(U)\exp(S(U)), \end{aligned} \tag{1.15}$$

for the ground- and excited states, respectively.

These exp$S$ Ansätze guarantee the correct volume dependence of the solutions. The ground state (vacuum) energy E_0 has to be proportional to the volume of the state (the volume of the lattice) (see ref. [19]) and the energy gap between the excited states and the vacuum should be independent of the volume. The validity of these volume dependencies is related to the properties of S and F. They can be expressed with the help of projection operators on localised functions (see ref. [56]):

$$S(U) = \sum_{\alpha>0} S_\alpha \eta^\alpha(U) \tag{1.16}$$

$$F(U) = F^K(U) = \sum_{\alpha} F^K_\alpha \eta^\alpha_K(U) \tag{1.17}$$

$$\eta^\alpha(U) = \frac{\tilde{\Pi}^0 \chi^\alpha(U)}{||\tilde{\Pi}^0 \chi^\alpha(U)||} \tag{1.18}$$

$$\eta^\alpha_K(U) = \frac{\tilde{\Pi}^K \chi^\alpha(U)}{||\tilde{\Pi}^K \chi^\alpha(U)||}\,. \tag{1.19}$$

The localised functions $\{\chi^\alpha\}$ will be described below. χ^0 is the constant function. It is omitted in the ground state correlation function since it just gives a scalar factor.

The quantities $\tilde{\Pi}^K$, where K stands for a set of quantum numbers of commuting operators, are the projection operators reflecting the symmetries of the lattice. These are

the translation and the rotation/reflection symmetry and the charge conjugation. We denote the symmetry groups by G_{lr} for lattice rotations and reflections and G_{lt} for lattice translations. We write $|G|$ for the order of the groups. The projectors are given by

$$\begin{aligned}\tilde{\Pi}^K &= \Pi^{\mathbf{p}}\Pi^{J^P}_{\nu\sigma}\Pi^{\pm}_C = \Pi^0\Pi^{J^P}_{\nu\sigma}\Pi^{\pm}_C \\ &= \Big(\sum_{t_{\mathbf{a}}\in G_{lt}} T_{\mathbf{a}}\Big)\Big(\frac{\dim J^P}{|G_{lr}|}\sum_{R\in G_{lr}} D^{J^P}_{\nu\sigma}(R^{-1})T(R)\Big)\frac{1}{2}(1\pm T_C).\end{aligned}$$

They project onto states with vanishing (lattice) momentum $\mathbf{p}=0$, angular momentum/parity $J^P=(0^+,0^-,2^+,2^-,1^\pm)$ and onto charge parity ± 1. The irreducible representation D^{J^P} of G_{lr} has the dimension $\dim J^P$. Magnetic quantum numbers labelling states in an irreducible representation are denoted by ν and σ. These projectors will be discussed in detail in chapter 3. K denotes the set of quantum numbers J^{PC}, ν and σ. In the trivial case $J^{PC}=0^{++}$ we omit K and the projector $\tilde{\Pi}^0$ is given by:

$$\begin{aligned}\tilde{\Pi}^0 &= \Pi^0\Pi^{0^+}\Pi^+_C \\ &= \Big(\sum_{t_{\mathbf{a}}\in G_{lt}} T_{\mathbf{a}}\Big)\Big(\frac{1}{|G_{lr}|}\sum_{R\in G_{lr}} T(R)\Big)\frac{1}{2}(1+T_C)\,.\end{aligned}$$

Localised functions $\{\chi^\alpha\}$ will be constructed in chapter 2 under the following conditions:

- χ^α is gauge invariant. It will be constructed of functions that consist of parallel transporters along loops (loop space). This provides the invariance under gauge transformation as we discussed in section 1.1.4.
- χ^α is localised, i.e. it has a finite support, as this is essential for the coupled cluster method.
- χ^α is a strong coupling eigenfunction. In the strong coupling limit $g\to\infty$, where $H\to\sum_{l,a}E^a_lE^a_l$, we have

$$\sum_{l,a} E^a_l E^a_l \chi^\alpha = \epsilon_\alpha \chi^\alpha\,. \tag{1.20}$$

- The set of functions $\{\chi^\alpha\}$ is linear independent under symmetry transformations on the lattice:

$$\sum_\alpha \sum_{t_{\mathbf{a}},R} c_{\alpha,\mathbf{a},R,C} T_{\mathbf{a}} T(R) T_C \chi^\alpha = 0 \Rightarrow c_{\alpha,\mathbf{a},R,C} = 0\,.$$

  Especially, this means no χ^α can be constructed from another element by symmetry transformations, i.e.

$$T_{\mathbf{a}}T(R)T_C\chi^\alpha = \chi^\beta \Rightarrow \alpha=\beta\,. \tag{1.21}$$

  For any element of course there can be nontrivial symmetry transformations, which map χ^α on itself. In chapter 3 these internal symmetries will be discussed and classified.

- The set of functions $\{\chi^\alpha\}$ is orthonormal:

$$\langle\chi^\alpha,\chi^\beta\rangle = \int DU(\chi^\alpha)^*\chi^\beta = \delta_{\alpha\beta}\,.$$

χ is called the loop space basis.

If we transfer its properties, i.e. after the projection $\tilde{\Pi}^K$, to η_K, we get η_K to be a (linear independent) basis, which is orthonormal via construction (see eq. (1.18) and eq. (1.19)):

$$\langle \eta_K^\alpha, \eta_{K'}^\beta \rangle = \delta_{\alpha\beta}\delta_{KK'} .$$

The norm will be determined in chapter 3, where we discuss the projection operators. The elements of η are also strong coupling eigenfunctions

$$\sum_{l,a} E_l^a E_l^a \eta_K^\alpha = \sum_{l,a} \frac{E_l^a E_l^a [\tilde{\Pi}^K \chi^\alpha]}{||\tilde{\Pi}^K \chi^\alpha||} = \frac{\epsilon_\alpha \tilde{\Pi}^K \chi^\alpha}{||\tilde{\Pi}^K \chi^\alpha||} = \epsilon_\alpha \eta_K^\alpha \tag{1.22}$$

and they are gauge invariant.

For the numerical calculations a truncation scheme for the basis will be introduced in chapter 4.

1.2.2 The coupled cluster equations

Within the coupled cluster approach we can now derive the coupled cluster equations, which are the lattice Schrödinger equations written in the basis η. This has been shown explicitly in refs. [63, 64]. Here we present merely the important steps.

The first step is to rewrite the Schrödinger equations in terms of the ground state correlation function S and the excitation operator F. For the ground state we have

$$\begin{aligned} H\Psi_0 &= E_0\Psi_0 \\ \Leftrightarrow e^{-S} H e^S &= E_0 \end{aligned} \tag{1.23}$$

and for the excited states we get

$$\begin{aligned} H\Psi &= E\Psi \\ \Leftrightarrow HF^K e^S &= EF^K e^S \qquad (1.24) \\ \Leftrightarrow [e^{-S} H e^S, F^K] &= (E - E_0) F^K . \qquad (1.25) \end{aligned}$$

For the last form we subtracted eq. (1.24) from eq. (1.23) multiplied by F^K. Inserting the Hamiltonian (eq. (1.13)) and using the relations between the link variables U_l and the Casimir operators $\sum_a E_l^a E_l^a$ (see eq. (1.12)) one can show that the terms in the expansion of the exponential in the equations above vanishes for orders > 2 (see ref. [63]). We then get the following equation for the ground state

$$\sum_\mu (S_{\mu\mu} + S_\mu S_\mu) - \sum_{\mathrm{p}} \frac{\beta^2}{2N_c^2} \mathrm{Tr}(\square + \square) = E_0$$

and for the excited states

$$\sum_\mu (F_{\mu\mu}^K + 2S_\mu F_\mu^K) = (E - E_0) F^K ,$$

with the abbreviations:

$$\begin{aligned} f_{(l,a)} &:= [E_l^a, f] \\ f_{(l,a)(l,a)} &:= [E_l^a, f_{(l,a)}] \\ \mu &:= (l,a) . \end{aligned}$$

In the second step we use the fact that S and F can be expanded in the basis η. This yields:

$$\sum_\mu \Big([\sum_{\alpha>0} S_\alpha \eta^\alpha]_{\mu\mu} + [\sum_{\alpha_1>0} S_{\alpha_1}\eta^{\alpha_1}]_\mu [\sum_{\alpha_2>0} S_{\alpha_2}\eta^{\alpha_2}]_\mu \Big) = \frac{||\tilde{\Pi}^0\chi^1||\beta^2}{N_c^2}\eta^1 + \frac{E_0}{N}\eta^0 \tag{1.26}$$

$$\sum_\mu \Big([\sum_{\alpha} F_\alpha^K \eta_K^\alpha]_{\mu\mu} + 2[\sum_{\alpha_1>0} S_{\alpha_1}\eta^{\alpha_1}]_\mu [\sum_{\alpha_2} F_{\alpha_2}^K \eta_K^{\alpha_2}]_\mu \Big) = (E-E_0)\sum_\alpha F_\alpha^K \eta_K^\alpha \,. \tag{1.27}$$

Here η^0 and η^1 are the first two basis elements: As χ^0 is chosen to be the identity on the lattice, which has the strong-coupling eigenvalue 0, we have to scale $\eta^0 = \frac{\tilde{\Pi}^0\chi^0}{||\tilde{\Pi}^0\chi^0||}$ with a factor N, which is a number characterising the volume of the lattice, to get well-defined equations (see as well section 3.4.2):

$$\frac{\eta^0}{N} = \mathbf{1}_{\text{Lattice}}$$

The element η^1 merely is the loop space basis element χ^1, which is the plaquette function as will be shown in chapter 2. After projection onto definite charge parity the plaquette function is symmetric under all rotations and reflections (see section 3.4.1) and we get:

$$\begin{aligned}
\eta^1 &= \frac{\tilde{\Pi}^0\chi^1}{||\tilde{\Pi}^0\chi^1||} = \frac{1}{||\tilde{\Pi}^0\chi^1||}\Pi^{\mathbf{p}=0}\Pi^{J^P=0^+}\Pi_c^+\chi^1 \\
&= \frac{1}{||\tilde{\Pi}^0\chi^1||}\Pi^0\Pi^{0^+}\frac{1}{2}\mathrm{Tr}(\square + \square) \\
&= \frac{1}{||\tilde{\Pi}^0\chi^1||}\frac{1}{2}\sum_{\mathrm{p}}\mathrm{Tr}(\square + \square)\,.
\end{aligned} \tag{1.28}$$

In the third step of the determination of the coupled cluster equations we inspect the various terms in eq. (1.26) and eq. (1.27) separately. For the first terms we get:

$$\begin{aligned}
\sum_\mu [\sum_{\alpha>0} S_\alpha \eta^\alpha]_{\mu\mu} &= \sum_{\alpha>0} \epsilon_\alpha S_\alpha \eta^\alpha \,, \\
\sum_\mu [\sum_{\alpha} F_\alpha^K \eta_K^\alpha]_{\mu\mu} &= \sum_{\alpha} \epsilon_\alpha F_\alpha^K \eta_K^\alpha \,.
\end{aligned}$$

Here we used the fact that the η are strong coupling eigenfunctions (see eq. (1.22)). The second terms contain products of basis elements:

$$\begin{aligned}
\textstyle\sum_\mu \; [\sum_{\alpha_1>0} S_{\alpha_1}\eta^{\alpha_1}]_\mu [\sum_{\alpha_2>0} S_{\alpha_2}\eta^{\alpha_2}]_\mu &= \sum_{\alpha_1>0,\alpha_2>0} S_{\alpha_1}S_{\alpha_2}\sum_\mu [\eta^{\alpha_1}]_\mu [\eta^{\alpha_2}]_\mu \\
&= \sum_{\alpha_1>0,\alpha_2>0,\alpha_3} S_{\alpha_1}S_{\alpha_2}C_{\alpha_3}^{\alpha_1,\alpha_2}(0^{++})\;\eta^{\alpha_3}\,,
\end{aligned} \tag{1.29}$$

$$\begin{aligned}
\textstyle\sum_\mu \; [\sum_{\alpha_1>0} S_{\alpha_1}\eta^{\alpha_1}]_\mu [\sum_{\alpha_2} F_{\alpha_2}^K \eta_K^{\alpha_2}]_\mu &= \sum_{\alpha_1>0,\alpha_2} S_{\alpha_1}F_{\alpha_2}^K\sum_\mu [\eta^{\alpha_1}]_\mu [\eta_K^{\alpha_2}]_\mu \\
&= \sum_{\alpha_1>0,\alpha_2} S_{\alpha_1}F_{\alpha_2}^{J^{PC}}\sum_\mu [\eta^{\alpha_1}]_\mu [\eta^{\alpha_2}_{J^{PC},\nu_2\sigma}]_\mu \\
&= \sum_{\alpha_1>0,\alpha_2,\alpha_3}\sum_\kappa S_{\alpha_1}F_{\alpha_2}^{J^{PC}}\,C_{\alpha_3,\nu_2\kappa}^{\alpha_1\alpha_2}(J^{PC})\;\eta^{\alpha_3}_{J^{PC},\kappa\sigma}\,.
\end{aligned} \tag{1.30}$$

These products will be calculated explicitly in appendix A. The correct coefficients, called the coupled cluster matrix elements, will also be defined there (see eq. (A.3)):

$$\begin{aligned} C^{\alpha_1\alpha_2}_{\alpha_3,\nu\kappa}(J^{PC}) &= \frac{1}{|G_{lr}|}\frac{||\tilde{\Pi}^K\chi^{\alpha_3}||}{||\tilde{\Pi}^0\chi^{\alpha_1}||||\tilde{\Pi}^K\chi^{\alpha_2}||} \\ &\times \sum_{\substack{t_{\mathbf{a}_2},t_{\mathbf{a}_3}\in G_{lt}\\ R_2,R_3\in G_{lr}}} D^{J^P}_{\nu\kappa}(R_2^{-1}R_3)\frac{1}{4}(\epsilon_{\alpha_3}-\epsilon_{\alpha_1}-\epsilon_{\alpha_2})(c^{\alpha_1\alpha_2}_{\alpha_3,\mathbf{a}_2,\mathbf{a}_3,R_2,R_3}+c^{\bar{\alpha}_1\alpha_2}_{\alpha_3,\mathbf{a}_2,\mathbf{a}_3,R_2,R_3})\,. \end{aligned}$$

The c-coefficients are coefficients in the expansion in the loop space basis χ. In chapter 2 they are defined by

$$\begin{aligned} \sum_{\substack{t_{\mathbf{a}_3}\in G_{lt},\\ R_3\in G_{lr}}}\sum_{\alpha_3} c^{\alpha_1\alpha_2}_{\alpha_3,\mathbf{a}_2,\mathbf{a}_3,R_2,R_3}T_{\mathbf{a}_3}T(R_3)\Pi^{\pm}_c\chi^{\alpha_3} &= \chi^{\alpha_1}T_{\mathbf{a}_2}T(R_2)\chi^{\alpha_2} \\ \sum_{\substack{t_{\mathbf{a}_3}\in G_{lt},\\ R_3\in G_{lr}}}\sum_{\alpha_3} c^{\bar{\alpha}_1\alpha_2}_{\alpha_3,\mathbf{a}_2,\mathbf{a}_3,R_2,R_3}T_{\mathbf{a}_3}T(R_3)\Pi^{\pm}_c\chi^{\alpha_3} &= (T_c\chi^{\alpha_1})T_{\mathbf{a}_2}T(R_2)\chi^{\alpha_2}\,, \end{aligned}$$

and calculated in eq. (2.21) and eq. (2.22).

Bringing all terms together, we have for the vacuum the equation

$$\sum_{\alpha_3}\epsilon_{\alpha_3}S_{\alpha_3}\eta^{\alpha_3}+\sum_{\alpha_1>0,\alpha_2>0,\alpha_3}S_{\alpha_1}S_{\alpha_2}C^{\alpha_1,\alpha_2}_{\alpha_3}(0^{++})\;\eta^{\alpha_3} = \frac{||\tilde{\Pi}^0\chi^1||\beta^2}{N_c^2}\eta^1+\frac{E_0}{N}\eta^0$$

and for the excited (glueball) states

$$\begin{aligned} &\sum_{\alpha_3}\epsilon_{\alpha_3}F^{J^{PC}}_{\alpha_3}\eta^{\alpha_3}_{J^{PC}\nu_3\sigma}+2\sum_{\alpha_1>0,\alpha_2,\alpha_3}\sum_{\kappa}S_{\alpha_1}F^{J^{PC}}_{\alpha_2}C^{\alpha_1,\alpha_2}_{\alpha_3,\nu_2\kappa}(J^{PC})\eta^{\alpha_3}_{J^{PC}\kappa\sigma} \\ &\quad = (E-E_0)\sum_{\alpha_3}F^{J^{PC}}_{\alpha_3}\eta^{\alpha_3}_{J^{PC}\nu_3\sigma}\,. \end{aligned}$$

As the equation for the excited states is independent of σ, we take one representative, choose it to be zero and omit it:

$$\begin{aligned} \sum_{\alpha_3}\epsilon_{\alpha_3}F^{J^{PC}}_{\alpha_3}\eta^{\alpha_3}_{J^{PC}\nu_3}+2\sum_{\alpha_1>0,\alpha_2,\alpha_3}\sum_{\kappa}S_{\alpha_1}F^{J^{PC}}_{\alpha_2}C^{\alpha_1,\alpha_2}_{\alpha_3,\nu_2\kappa}(J^{PC}) &\quad \eta^{\alpha_3}_{J^{PC}\kappa} \\ = &\quad (E-E_0)\sum_{\alpha_3}F^{J^{PC}}_{\alpha_3}\eta^{\alpha_3}_{J^{PC}\nu_3}\,. \end{aligned}$$

Since the basis elements η^{α} are orthonormal the ground state is determined by the following the set of equations

$$\epsilon_{\alpha_3}S_{\alpha_3}+\sum_{\alpha_1>0,\alpha_2>0}S_{\alpha_1}S_{\alpha_2}C^{\alpha_1,\alpha_2}_{\alpha_3}(0^{++}) = \frac{||\tilde{\Pi}^0\chi^1||\beta^2}{N_c^2}\delta_{\alpha_3 1}+\frac{E_0}{N}\delta_{\alpha_3 0}\,. \qquad (1.31)$$

The equation for the excited states is then a simple eigenvalue equation for $F^{J^{PC}}$:

$$\epsilon_{\alpha_3}F^{J^{PC}}_{\alpha_3}+2\sum_{\alpha_1>0,\alpha_2}S_{\alpha_1}F^{J^{PC}}_{\alpha_2}C^{\alpha_1,\alpha_2}_{\alpha_3,\nu_2\nu_3}(J^{PC}) = (E-E_0)F^{J^{PC}}_{\alpha_3}\,, \qquad (1.32)$$

where ν_2 and ν_3 denote the indices of the coupled cluster matrix element.

The procedure of solving these equations will be presented in section 4.2.1 for the vacuum state and in section 4.3.1 for the glueball states. In section 4.1 we will specify the range of α_3 for the vacuum state and the excited (glueball) states.

1.3 Improved Hamiltonian

The classical improvement and the tadpole improvement of the Wilson action discussed in section 1.1.3 can be applied to the Hamiltonian formalism simply by changing the plaquette term of the Kogut-Susskind Hamiltonian (see as well ref. [47]) according to:

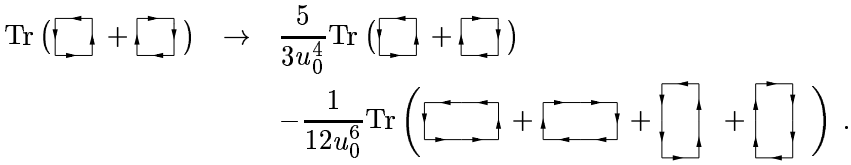

In chapter 2 we show that the rectangular term is related to the basis element η^6 (see section 2.2.3). Analogous to eq. (1.28) for the plaquette function one can show that

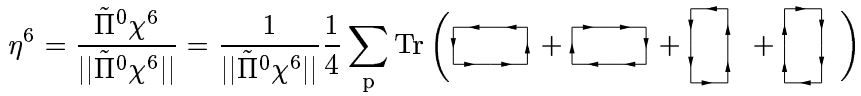

and to include the improvement we substitute in the equation for the vacuum:

$$\frac{||\tilde{\Pi}^0\chi^1||\beta^2}{N_c^2}\delta_{\alpha_3 1} \to \frac{\beta^2}{N_c^2}\left(\frac{5}{3u_0^4}||\tilde{\Pi}^0\chi^1||\delta_{\alpha_3 1} - \frac{1}{6u_0^6}||\tilde{\Pi}^0\chi^6||\delta_{\alpha_3 6}\right). \tag{1.33}$$

For the tadpole improvement we calculate the mean value u_0 of the link variables $\frac{1}{N_c}\mathrm{ReTr}U_l$ via the plaquette variable (see eq. (1.10)). In the Hamiltonian formalism this is done by calculating the expectation value of $H + \lambda\mathrm{Tr}\left(\square + \square\right)$ for some very small λ, and using the Feynman-Hellmann formula:

$$\langle 0|\mathrm{Tr}\left(\square + \square\right)|0\rangle = \frac{d}{d\lambda}\langle 0|H + \lambda\mathrm{Tr}\left(\square + \square\right)|0\rangle\big|_{\lambda=0}.$$

This was already implemented for SU(2) calculations in ref. [64]) and is applied here for SU(3). Results are given in chapter 4.

Chapter 2 **Construction of the basis**

In this chapter we will present the construction of the localised loop space basis χ introduced in chapter 1.

As the plaquette function is the basic element of this basis, its properties will be presented first. We will introduce the graphical notation for the SU(3) coupling we want to use in this chapter, following that of ref. [15] and of ref. [62] for SO(3). Then we give the recipe for building the basis and illustrate it by some examples. For the numerical calculation of the SU(3) recoupling coefficients a computer program [29] was kindly made available to us. We adopted it for our purpose. At the end we will check if the loop space basis has the properties we demanded in chapter 1 and calculate the coefficients needed for the multiplication of basis elements to determine the coupled cluster matrix element as given in appendix A.

2.1 The plaquette function

The plaquette function of eq. (1.6) is crucial for the construction of the loop space basis χ, as by multiplication with this function the whole basis is formed. It is the first non-trivial basis element of the loop space basis and we name it with χ^1.

In terms of the irreducible representation (IR) $D^{\Gamma}_{\gamma\gamma'}(U)$ of elements $U \in \mathrm{SU}(3)$, the plaquette function can be written as:

$$\chi^1 = \mathrm{Tr}\square \quad = \sum_{\gamma_1,\gamma_2,\gamma_3,\gamma_4} D^{\mathbf{3}}_{\gamma_1\gamma_2}(U_1) D^{\mathbf{3}}_{\gamma_2\gamma_3}(U_2) D^{\mathbf{3}}_{\gamma_3\gamma_4}(U_3^{-1}) D^{\mathbf{3}}_{\gamma_4\gamma_1}(U_4^{-1})\,. \tag{2.1}$$

We have used that for the plaquette function we obtain for the 3×3 matrix U_l, $l = 1,\ldots,4$, on the lattice links: $(U_l)_{\gamma\gamma'} = D^{\Gamma=\mathbf{3}}_{\gamma\gamma'}(U_l)$. Here $\Gamma = (p,q) = \mathbf{3} = (1,0)$ labels the three-dimensional fundamental IR of SU(3). The notations and conventions used in this thesis concerning general IRs of SU(3) will be presented in appendix B.

In terms of the graphical notation of ref. [62] for the IRs

$$D^{\Gamma}_{\gamma\gamma'}(U) \quad = \quad \gamma \xrightarrow[U]{\Gamma} \gamma'$$

$$D^{\Gamma}_{\gamma\gamma'}(U^{-1}) \quad = \quad \gamma \xrightarrow[U^{-1}]{\Gamma} \gamma'$$

we can write the plaquette functions as

χ^1 =

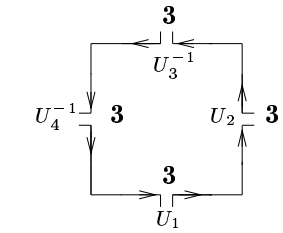

,

where the summation in eq. (2.1) is represented by linking the lines.

The plaquette function χ^1 is gauge invariant as it corresponds to a parallel transporter along a closed loop on the lattice and therefore to an element of the loop space of gauge invariant functions. It is determined completely by the IRs labelled with $\Gamma_l = \mathbf{3}$ on the links $l = 1, \ldots, 4$. By construction it is a strong coupling eigenfunction with the eigenvalue $\epsilon(\Gamma) = \epsilon(\mathbf{3}) = \frac{4}{3}$ of the Casimir operator (see eq. (B.1)) on every link l:

$$\sum_{l,a} E_l^a E_l^a \, \chi(\Gamma_1, \Gamma_2, \Gamma_3, \Gamma_4) \;=\; 4\frac{4}{3}\chi(\Gamma_1, \Gamma_2, \Gamma_3, \Gamma_4) = \frac{16}{3}\chi(\Gamma_1, \Gamma_2, \Gamma_3, \Gamma_4)\,. \qquad (2.2)$$

The normalisation eq. (B.2) implies that also χ^1 is normalised:

$$\langle \chi^1 | \chi^1 \rangle = \int \mathrm{D}U \; (\chi^1)^* \; \chi^1 \;=\; 1\,.$$

At a lattice site of χ^1 only two IRs couple, but generally in $D = 2$ space dimension we have four links with IRs coupling at a site and intermediate couplings have to be taken into account. This can be systematised, similar to the strategy of ref. [51] for SU(2), if we replace a lattice site by two vertices where now three links with IRs couple:

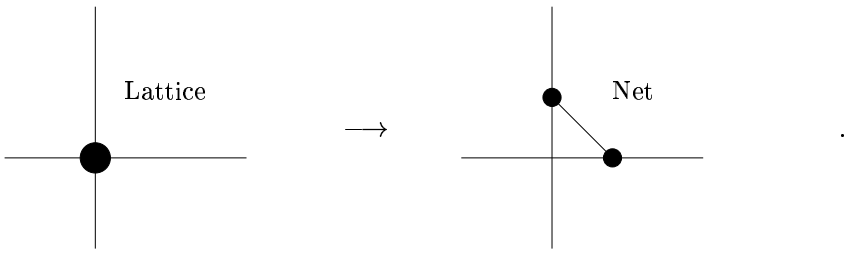

.

The collection of all vertices representing the coupling of three IRs on links we shall call a "net".

The plaquette function on a net

At a vertex on the newly introduced net three IRs (on two lattice and one intermediate link), say Γ_1, Γ_2 and Γ_3 of SU(3) couple and the corresponding coupling coefficients are the Clebsch-Gordan-coefficient (CGC), which will be presented in appendix B.2. The

graphical notation for the CGC on the two new vertices is the following:

$$\langle \Gamma_1\gamma_1\,;\Gamma_2\gamma_2\,|\Gamma_3\gamma_3\rangle_n \;=\;$$

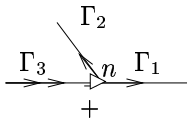

$$= {}_n\langle \Gamma_3\gamma_3\,|\Gamma_1\gamma_1\,;\Gamma_2\gamma_2\rangle \;=\;$$

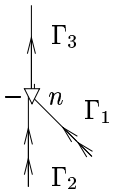

.

The sign at a vertex denotes the order of the coupling. Clockwise corresponds to $-$ and anti-clockwise to $+$. The outer multiplicity of the CGC is denoted with n.

Rewriting the plaquette function χ^1 by using CGC and employing their properties when coupling to a singlet $\Gamma = (p,q) = \mathbf{1} = (0,0)$ (see eq. (B.9)), we get with a normalisation factor $\hat{\Gamma} = \sqrt{\dim(\Gamma)}$:

$$\begin{aligned}\chi^1 = \sum_{\gamma_i,\gamma_i',i=1,\dots,8} \hat{\mathbf{3}}^4 \quad & D^{\Gamma_1}_{\gamma_1\gamma_1'}(U_1)\,\langle \mathbf{10};\Gamma_5\gamma_5\,\big|\Gamma_1\gamma_1'\rangle\, D^{\Gamma_5}_{\gamma_5\gamma_5'}(\mathbf{1})\,\big\langle \Gamma_5\gamma_5';\mathbf{10}\,|\Gamma_2\gamma_2\rangle \\ & D^{\Gamma_2}_{\gamma_2\gamma_2'}(U_2)\,\big\langle \Gamma_6\gamma_6';\Gamma_2\gamma_2'\,|\mathbf{10}\rangle\, D^{\Gamma_6}_{\gamma_6\gamma_6'}(\mathbf{1})\,\langle \mathbf{10};\Gamma_6\gamma_6\,\big|\Gamma_3\gamma_3'\big\rangle \\ & D^{\Gamma_3}_{\gamma_3\gamma_3'}(U_3)\,\langle \Gamma_3\gamma_3;\Gamma_7\gamma_7\,|\mathbf{10}\rangle\, D^{\Gamma_7}_{\gamma_7\gamma_7'}(\mathbf{1})\,\big\langle \Gamma_7\gamma_7';\Gamma_4\gamma_4'\,|\mathbf{10}\big\rangle \\ & D^{\Gamma_4}_{\gamma_4\gamma_4'}(U_4)\,\big\langle \Gamma_8\gamma_8';\mathbf{10}\,|\Gamma_4\gamma_4\big\rangle\, D^{\Gamma_8}_{\gamma_8\gamma_8'}(\mathbf{1})\,\langle \Gamma_1\gamma_1;\Gamma_8\gamma_8\,|\mathbf{10}\rangle\ , \\ & \text{where } \Gamma_1=\Gamma_5=\Gamma_2=\Gamma_7=\mathbf{3}\ ,\Gamma_6=\Gamma_3=\Gamma_4=\Gamma_8=\bar{\mathbf{3}}\,,\end{aligned}$$

which in graphical notation reads:

$$\chi^1 \;=\; \hat{\mathbf{3}}^4$$

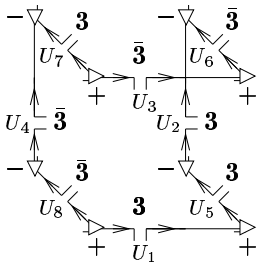

$$=$$

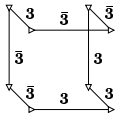

. (2.3)

For the IRs on the new intermediate link on the net we have that $D^{\Gamma}_{\gamma\gamma'}(\mathbf{1}) = \delta_{\gamma\gamma'}$ and $\Gamma = \bar{\mathbf{3}}$ is the conjugate IR of the fundamental IR of SU(3). It appears as we need the coupling $\mathbf{3}\otimes\bar{\mathbf{3}}\to\mathbf{1}$ to the singlet. For the outer multiplicity on the vertices we have here $n=1$ and therefore we omit it as well as the trivial links carrying the singlet IR $\Gamma=\mathbf{1}$.

We thus see that the plaquette function and also the other basis elements χ^α are determined by a set of IRs $\{\Gamma_l\}$ on the links l of the net. This we call a pattern of IRs. In order to simplify matters we sometimes reduce the graphical notation as on the right in eq. (2.3): The normalisation factor $\hat{\mathbf{3}}^4$ is tacitly implied.

Now with the plaquette function on the net we have the basic building block for the other loop space basis elements.

2.2 Recipe for the construction of the basis

The loop space basis χ is constructed in two steps. In the first step, subspaces are generated from geometrically inequivalent plaquette products. The second step is the construction of an orthogonal basis system in these subspaces.

We will start with the geometrical considerations.

2.2.1 Geometrical subspaces

At first the plaquette function χ^1 is assigned to a function $\Lambda^{1,1}$ corresponding to the geometrical plaquette on the spatial lattice:

$\Lambda^{1,1} =$ 

Using $\Lambda^{1,1}$ we built general geometrical functions $\Lambda^{\delta,k}$. They are given by linked, standardised δ-fold plaquette products of the type

$$\Lambda^{\delta,k} = \Lambda^{1,1}\ T_{\mathbf{a}_2(k)}T(R_2(k))\Lambda^{1,1} \dots\ T_{\mathbf{a}_\delta(k)}T(R_\delta(k))\Lambda^{1,1}\ ,\ \ k = 1, \dots, n_\delta\ ,$$

where $\mathbf{a}_\lambda(k) \in G_{lt}$ and $R_\lambda(k) \in G_{lr}$, $\lambda = 2, \dots \delta$ are suitable translations and rotations on the lattice. This means we look for all possible linked plaquette products up to a number δ, which defines the order of the subspace. The number k characterises the different, geometrically independent possibilities for building plaquette products of the same order. The total number of k is called n_δ. The functions $\Lambda^{\delta,k}$ generate the geometrical subspaces mentioned above. We denote them with $H^{\delta,k}$.

For completeness we assign the constant basis element χ^0 to the geometrical function $\Lambda^{0,1} = \mathbb{1}$, which spans the subspace $H^{0,1}$.

The $\Lambda^{\delta,k}$ are characterised by simple loop patterns, which are shown up to the order $\delta = 3$ in table 2.1. These results have already been shown in ref. [64].

In higher orders we get

$$\begin{aligned}
\delta = 4 &\ \rightarrow\ n_\delta = 84 \\
\delta = 5 &\ \rightarrow\ n_\delta = 582 \\
\delta = 6 &\ \rightarrow\ n_\delta = 4716 \\
\delta = 7 &\ \rightarrow\ n_\delta = 38628\,.
\end{aligned}$$

To choose a unique set of the $\Lambda^{\delta,k}$ in ref. [64] a standardisation scheme was defined for the geometrical subspaces, which also considers the lattice symmetries:

First a bounding box is defined, which is the smallest rectangle enclosing the $\Lambda^{\delta,k}$. This box has to be aligned, i.e. we define a coordinate system such that all coordinates of the box are positive and the box itself touches the axes. This fixes the properties of the subspaces with respect to translations. Then we require, that the extensions s_x and s_y of the bounding box fulfil $s_x \leq s_y$. Here x and y denote the two directions of the two-dimensional lattice. If after rotations (and a translation back into the box) more than one position of a $\Lambda^{\delta,k}$ fulfils these criteria, a characteristic number is created for each position from the coordinates of the $\Lambda^{\delta,k}$, considering the coordinates of all geometrical plaquettes the function is built of, and the position with the smallest number is chosen.

Table 2.1: The loop patterns of the geometrical functions $\Lambda^{\delta,k}$ up to the order $\delta = 3$.

order δ	$\Lambda^{\delta,k}$			n_δ
0	$\Lambda^{0,1}=\mathbb{1}$			1
1	$\Lambda^{1,1}=$ 			1
2	$\Lambda^{2,1}=$ 	$\Lambda^{2,2}=$ 	$\Lambda^{2,3}=$ 	
	$\Lambda^{2,4}=$ 			4
3	$\Lambda^{3,1}=$ 	$\Lambda^{3,2}=$ 	$\Lambda^{3,3}=$ 	
	$\Lambda^{3,4}=$ 	$\Lambda^{3,5}=$ 	$\Lambda^{3,6}=$ 	
	$\Lambda^{3,7}=$ 	$\Lambda^{3,8}=$ 	$\Lambda^{3,9}=$ 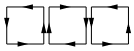	
	$\Lambda^{3,10}=$ 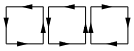	$\Lambda^{3,11}=$ 	$\Lambda^{3,12}=$ 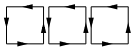	12

Consequently we can distinguish the different geometrical functions $\Lambda^{\delta,k}$. Of course the operation that transforms to a standard position is unique only up to the symmetries of the function under rotation and translation.

Now in the geometrical subspaces $H^{\delta,k}$ we can built up the loop space basis χ.

2.2.2 SU(3) coupling

In this section we point out the major issues in constructing the basis in the subspaces. As an example the subspaces $H^{\delta,k}$ with functions $\Lambda^{\delta,k}$ up to the second order $\delta = 2$ are given explicitly.

In the first two subspaces we have the two first basis elements per definition, the identity χ^0 on the lattice and the plaquette function χ^1:

$$\begin{aligned} H^{0,1} &: \chi^0 \\ H^{1,1} &: \chi^1 . \end{aligned}$$

Therefore we start with the construction of the new basis elements in subspace $H^{2,1}$ and we build them of products of the plaquette function in the way the subspace contains the geometrical plaquettes. In $H^{2,1}$, that consists of the geometrical function

$$\Lambda^{2,1} = \text{  },$$

we have to multiply two plaquette function at the same position

$\chi^1 \otimes \chi^1 =$ 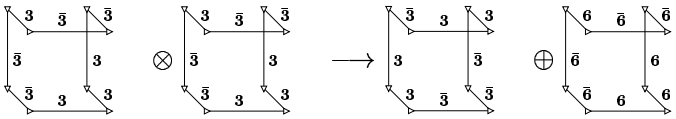 .

The multiplication rules are SU(3) coupling rules (i.e. the Clebsch-Gordan series). The multiplicity n_3 of a coupling

$$\Gamma^1 \otimes \Gamma^2 \longrightarrow \Gamma^3_{n_3}$$

is determined by a multiplicity formula given in ref. [65] based on that of ref. [49]. As we just want to select the new basis elements, the general rules containing the correct phases and factors when multiplying basis elements are not needed here. The correct coefficients are important for the coupled cluster matrix element (see appendix A) and therefore determined at the end of this chapter (see eq. (2.19) and eq. (2.20)).

The multiplicity formula for the subspace under consideration gives:

$$(\Gamma^1 = \mathbf{3}) \otimes (\Gamma^2 = \mathbf{3}) \quad \longrightarrow \quad (\Gamma^3_{n_3} = \bar{\mathbf{3}}_1) \oplus (\Gamma^3_{n_3} = \mathbf{6}_1)\,.$$

As we will show below the first part of the result

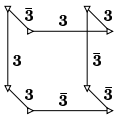 $= T_C \chi^1$ (2.4)

depends on χ^1 via charge conjugation T_C and in this sense is no new basis element, because we demand the basis to be linear independent under symmetry transformations on the lattice (see eq. (1.21)). Thus in the subspace

$H^{2,1} \quad : \quad \chi^2 =$ 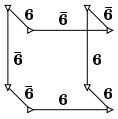

we have only one new basis element. The normalisation will be computed in the next section.

As we have seen we need to know how a symmetry transformation acts on a basis element. On the lattice we have translations $t_{\mathbf{a}} \in G_{lt}$, rotation/reflections $R \in G_{lr}$ and charge conjugation T_C. These symmetry groups will be discussed in detail in chapter 3. The general rules for the symmetry operations on the basis containing the correct phase factors are given in section 2.3.4. For our selection of the χ^α the phases are not needed.

Charge conjugation implies a complex conjugation of the basis element (see eq. (2.11)), and for the IR on the link this implies $\Gamma \to \bar{\Gamma}$ as we will see below. Thus the charge conjugated plaquette function is given by eq. (2.4). An example of the role of charge conjugation is found in subspace $H^{2,2}$ containing the geometrical element

$\Lambda^{2,2} =$  .

The geometrical aspect of complex conjugation of a basis element is changing the direction of the links it contains (see eq. (2.12) below). Thus we have to multiply the plaquette function by the charge conjugated plaquette function of eq. (2.4):

$\chi^1 \otimes T_C \chi^1 =$ 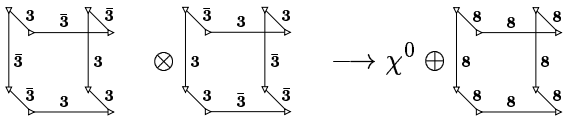 $\longrightarrow \chi^0 \oplus$.

The corresponding SU(3) coupling used here is $\mathbf{3} \otimes \bar{\mathbf{3}} \longrightarrow \mathbf{1} \oplus \mathbf{8}$ and we find that

$H^{2,2} \quad : \quad \chi^3 =$ 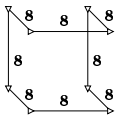

contains one new basis element.

Of course the operation of translation implies just moving the IRs on the lattice (see eq. (2.17) below). An example of translation and charge conjugation is found in subspace $H^{2,3}$ containing the geometrical function

$\Lambda^{2,3} =$  .

We have to multiply the plaquette function by the charge conjugated plaquette function translated by 1 in the x-direction:

$\chi^1 \otimes T_{\mathbf{a}=\binom{1}{0}} T_C \chi^1 \quad =$ 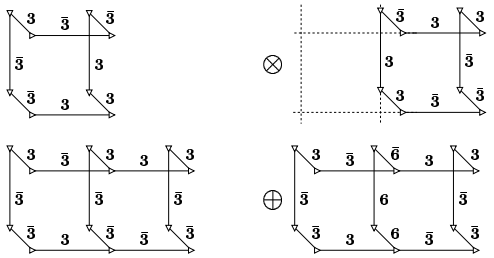

$\longrightarrow$

,

and we find that

$H^{2,3} \quad : \quad \chi^4 =$ 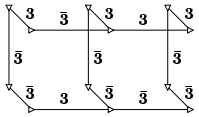 , $\chi^5 =$ 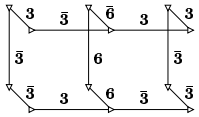

contains two new basis elements. To complete the second order we give here in addition subspace $H^{2,4}$, which contains

$\Lambda^{2,5} =$  ,

and thus we have to multiply the plaquette function with the plaquette function translated by 1 in x-direction and we get:

$H^{2,4} \quad : \quad \chi^6 =$ 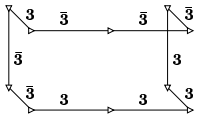 , $\chi^7 =$ 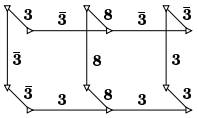 .

Going on with the SU(3) coupling in the subspaces we get up to the third order $\delta = 3$ the number of basis elements $n_{H^{\delta,k}}$ in the subspaces given in table 2.2. Altogether we find 51 basis elements up to the third order. They are graphically presented in the next section.

To avoid double counting and to ensure that the basis χ is independent with respect to symmetry transformations on the lattice (see eq. (1.21)), also here we have to define a standardisation scheme. This will be done in analogy to the standardisation of the geometrical functions $\Lambda^{\delta,k}$ of the previous section, which already takes care of the lattice symmetries. With a bounding box the basis element is brought to a standard form. To distinguish basis elements with the same box a characteristic number is created by the

Table 2.2: Number $n_{H^{\delta,k}}$ of basis elements in the subspaces $H^{\delta,k}$ up to third order.

δ	$H^{\delta,k}$	$n_{H^{\delta,k}}$	$H^{\delta,k}$	$n_{H^{\delta,k}}$	$H^{\delta,k}$	$n_{H^{\delta,k}}$	$H^{\delta,k}$	$n_{H^{\delta,k}}$	$H^{\delta,k}$	$n_{H^{\delta,k}}$
0	$H^{0,1}$:	1								
1	$H^{1,1}$:	1								
2	$H^{2,1}$:	1	$H^{2,2}$:	1	$H^{2,3}$:	2	$H^{2,4}$:	2		
3	$H^{3,1}$:	1	$H^{3,2}$:	1	$H^{3,3}$:	2	$H^{3,4}$:	2	$H^{3,5}$:	3
	$H^{3,6}$:	6	$H^{3,7}$:	6	$H^{3,8}$:	6	$H^{3,9}$:	3	$H^{3,10}$:	4
	$H^{3,11}$:	6	$H^{3,12}$:	3						

following process: We number the links of the element and after a symmetry transformation we demand the link with a smaller number to have an IR with a higher dimension. An IR precedes its conjugated one.

Up to now we have given many examples of the construction of the basis, but none contained a multiplicity $n > 1$ on a vertex. The reason for this is that basis elements with multiplicity occur at first in the fourth order $\delta = 4$. To show how we handle multiplicities we give an example of the fourth order:

Here we have a subspace $H^{4,49}$ with the geometrical function

$\Lambda^{4,49} =$  .

Starting in the third order with the geometrical function

$\Lambda^{3,5} =$ 

we get the following subspace with standardised basis elements

$H^{3,5}$: $\chi^{14} =$ 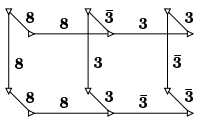 , $\chi^{15} =$ 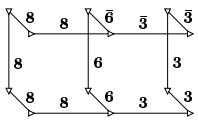 , $\chi^{16} =$ 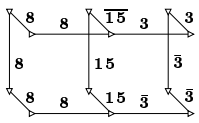 .

Going in the fourth order to subspace $H^{4,49}$ we have to multiply these basis elements in

the third order by the translated plaquette function. If we take for example χ^{14} we get:

$\chi^{14} \otimes T_{\mathbf{a}=\binom{1}{0}} \chi^1$ =

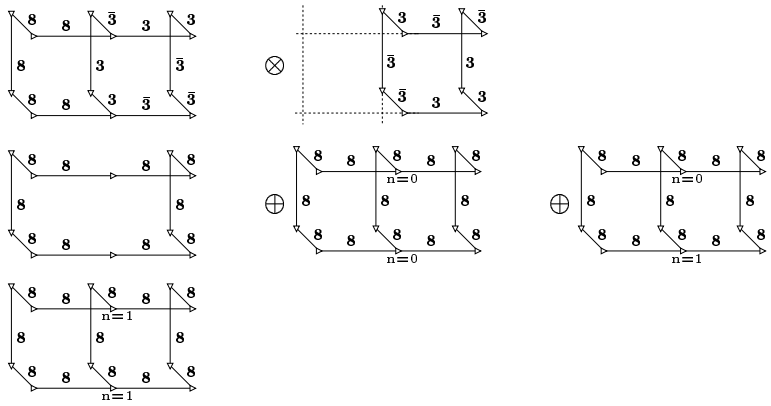

$$= \chi^{211} \oplus \chi^{212} \oplus \chi^{213} \oplus \chi^{214} .$$

Here we have used the coupling $\mathbf{8} \otimes \mathbf{8} \to \mathbf{8}_1 \oplus \mathbf{8}_2 \oplus \ldots$. We distinguish three basis elements $\chi^{212}, \chi^{213}, \chi^{214}$ with the same IRs on the links, but with different multiplicity indices on the vertices.

Checking this together with the standardisation is the way we identify a basis element as a new one.

We have to mention that with this construction of the basis, still there are some basis elements missing. We see this if we try to expand products of basis elements again in the basis. This problem is cured by multiplying all basis elements, again using the multiplicity formula discussed above and adding the newly appearing elements to the basis.

2.2.3 Basis up to third order

We give here the basis elements up to third order $\delta = 3$ in graphical notation.

1

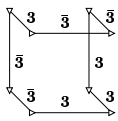
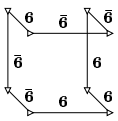
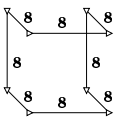
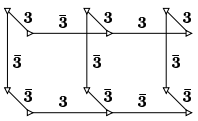

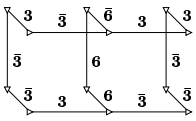
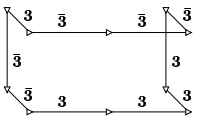
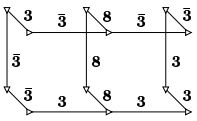
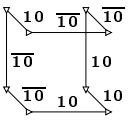
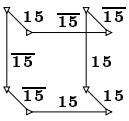

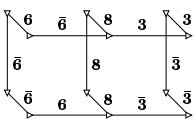
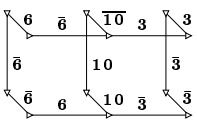
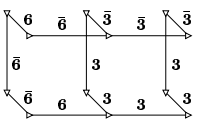
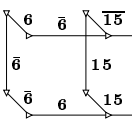
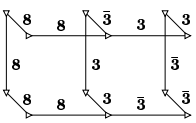

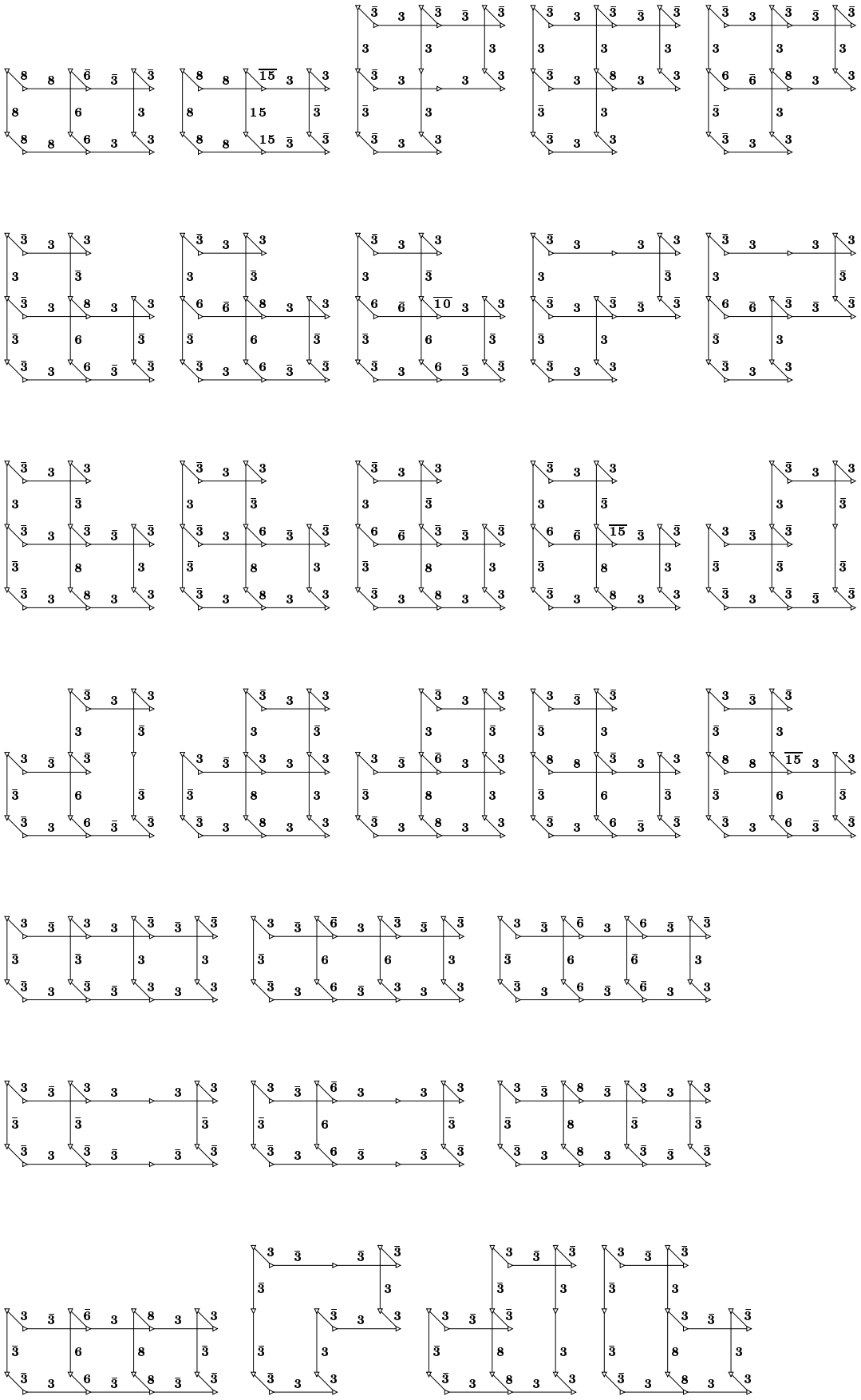

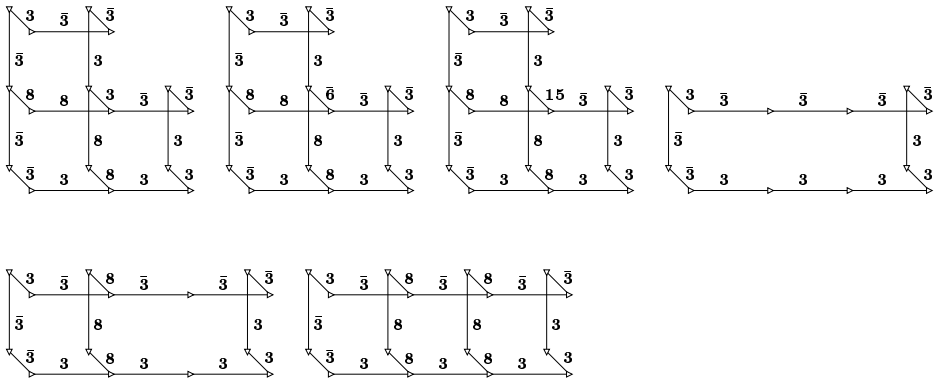

We thus have one basis element in the zeroth order, two basis elements up to the first order, eight basis elements up to the second order and fifty-one basis elements in the third order.

For higher orders the number of basis elements is shown in table 2.3.

Table 2.3: Number of basis elements n_{χ^α} up to sixth order.

order δ	1	2	3	4	5	6
number of basis elements n_{χ^α}	2	8	51	821	17012	379226

2.3 Properties of the basis

Now as we have constructed the loop space basis we will check whether it satisfies the requirements listed in section 1.2.1.

2.3.1 Gauge invariant and localised basis

The basis elements are built from products of the plaquette function and, because the plaquette corresponds to the trace over the smallest closed loop on the lattice, they also belong to the loop space of gauge invariant functions. We therefore have called this basis the loop space basis.

That the basis elements are localised is guaranteed by their construction via linked products and by the standardisation scheme described in the previous section.

2.3.2 Strong coupling basis

In the strong coupling limit $g \to \infty$, where the Kogut-Susskind Hamiltonian has the form $H \to \sum_{l,a} E_l^a E_l^a$, we have

$$\sum_{l,a} E_l^a E_l^a \chi^\alpha = \epsilon_\alpha \chi^\alpha \,. \tag{2.5}$$

Here ϵ_α is given by the eigenvalue of the Casimir operator (see eq. (B.1)) on every link l of the basis function (excluding intermediate links):

$$\epsilon_\alpha = \sum_{l \text{ not intermediate}} \epsilon(\Gamma_l) \,. \tag{2.6}$$

Γ_l is the IR on the link l of χ^α. Thus the basis consists of strong coupling eigenfunctions.

2.3.3 Normalisation

For the plaquette function we have a normalisation factor of $\hat{\mathbf{3}}^4$:

$\chi^1 \;=\; \hat{\mathbf{3}}^4$

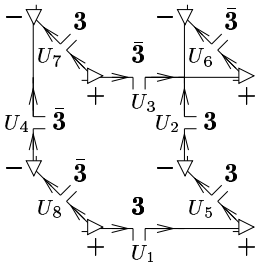

. (2.7)

To generalise this to the other basis elements we merely have to inspect a general site of a basis element:

site $=$

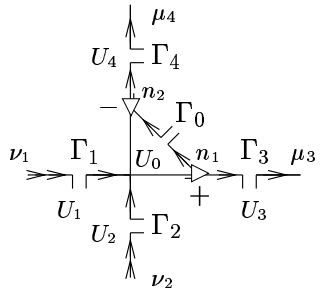

$$= \sum_{\substack{\mu_1,\,\nu_3,\,\nu_0 \\ \mu_0,\,\mu_2\,\nu_4}} D^{\Gamma_1}_{\nu_1\mu_1}(U_1)\,\langle \Gamma_3\nu_3;\Gamma_0\nu_0\,|\Gamma_1\mu_1\rangle_{n_1}\, D^{\Gamma_3}_{\nu_3\mu_3}(U_3) D^{\Gamma_0}_{\nu_0\mu_0}(U_0)$$
$$D^{\Gamma_2}_{\nu_2\mu_2}(U_2)\,\langle \Gamma_0\mu_0;\Gamma_2\mu_2\,|\Gamma_4\nu_4\rangle_{n_2}\, D^{\Gamma_4}_{\nu_4\mu_4}(U_4) \,. \tag{2.8}$$

Any basis element consisting of N_s sites is given by composing N_s general sites and summing over the indices ν_1, ν_2, μ_3 and μ_4 on the open links. We denote here a matrix element of the IR on the link l with ν at the incoming link and μ at the outgoing link by $D^\Gamma_{\nu\mu}(U_l)$.

With the normalisation of the IR of eq. (B.2) and of the CGC of eq. (B.6) we can check via integration with respect to the Haar measure of eq. (1.14), if a general site is normalised

and also orthogonal:

$$\langle \text{site}|\text{site}'\rangle = \int DU$$

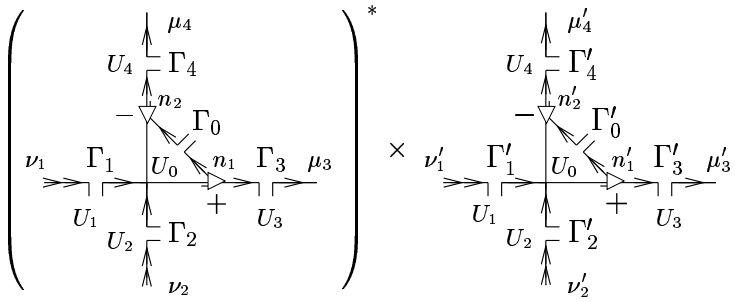

$$= \frac{1}{\hat{\Gamma}_0^2}\delta_{\Gamma_1\Gamma_1'}\delta_{\Gamma_2\Gamma_2'}\delta_{\Gamma_3\Gamma_3'}\delta_{\Gamma_4\Gamma_4'}\delta_{\Gamma_5\Gamma_5'}\delta_{n_1n_1'}\delta_{n_2n_2'}$$
$$\times\left(\delta_{\nu_1\nu_1'}\delta_{\nu_2\nu_2'}\delta_{\mu_3\mu_3'}\delta_{\mu_4\mu_4'}\frac{1}{\hat{\Gamma}_2^2}\frac{1}{\hat{\Gamma}_3^2}\right) \text{ factor on open links.}$$

The factors on the open links $\frac{1}{\hat{\Gamma}_2^2}$ and $\frac{1}{\hat{\Gamma}_3^2}$ will be absorbed in the composition of the site to a complete basis element and we are left with a factor $\frac{1}{\hat{\Gamma}_0^2}$. This means we have a factor $\frac{1}{\hat{\Gamma}_0}$ for the norm $||\text{site}||$ of the site, where Γ_0 is the IR on the intermediate link.

Thus in general each site contributes with a factor $\frac{1}{\hat{\Gamma}_i}$, where i denotes the intermediate link, to the norm of the basis element. By defining an appropriate normalisation, an orthogonal basis is obtained:

$$\langle\chi^\alpha|\chi^\beta\rangle = \langle\chi^{\{\Gamma_l\},\{n_v\}}|\chi^{\{\Gamma_l'\}\{n_v'\}}\rangle = \delta_{\{\Gamma_l\}\{\Gamma_l'\}}\delta_{\{n_v\}\{n_v'\}} = \delta_{\alpha\beta}\,,$$

where $\{\Gamma_l\}$ denotes the set of IRs on the lattice links l and $\{n_v\}$ the set of multiplicities on the vertices v the basis element depends on.

We see that for example the plaquette function consists four sites with an IR $\Gamma = \mathbf{3}$ on the intermediate link and accordingly we get a normalisation factor $\hat{\Gamma}^4 = \hat{\mathbf{3}}^4$.

2.3.4 Symmetry transformation of the basis

The linear independence under symmetry transformations (see eq. (1.21)) is guaranteed by the standardisation scheme defined above. No χ^α can be created from a different one by any such transformation. There are, however, nontrivial symmetry transformations which map χ^α on itself.

To classify these internal symmetries of a basis element, which will be done in chapter 3, we have to determine the right phase factors for the action of the symmetry transformations on the basis. This will be done here.

We define a translation $T_\mathbf{a}, t_\mathbf{a} \in G_{lt}$ on a basis element χ^α specified by a set of IRs $\{\Gamma_l\}$ on the links l via

$$T_\mathbf{a}\chi^\alpha(\{\Gamma_l\}) \;=\; p^\mathbf{a}\chi^\alpha(\{\Gamma_{l'}\})\,,\; t_\mathbf{a} : l \to l' = l - \mathbf{a}\,, \tag{2.9}$$

a reflection and rotation $T(R), R \in G_{lr}$ via

$$T(R)\chi^\alpha(\{\Gamma_l\}) \;=\; p^R\chi^\alpha(\{\Gamma_{l'}\})\,,\; l' = R^{-1}l\,, \tag{2.10}$$

and the operation of charge conjugation T_C via

$$T_C\chi^\alpha(\{\Gamma_l\}) \quad = \quad (\chi^\alpha(\{\Gamma_l\}))^* = p^C\chi^\alpha(\{\bar{\Gamma}_l\})\,, \tag{2.11}$$

where $\bar{\Gamma}$ is the IR conjugate to Γ. The phase factors $p^{\mathbf{a}}, p^R$ and p^C will now be determined separately for the three symmetry transformations.

Charge conjugation

Following ref. [7] we have defined the operation of charge conjugation T_C by complex conjugation of the basis element. For the IRs of SU(3) we get (see eq. B.4):

$$(D^\Gamma_{\nu\mu})^*(U) \quad = D^\Gamma_{\mu\nu}(U^{-1}) \quad \propto D^{\bar{\Gamma}}_{\bar{\nu}\bar{\mu}}(U) \tag{2.12}$$

$$\Big(\ \nu \xrightarrow[U]{\Gamma} \mu\ \Big)^* \qquad \propto \qquad \bar{\nu} \xrightarrow[U]{\bar{\Gamma}} \bar{\mu} \quad .$$

Again considering the graphical notation of a general site of a basis element as in eq. (2.8), omitting here the $U_0, \ldots, U_4$ as they will not change their position, charge conjugation involves the following:

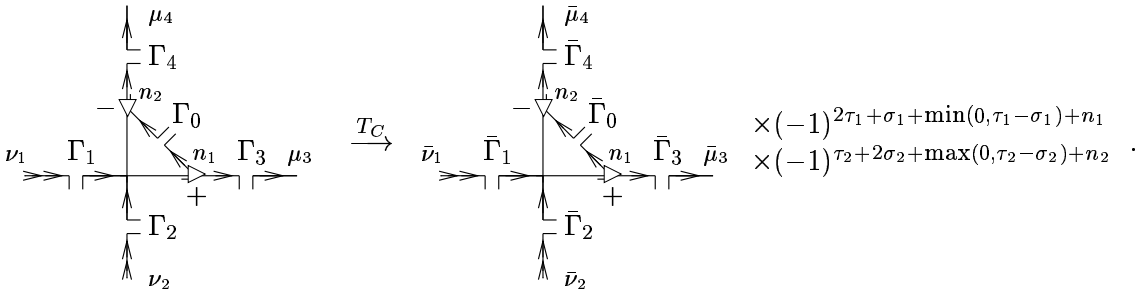

The phases we get depend on the three IRs, say Γ_1, Γ_2 and Γ_3 with multiplicity n, coupling at a vertex v of the general site. This is encoded in the τ and σ, which are given as in eq. (B.8):

$$\tau := \frac{1}{3}(p_1 + p_2 - p_3); \qquad \sigma := \frac{1}{3}(q_1 + q_2 - q_3)\,.$$

Here we have $\Gamma_1 = (p_1, q_1), \Gamma_2 = (p_2, q_2)$ and $\Gamma_3 = (p_3, q_3)$. Thus at a vertex we get a phase factor $p^C = p^C_{(\tau_v, \sigma_v, n_v)}$.

In composing the general site to a basis element χ^α under charge conjugation we have to conjugate the IRs on the links and multiply the elements by the phase factors on the vertices:

$$T_C\chi^\alpha(\{\Gamma_l\}) = \chi^\alpha(\{\bar{\Gamma}_l\}) \prod_v p^C_{(\tau^\alpha_v, \sigma^\alpha_v, n^\alpha_v)} \tag{2.13}$$

We have to mention that at the site shown above we omit phases on the outer links, as they cancel when the site is composed to a complete basis element.

Rotation and reflection

Concerning rotations and reflections we proceed as we did for charge conjugation. We determine how a rotation and a reflection act on a general site and thus infer the general rule for the transformation of a basis element. In chapter 3 we will see that the group G_{lr} of rotations and reflections has eight elements in $D = 2$ space dimensions and accordingly we have eight transformations acting on the loop space basis:

$$\begin{array}{lcllcl} T_0 &=& T(R(0)) & T_4 &=& T(I) \\ T_1 &=& T(IR(\frac{3\pi}{2}))) & T_5 &=& T(R(\frac{3\pi}{2})) \\ T_2 &=& T(IR(\frac{\pi}{2})) & T_6 &=& T(R(\frac{\pi}{2})) \\ T_3 &=& T(R(\pi)) & T_7 &=& T(IR(\pi))\,. \end{array} \tag{2.14}$$

Here the rotations are denoted with $R(\theta)$ with the rotation angle θ and I is the reflection that swaps the x and the y axis. For a general site we get:

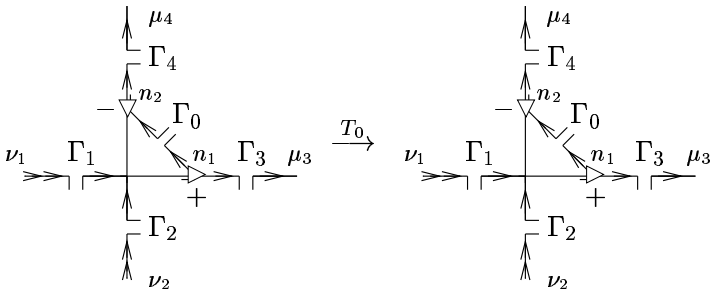

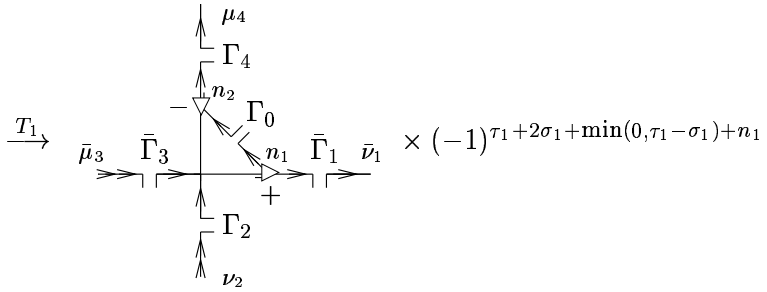

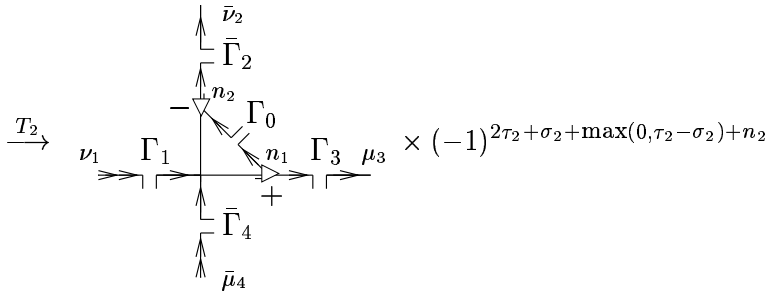

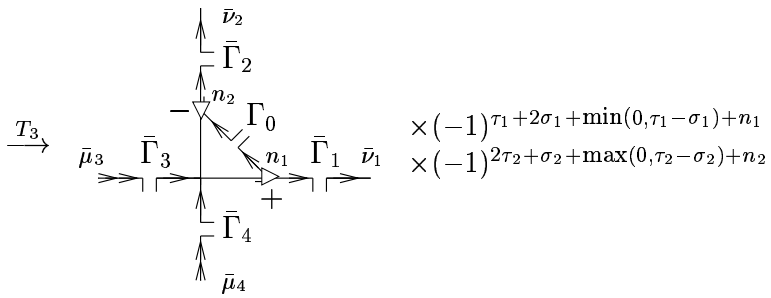

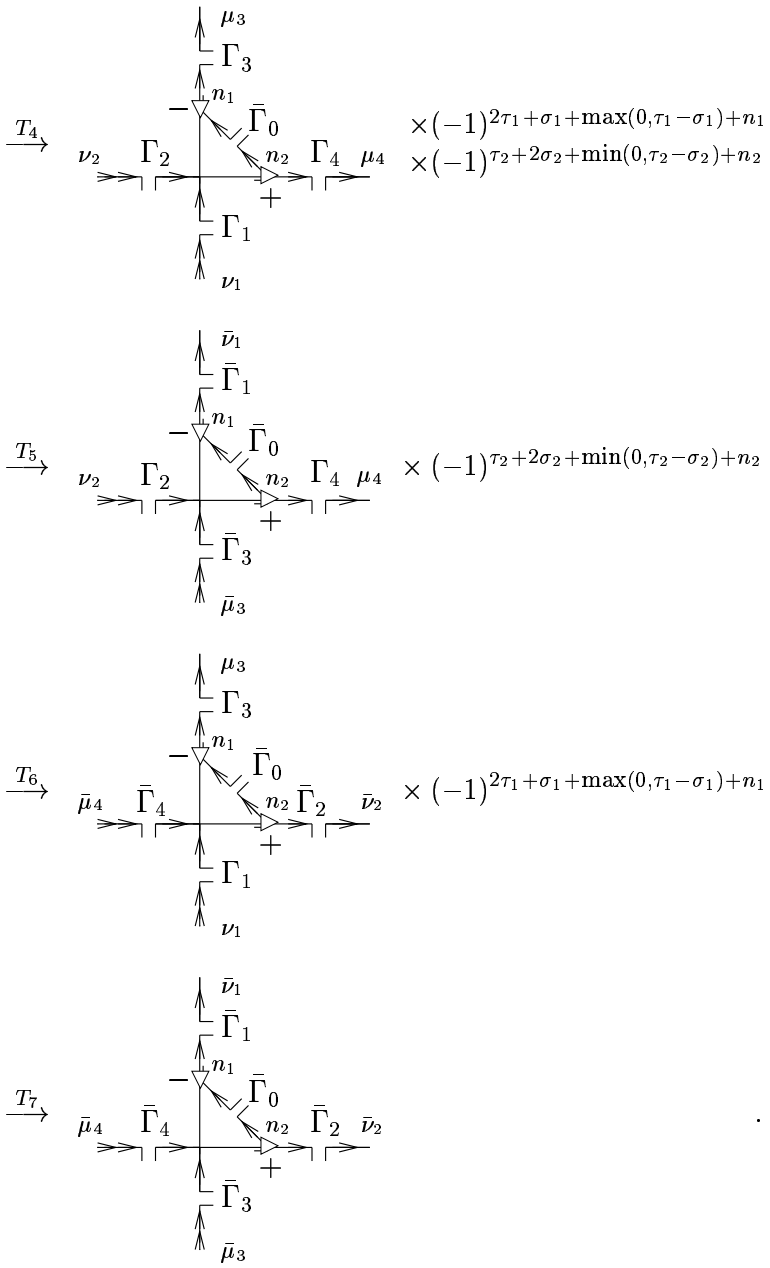

This implies a phase factor p^R for every vertex v of a basis element and we get:

$$T(R)\chi^\alpha(\{\Gamma_l\}) = \chi^\alpha(\{\Gamma_{R^{-1}l}\}) \prod_v p^R_{(\tau_v^\alpha,\sigma_v^\alpha,n_v^\alpha)} \,. \tag{2.15}$$

If the rotation or reflection changes the direction of the link $l \to l^{-1}$ the IR on the link l has to be conjugated $\Gamma_l \to \bar{\Gamma}_l$ because of the property of the IR of eq. (B.4):

$$D^\Gamma_{\nu\mu}(U_{l^{-1}}) = D^\Gamma_{\nu\mu}(U_l^{-1}) \propto D^{\bar{\Gamma}}_{\bar{\mu}\bar{\nu}}(U_l) \,.$$

Again the phase factors on the open links of a general site will cancel, if we compose sites to a basis element and therefore we omit them.

Rotation/reflections commute with charge conjugation, thus:

$$[T_C, T_i] = 0 \,, \tag{2.16}$$

where the $T_i, i = 0, \ldots, 7$ are defined as in eq. (2.14).

Translation

Under translations there is no phase factor and we just get:

$$T_{\mathbf{a}}\chi^{\alpha}(\{\Gamma_l\}) = \chi^{\alpha}(\{\Gamma_{l-\mathbf{a}}\})\,. \tag{2.17}$$

Also translations commute with charge conjugation:

$$[T_C, T_{\mathbf{a}}] = 0 \tag{2.18}$$

2.3.5 Product of basis elements

To solve the coupled cluster equations (see eq. (1.26) and eq. (1.27)) we need to determine the coupled cluster matrix elements. This will be done in appendix A. It contains the correct coefficient when multiplying two basis elements of the basis η. As η is the loop space basis χ reordered with respect to the symmetries of the lattice (see eq. (1.18) and eq. (1.19)), we need for the calculation of the coupled cluster matrix element the correct coefficients when multiplying two basis elements of χ. These coefficients, which we call c-coefficients, are defined via:

$$\sum_{\substack{t_{\mathbf{a}_3}\in G_{lt},\\ R_3\in G_{lr}}} \sum_{\alpha_3} c^{\alpha_1\alpha_2}_{\alpha_3,\mathbf{a}_2,\mathbf{a}_3,R_2,R_3} T_{\mathbf{a}_3} T(R_3)\Pi_C^{\pm}\chi^{\alpha_3} = \chi^{\alpha_1} T_{\mathbf{a}_2} T(R_2)\chi^{\alpha_2}\,, \tag{2.19}$$

$$\sum_{\substack{t_{\mathbf{a}_3}\in G_{lt},\\ R_3\in G_{lr}}} \sum_{\alpha_3} c^{\bar{\alpha}_1\alpha_2}_{\alpha_3,\mathbf{a}_2,\mathbf{a}_3,R_2,R_3} T_{\mathbf{a}_3} T(R_3)\Pi_C^{\pm}\chi^{\alpha_3} = (T_C\chi^{\alpha_1}) T_{\mathbf{a}_2} T(R_2)\chi^{\alpha_2}\,. \tag{2.20}$$

The operator $\Pi_C^{\pm} = \frac{1}{2}(1 \pm T_C)$ is the projection operator on states with definite charge parity.

The phases with respect to symmetry transformations of the basis elements given in the last section imply:

$$\begin{aligned} \chi^{\alpha_1} T_{\mathbf{a}_2} T(R_2)\chi^{\alpha_2} &= \chi^{\alpha_1}\chi^{\alpha_2'} \prod_v p^{R_2}_{(\tau_v^{\alpha_2},\sigma_v^{\alpha_2},n_v^{\alpha_2})} \\ T_C\chi^{\alpha_1} T_{\mathbf{a}_2} T(R_2)\chi^{\alpha_2} &= \chi^{\bar{\alpha}_1}\chi^{\alpha_2'} \prod_v p^{C}_{(\tau_v^{\alpha_1},\sigma_v^{\alpha_1},n_v^{\alpha_1})} p^{R_2}_{(\tau_v^{\alpha_2},\sigma_v^{\alpha_2},n_v^{\alpha_2})} \end{aligned}$$

Here α' denotes the rotated and translated set of IRs of the basis element labelled by α and $\bar{\alpha}$ the corresponding conjugated IRs (see eq. (2.17), eq. (2.15) and eq. (2.13)).

We determine the c-coefficients for general basis elements again by inspecting a general

site as in eq. (2.8). Multiplication of two sites gives:

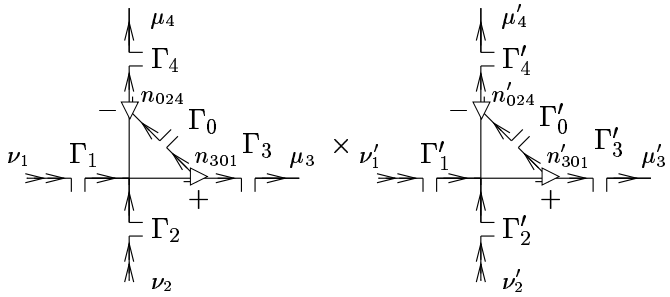

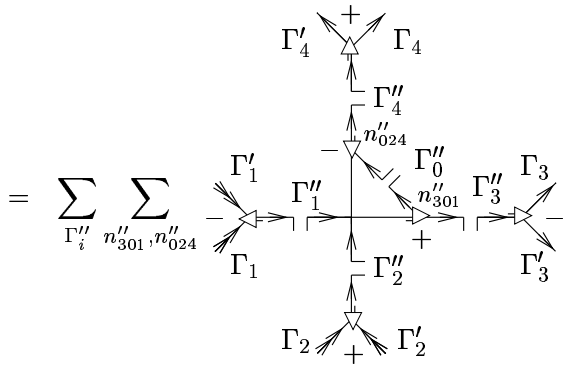

$$\times \sum_{n_1,n_3,n_2,n_4,n_0} X \begin{pmatrix} \Gamma_3 & \Gamma'_3 & \Gamma''_{3,n_3} \\ \Gamma_0 & \Gamma'_0 & \Gamma''_{0,n_0} \\ \Gamma_{1,n_{301}} & \Gamma'_{1,n'_{301}} & \Gamma''_{1,n''_{301},n_1} \end{pmatrix} X \begin{pmatrix} \Gamma_0 & \Gamma'_0 & \Gamma''_{0,n_0} \\ \Gamma_2 & \Gamma'_2 & \Gamma''_{2,n_2} \\ \Gamma_{4,n_{024}} & \Gamma'_{4,n'_{024}} & \Gamma''_{4,n''_{024},n_4} \end{pmatrix} .$$

In eq. (B.10) the $X9\Gamma$-symbols, the SU(3) analogues to the usual SU(2)-$9j$ symbols, are defined. They are recoupling coefficients involving nine IRs. The multiplicities n_l, $l = 1,\ldots,4$ are obtained by the coupling

$$\Gamma_i \otimes \Gamma'_i \to \Gamma''_{i,n_i}$$

on the lattice links. If we denote the three links at a general vertex v by l_v^1, l_v^2, l_v^3 and the corresponding multiplicities on these links by n_{l^1}, n_{l^2} and n_{l^1} and on the vertex by n_v, we get the following rule for the product of two basis elements:

$$\begin{aligned} \chi^{\alpha_1}\chi^{\alpha_2} \;=\; & \sum_{\substack{t_{\mathbf{a}_3}\in G_{lt},\\ R_3\in G_{lr}}} \sum_{\alpha_3} T_{\mathbf{a}_3} T(R_3) \chi^{\alpha_3} \\ & \times \sum_{n_{l^1},n_{l^2},n_{l^3}} \prod_v p^{R_3}_{(\tau_v^{\alpha_3},\sigma_v^{\alpha_3},n_v^{\alpha_3})} X \begin{pmatrix} \Gamma^{\alpha_1}_{l_v^1} & \Gamma^{\alpha_2}_{l_v^1} & \Gamma^{\alpha_3}_{l_v^1,n_{l^1}} \\ \Gamma^{\alpha_1}_{l_v^2} & \Gamma^{\alpha_2}_{l_v^2} & \Gamma^{\alpha_3}_{l_v^2,n_{l^2}} \\ \Gamma^{\alpha_1}_{l_v^3,n_v^{\alpha_1}} & \Gamma^{\alpha_2}_{l_v^3,n_v^{\alpha_2}} & \Gamma^{\alpha_3}_{l_v^3,n_v^{\alpha_3},n_{l^3}} \end{pmatrix} . \end{aligned}$$

The translation $T_{\mathbf{a}_3}$ and rotation $T(R_3)$ account for the correct standardisation of the basis element χ^{α_3}.

The c-coefficients are then given as:

$$
\begin{aligned}
c^{\alpha_1\,\alpha_2}_{\alpha_3,\mathbf{a}_2,\mathbf{a}_3,R_2,R_3} &= \sum_{n_{l^1},n_{l^2},n_{l^3}} \prod_v p^{R_2}_{(\tau_v^{\alpha_2},\sigma_v^{\alpha_2},n_v^{\alpha_2})} p^{R_3}_{(\tau_v^{\alpha_3},\sigma_v^{\alpha_3},n_v^{\alpha_3})} \\
&\quad \times X \begin{pmatrix} \Gamma^{\alpha_1}_{l_v^1} & \Gamma^{\alpha_2'}_{l_v^1} & \Gamma^{\alpha_3}_{l_v^1,n_{l^1}} \\ \Gamma^{\alpha_1}_{l_v^2} & \Gamma^{\alpha_2'}_{l_v^2} & \Gamma^{\alpha_3}_{l_v^2,n_{l^2}} \\ \Gamma^{\alpha_1}_{l_v^3,n_v^{\alpha_1}} & \Gamma^{\alpha_2'}_{l_v^3,n_v^{\alpha_2'}} & \Gamma^{\alpha_3}_{l_v^3,n_v^{\alpha_3},n_{l^3}} \end{pmatrix} \qquad (2.21) \\
c^{\bar{\alpha}_1\,\alpha_2}_{\alpha_3,\mathbf{a}_2,\mathbf{a}_3,R_2,R_3} &= \sum_{n_{l^1},n_{l^2},n_{l^3}} \prod_v p^{c}_{(\tau_v^{\bar{\alpha}_1},\sigma_v^{\bar{\alpha}_1},n_v^{\bar{\alpha}_1})} p^{R_2}_{(\tau_v^{\alpha_2'},\sigma_v^{\alpha_2'},n_v^{\alpha_2'})} p^{R_3}_{(\tau_v^{\alpha_3},\sigma_v^{\alpha_3},n_v^{\alpha_3})} \\
&\quad \times X \begin{pmatrix} \bar{\Gamma}^{\alpha_1}_{l_v^1} & \Gamma^{\alpha_2'}_{l_v^1} & \Gamma^{\alpha_3}_{l_v^1,n_{l^1}} \\ \bar{\Gamma}^{\alpha_1}_{l_v^2} & \Gamma^{\alpha_2'}_{l_v^2} & \Gamma^{\alpha_3}_{l_v^2,n_{l^2}} \\ \bar{\Gamma}^{\alpha_1}_{l_v^3,n_v^{\alpha_1}} & \Gamma^{\alpha_2'}_{l_v^3,n_v^{\alpha_2'}} & \Gamma^{\alpha_3}_{l_v^3,n_v^{\alpha_3},n_{l^3}} \end{pmatrix} . \qquad (2.22)
\end{aligned}
$$

Here α_2' refers to IRs of the basis element χ^{α_2} rotated by $T(R_2)$ and translated by $T_{\mathbf{a}_2}$ and as the basis element χ^{α_1} is charge conjugated for the second c-coefficient the corresponding IRs have to be conjugated $\bar{\Gamma}^{\alpha_1}$.

Concluding remark

At the end of this chapter we can state that the loop space basis χ fulfils all the requirements stated in chapter 1 and we are able to multiply two basis elements. Thus we can now construct the elements of the basis η of eq. (1.18) and eq. (1.19) which, in addition are eigenstates of the lattice symmetry operations.

Chapter 3 Symmetries on the lattice

In this chapter we will discuss the symmetries on the lattice, i.e. the translational symmetry, the symmetry under rotation and reflection and charge conjugation. They are taken into account via projection operators acting on the loop space basis χ to obtain a basis η, which has the correct symmetry. In chapter 2 the loop space basis χ has been constructed to be linear independent under symmetry transformations. There are however internal symmetries, which map a basis element on itself. The treatment of these internal symmetries will be presented at the end of this chapter and we will get a prescription how to construct an orthonormal basis η.

3.1 Lattice translations

The elements $t_{\mathbf{a}}$ of the lattice translation group G_{lt} on a two-dimensional lattice with space points $\mathbf{x}$ are given by the prescription

$$t_{\mathbf{a}} : \mathbf{x} \to \mathbf{x} + \mathbf{a}. \tag{3.1}$$

These translations should leave the (infinite) lattice invariant. Thus for the translation vector

$$\mathbf{a} = a_1\mathbf{e}_1 + a_2\mathbf{e}_2\,, \text{ with } \mathbf{e}_1 = \begin{pmatrix}1\\0\end{pmatrix} \text{ and } \mathbf{e}_2 = \begin{pmatrix}0\\1\end{pmatrix},$$

the numbers a_1 and a_2 have to be integers, as on the lattice all distances are measured in units of the lattice spacing. Note that the lattice spacing is denoted with 'a' and the translation vector with '$\mathbf{a}$'.

As given in eq. (2.17) the group G_{lt} acts on the loop space basis χ as follows:

$$T_{\mathbf{a}}\chi^{\alpha}(\{\Gamma_l\}) = \chi^{\alpha}(\{\Gamma_{l-\mathbf{a}}\})\,. \tag{3.2}$$

With $\{\Gamma_l\}$ we denote the set of irreducible representations (IRs) of SU(3) on the links l the basis elements χ^{α} depends on. The translation of the links $l \to l - \mathbf{a}$, which are straight paths from one lattice point to the neighbouring point, is given by shifting these two points via eq. (3.1).

Generally spatial translations are generated by the momentum operator. Thus the projection operator for momentum $\mathbf{p}$ is given by

$$\Pi^{\mathbf{p}} = \sum_{t_{\mathbf{a}} \in G_{lt}} \mathrm{e}^{i\mathbf{p}\mathbf{a}}\, T_{\mathbf{a}}\,.$$

In this thesis we only consider (lattice) momentum $\mathbf{p} = 0$ and accordingly

$$\Pi^{0} = \sum_{t_{\mathbf{a}} \in G_{lt}} T_{\mathbf{a}}\,. \tag{3.3}$$

The difficulties to handle momentum $\mathbf{p} \neq 0$ were discussed in ref. [63]. Choosing $\mathbf{p} = 0$ we have a projector that commutes with the Hamiltonian, the projector onto angular momentum/parity J^P (see eq. (3.5)) and the projectors onto charge parity (see eq. (3.10)):

$$[\Pi^0, H] = [\Pi^0, \Pi^{J^P}] = [\Pi^0, \Pi_C^{\pm}] = 0\,. \tag{3.4}$$

The restriction we have on the lattice for the spatial translations implies a restriction of momentum to the first Brillouin zone and thus we have the cut-off the lattice provides to regularise the continuum theory.

3.2 Lattice rotations and reflections

The group G_{lr} of lattice rotations and reflections in $D = 2$ space dimensions corresponds to the orthogonal group O(2) in the continuum restricted by the condition to leave the lattice invariant. The group O(2) consists of two disjoint sets of elements, rotations $R(\theta) \in \mathrm{SO}(2)$, with the rotation angle θ, and general reflections $I \cdot R(\theta)$, with $R(\theta) \in \mathrm{SO}(2)$ and a special reflection I. Without loss of generality one can fix the reflection I in two dimensions (see ref. [61]). We choose the reflection which swaps the x and the y axes:

$$I = \begin{pmatrix} 0 & 1 \\ 1 & 0 \end{pmatrix}.$$

General rotations $R(\theta) \in \mathrm{SO}(2)$ are given by the 2×2 matrix:

$$R(\theta) = \begin{pmatrix} \cos(\theta) & -\sin(\theta) \\ \sin(\theta) & \cos(\theta) \end{pmatrix}.$$

On the lattice θ is restricted to $\theta = 0, \frac{\pi}{2}, \pi, \frac{3\pi}{2}$ and we get the following eight elements of G_{lr}:

$$\begin{aligned}
R_0 &= R(0) = \begin{pmatrix} 1 & 0 \\ 0 & 1 \end{pmatrix} \\
R_1 &= IR(\frac{3\pi}{2}) = \begin{pmatrix} 0 & 1 \\ 1 & 0 \end{pmatrix}\begin{pmatrix} 0 & 1 \\ -1 & 0 \end{pmatrix} = \begin{pmatrix} -1 & 0 \\ 0 & 1 \end{pmatrix} \\
R_2 &= IR(\frac{\pi}{2}) = \begin{pmatrix} 0 & 1 \\ 1 & 0 \end{pmatrix}\begin{pmatrix} 0 & -1 \\ 1 & 0 \end{pmatrix} = \begin{pmatrix} 1 & 0 \\ 0 & -1 \end{pmatrix} \\
R_3 &= R(\pi) = \begin{pmatrix} -1 & 0 \\ 0 & -1 \end{pmatrix} \\
R_4 &= I = \begin{pmatrix} 0 & 1 \\ 1 & 0 \end{pmatrix} \\
R_5 &= R(\frac{3\pi}{2}) = \begin{pmatrix} 0 & 1 \\ -1 & 0 \end{pmatrix} \\
R_6 &= R(\frac{\pi}{2}) = \begin{pmatrix} 0 & -1 \\ 1 & 0 \end{pmatrix} \\
R_7 &= IR(\pi) = \begin{pmatrix} 0 & 1 \\ 1 & 0 \end{pmatrix}\begin{pmatrix} -1 & 0 \\ 0 & -1 \end{pmatrix} = \begin{pmatrix} 0 & -1 \\ -1 & 0 \end{pmatrix}
\end{aligned}$$

They transform the lattice points $\mathbf{x}$ via:

$$\mathbf{x} \to R\mathbf{x}\,.$$

As given in eq. (2.15) the group G_{lr} acts on the loop space basis elements depending on a set of IRs $\{\Gamma_l\}$ of SU(3) on the links l as follows:

$$T(R)\chi^\alpha(\{\Gamma_l\}) = p^R\chi^\alpha(\{\Gamma_{R^{-1}l}\})\,.$$

The transformation of the links $l \to R^{-1}l$ is given by the rotation or reflection of the start and the end point of the link. We denote the eight transformations by

$$T_i = T(R_i)\,,\ i = 0,\ldots,7\,.$$

Projection operators on states of definite angular momentum and parity are given by:

$$\Pi^{J^P}_{\nu\sigma} = \frac{\dim J^P}{|G_{lr}|}\sum_{R\in G_{lr}} D^{J^P}_{\nu\sigma}T(R)\,. \tag{3.5}$$

The quantity $|G_{lr}| = 8$ denotes the order of the group and $D^{J^P}_{\nu\sigma}$ are the IRs of G_{lr} labelled with lattice angular momentum/parity J^P and magnetic quantum numbers ν and σ. The dimension of the IR is denoted with $\dim J^P$. In the next section we will present these IRs.

3.2.1 Irreducible representations

The group G_{lr} consists of five classes of conjugate elements. The classes are:

1. class: $\{R_0\}$
2. class: $\{R_1, R_2\}$
3. class: $\{R_3\}$
4. class: $\{R_5, R_6\}$
5. class: $\{R_4, R_7\}$

As the number of IRs of a group is equal to the number of classes in the group, we have five IRs of G_{lr}. For the dimension $\dim J^P$ of the IR we have to fulfil (see ref. [61]):

$$\begin{aligned}\sum_{J^P}(\dim J^P)^2 &= |G_{lr}| = 8\\ 1^2+1^2+1^2+1^2+2^2 &= 8\,.\end{aligned}$$

Thus we can conclude that we have four one-dimensional and one two-dimensional IR.

The group G_{lr} corresponds to the crystal group C_{4v}. Its IRs are well known (see e.g. ref. [16]). There are two one-dimensional IRs corresponding to lattice angular momentum $J = 0$. The one with positive parity we label with $J^P = 0^+$ and the one with negative parity we label with $J^P = 0^-$. In addition there are two one-dimensional IRs corresponding to $J = 2$. We can assign a parity ± 1 to them and label them with lattice angular momentum/parity $J^P = 2^+$ and $J^P = 2^-$. Considering $J = 1$, this yields the two-dimensional representation labelled with lattice angular momentum/parity $J^P = 1^\pm$. The labelling $J^P = 0^+, 0^-, 1^\pm, 2^+, 2^-$ will be clear below, when we discuss the contribution of these IRs to the continuum angular momentum and parity.

We will list the IRs in appendix C and in table 3.1 give only the corresponding characters c^{J^P}.

Table 3.1: The characters c^{J^P} of the irreducible representations labelled with J^P of the group G_{lr} of lattice rotations and reflections.

	1st class $\{R_0\}$	2nd class $\{R_1, R_2\}$	3rd class $\{R_3\}$	4th class $\{R_5, R_6\}$	5th class $\{R_4, R_7\}$
$J^P = 0^+$	1	1	1	1	1
$J^P = 0^-$	1	-1	1	1	-1
$J^P = 1^\pm$	2	0	-2	0	0
$J^P = 2^+$	1	1	1	-1	-1
$J^P = 2^-$	1	-1	1	-1	1

3.2.2 Continuum and lattice angular momentum

We have seen that the group G_{lr} is the group O(2) restricted to lattice rotations and reflections. Here we want to compare the IRs of G_{lr} and $O(2)$ labelled by the angular momentum. We therefore present the IRs of O(2) first (see e.g. ref. [61]).

There are two one-dimensional IRs of O(2) corresponding to the continuum angular momentum $J_c = 0$. They are characterised by the eigenvalue of parity $P = \pm 1$:

$$\begin{aligned} D^{0^\pm}(R(\theta)) &= 1 \\ D^{0^+}(I) = 1 \quad &\text{and} \quad D^{0^-}(I) = -1\,. \end{aligned} \tag{3.6}$$

In addition there is an infinite number of two-dimensional IRs of O(2). They are characterised by a continuum angular momentum $J_c = 1, 2, \ldots$:

$$\begin{aligned} D^{J_c^P}(R(\theta)) &= \begin{pmatrix} \mathrm{e}^{-\mathrm{i}J_c\theta} & 0 \\ 0 & \mathrm{e}^{\mathrm{i}J_c\theta} \end{pmatrix} \\ D^{J_c^P}(I) &= \begin{pmatrix} 0 & 1 \\ 1 & 0 \end{pmatrix}. \end{aligned} \tag{3.7}$$

To compare the continuum and the lattice angular momentum/parity we follow refs. [1, 28], where similar calculations have been performed in $D = 3$ space dimensions comparing the continuum group O(3) and the crystal group O_h.

Here we want to compare O(2) and G_{lr}. As the lattice group G_{lr} is a subgroup of the continuum group O(2) we can apply the concept of subduced representations.

The IRs of O(2) were labelled with J_c^P and those of the subgroup G_{lr} with J^P. A subduced representation is obtained by restricting an IR of a group to the elements of a subgroup. These are only those matrices of the IRs of O(2) that are images of elements of G_{lr}. We can apply Frobenius first theorem (see e.g. ref. [37]), which is a formal statement of the fact that a subduced representation of a subgroup can be decomposed into IRs of this subgroup. Following the notation of ref. [10] we write for a subduced representation:

$$D^{J_c^P} \downarrow G_{lr} = \sum_{J^P} \oplus\, m_{J_c^P}^{J^P}\, D^{J^P}(G_{lr})\,.$$

Table 3.2: The characters $c^{J_c^P}$ of the subduced representations $D^{J_c^P} \downarrow G_{lr}$ from the IRs of the group O(2) labelled with J_c^P on the group G_{lr}, which consists of rotations by an angle θ and reflections.

	1st class $\{R_0\}$ $\theta = 0$	2nd class $\{R_1, R_2\}$ reflections	3rd class $\{R_3\}$ $\theta = \pi$	4th class $\{R_5, R_6\}$ $\theta = \frac{\pi}{2}$	5th class $\{R_4, R_7\}$ reflections
$J_c^P = 0^+$	1	1	1	1	1
$J_c^P = 0^-$	1	−1	1	1	−1
$J_c^P = 1^\pm$	2	0	−2	0	0
$J_c^P = 2^\pm$	2	0	2	−2	0
$J_c^P = 3^\pm$	2	0	−2	0	0
$J_c^P = 4^\pm$	2	0	2	2	0
$J_c^P = 5^\pm$	2	0	−2	0	0
$J_c^P = 6^\pm$	2	0	2	−2	0
⋮					

Here $\oplus$ denotes the direct sum of inequivalent IRs. The integers $m_{J_c^P}^{J^P}$ give the multiplicities how often an IR J^P is contained in J_c^P. They can be calculated with the formula:

$$m_{J_c^P}^{J^P} = \frac{1}{|G_{lr}|} \sum_k n_k c_k^{J_c^P} c_k^{J^P} , \tag{3.8}$$

where the order of G_{lr} is $|G_{lr}| = 8$ and the order of the kth class of G_{lr} is denoted by n_k. The numbers c^{J^P} and $c^{J_c^P}$ are the characters of the subduced and the irreducible representation of G_{lr}. In table 3.1 we have listed the characters c^{J^P}.

To get the characters of the subduced representations, we have to evaluate the characters of the IRs of O(2) for the elements of G_{lr}. The characters for the one-dimensional IR (see eq. (3.6)) are 1 for all pure rotations and ± 1 for all reflections. For the two-dimensional IR (see eq. (3.7)) the characters for the rotations by an angle θ are given by

$$c^{J_c^P} = \mathrm{Tr}(D^{J_c^P}(R(\theta))) = 2\cos(J_c\theta)$$

and for reflections they are:

$$c^{J_c^P} = \mathrm{Tr}\left(D^{J_c^P}(IR(\theta))\right) = \mathrm{Tr}\left(D^{J_c^P}(I)D^{J_c^P}(R(\theta))\right) = \mathrm{Tr}\begin{pmatrix} 0 & \mathrm{e}^{\mathrm{i}J_c\theta} \\ \mathrm{e}^{-\mathrm{i}J_c\theta} & 0 \end{pmatrix} = 0\,.$$

Table 3.2 gives the corresponding characters of the subduced representation.

Applying formula (3.8) we get the results for the multiplicities $m_{J_c^P}^{J^P}$ of table 3.3. With these we know the contributions of the lattice angular momentum/parity J^P to the continuum angular momentum/parity J_c^P. We see that e.g. the lowest continuum angular momentum/parity J_c^P, the lattice angular momentum/parity $J^P = 0^+$ contributes to, is $J_c^P = 0^+$, the $J^P = 0^-$ contributes to $J_c^P = 0^-$ and so on. This justifies the labelling of the lattice angular momentum/parity by the same symbols.

Table 3.3: The multiplicities $m_{J_c^P}^{J^P}$,i.e how often an irreducible representation IR of the group of lattice rotations and reflections Glr, labelled with J^P, is contained in the IR of O(2), labelled with J_c^P.

	$J^P=0^+$	$J^P=0^-$	$J^P=1^\pm$	$J^P=2^+$	$J^P=2^-$
$J_c^P=0^+$	1	0	0	0	0
$J_c^P=0^-$	0	1	0	0	0
$J_c^P=1^\pm$	0	0	1	0	0
$J_c^P=2^\pm$	0	0	0	1	1
$J_c^P=3^\pm$	0	0	1	0	0
$J_c^P=4^\pm$	1	1	0	0	0
$J_c^P=5^\pm$	0	0	1	0	0
$J_c^P=6^\pm$	0	0	0	1	1
$\vdots$					

3.3 Charge conjugation

As we already mentioned in section 2.3.4 the operation of charge conjugation on the loop space basis corresponds to complex conjugation and this implies for a set of IRs $\{\Gamma_l\}$ of SU(3) on the links l of the basis elements (see as well eq. (2.13)):

$$T_C\chi^\alpha(\{\Gamma_l\}) = (\chi^\alpha(\{\Gamma_l\}))^* = p^C\chi^\alpha(\{\bar{\Gamma}_l\})\,. \tag{3.9}$$

Accordingly the operators which project onto states with charge parity ± 1 are

$$\Pi_C^\pm\chi^\alpha \;=\; \frac{1}{2}(1\pm T_C)\chi^\alpha\,. \tag{3.10}$$

The Hamiltonian commutes with these projectors and therefore we can classify its eigenstates with the two charge parities.

3.4 The symmetry projected basis

In the first part of this chapter we presented the projection operators for the lattice symmetries. Now we will discuss their action on the loop space basis.

3.4.1 Internal symmetries

As we have mentioned before there are internal symmetries of the elements of the loop space basis. These are symmetry transformations which map an element on itself and have to be considered as they affect the projection operators. The internal symmetries for SU(2) in $D=2$ space dimensions were discussed in ref. [64] and have to be extended for SU(3) in $D=2$ space dimensions. Additional phases can occur and, moreover, we have to consider charge conjugation. For example, we find that the plaquette function

(see eq. (2.3)), which is the first basis element, transforms under rotation/reflections $T(R)$ and charge conjugation T_C as follows:

$T_0\chi^1 =$ 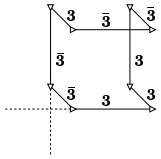
$T_1\chi^1 =$ 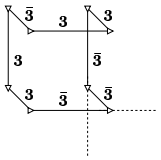
$T_2\chi^1 =$ 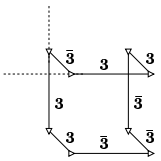

$T_3\chi^1 =$ 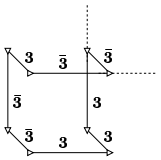
$T_4\chi^1 =$ 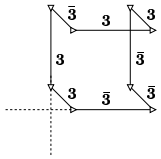
$T_5\chi^1 =$ 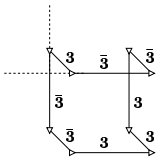

$T_6\chi^1 =$ 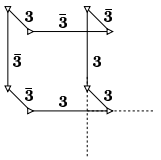
$T_7\chi^1 =$ 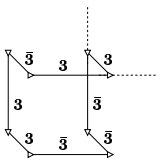
$T_C\chi^1 =$ 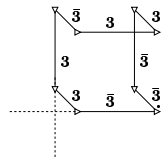

All phases are +1. The internal symmetries under rotation/reflections and translations $T_{\mathbf{a}}$ are then:

$$\begin{aligned} T_0\chi^1 &= T_{\mathbf{a}=\binom{1}{1}}T_3\chi^1 = T_{\mathbf{a}=\binom{0}{1}}T_5\chi^1 = T_{\mathbf{a}=\binom{1}{0}}T_6\chi^1 \\ T_4\chi^1 &= T_{\mathbf{a}=\binom{1}{0}}T_1\chi^1 = T_{\mathbf{a}=\binom{0}{1}}T_2\chi^1 = T_{\mathbf{a}=\binom{1}{1}}T_7\chi^1 \\ &= T_C\chi^1 . \end{aligned}$$

As the projector $\Pi^{\mathbf{p}=0}$ commutes with all other projectors (see eq. (3.4)), we assume from now on that the basis elements are already projected on momentum $\mathbf{p} = 0$. In this section we use the following abbreviation:

$$\underline{\chi}^\alpha = \Pi^0\chi^\alpha = \sum_{t_{\mathbf{a}}\in G_{lt}} T_{\mathbf{a}}\chi^\alpha .$$

For the plaquette function we then get:

$$\begin{aligned} T_0\underline{\chi}^1 &= T_3\underline{\chi}^1 = T_5\underline{\chi}^1 = T_6\underline{\chi}^1 \\ T_4\underline{\chi}^1 &= T_1\underline{\chi}^1 = T_2\underline{\chi}^1 = T_7\underline{\chi}^1 \\ &= T_C\underline{\chi}^1 . \end{aligned}$$

Thus it remains to discuss the internal symmetries with respect to rotations/reflections and charge conjugation.

As we project at first on charge parity and then on angular momentum and parity, we have to check the internal symmetries under rotation/reflections of the basis elements with

definite charge parity. For the plaquette function we get for positive charge parity

$$\begin{aligned} T_0\Pi^+\underline{\chi}^1 &= \frac{1}{2}(1+T_C)\underline{\chi}^1 = T_3\Pi^+\underline{\chi}^1 = T_5\Pi^+\underline{\chi}^1 = T_6\Pi^+\underline{\chi}^1 = \\ = T_1\Pi^+\underline{\chi}^1 &\overset{T_1\underline{\chi}^1=T_C\underline{\chi}^1}{=} \frac{1}{2}(T_C+1)\underline{\chi}^1 = T_2\Pi^+\underline{\chi}^1 = T_4\Pi^+\underline{\chi}^1 = T_7\Pi^+\underline{\chi}^1 . \end{aligned} \tag{3.11}$$

Thus $\Pi^+\underline{\chi}^1$ is symmetric under all rotations and reflections. For negative charge parity we get

$$\begin{aligned} T_0\Pi^-\underline{\chi}^1 &= \frac{1}{2}(1-T_C)\underline{\chi}^1 = T_3\Pi^-\underline{\chi}^1 = T_5\Pi^-\underline{\chi}^1 = T_6\Pi^-\underline{\chi}^1 = \\ = -T_1\Pi^-\underline{\chi}^1 &\overset{T_1\underline{\chi}^1=T_C\underline{\chi}^1}{=} \frac{1}{2}(T_C-1)\underline{\chi}^1 = -T_2\Pi^-\underline{\chi}^1 = -T_4\Pi^-\underline{\chi}^1 = -T_7\Pi^-\underline{\chi}^1 . \end{aligned} \tag{3.12}$$

Thus $\Pi^-\underline{\chi}^1$ changes sign under reflections.

For general basis elements $\underline{\chi}^\alpha$ we have to take into account the following cases of symmetries of $\underline{\chi}^\alpha$ to check the internal symmetries of $\Pi^\pm\underline{\chi}^\alpha$. For positive charge parity we get for a general element $R \in G_{lr}$:

- $T(R)\underline{\chi}^\alpha \neq \pm\underline{\chi}^\alpha$ and $T_C\underline{\chi}^\alpha = \pm T(R)\underline{\chi}^\alpha \rightarrow T(R)\Pi^+\underline{\chi}^\alpha = \pm\Pi^+\underline{\chi}^\alpha$
- $T(R)\underline{\chi}^\alpha = \pm\underline{\chi}^\alpha$ and $T_C\underline{\chi}^\alpha \neq \pm T(R)\underline{\chi}^\alpha \rightarrow T(R)\Pi^+\underline{\chi}^\alpha = \pm\Pi^+\underline{\chi}^\alpha$
- $T(R)\underline{\chi}^\alpha = \underline{\chi}^\alpha$ and $T_C\underline{\chi}^\alpha = \pm T(R)\underline{\chi}^\alpha \rightarrow T(R)\Pi^+\underline{\chi}^\alpha = \begin{cases} \Pi^+\underline{\chi}^\alpha \\ 0 \end{cases} = \begin{cases} \underline{\chi}^\alpha \\ 0 \end{cases}$
- $T(R)\underline{\chi}^\alpha = -\underline{\chi}^\alpha$ and $T_C\underline{\chi}^\alpha = \pm T(R)\underline{\chi}^\alpha \rightarrow T(R)\Pi^+\underline{\chi}^\alpha = \begin{cases} 0 \\ -\Pi^+\underline{\chi}^\alpha \end{cases} = \begin{cases} 0 \\ -\underline{\chi}^\alpha \end{cases}$.

And for negative charge parity we have:

- $T(R)\underline{\chi}^\alpha \neq \pm\underline{\chi}^\alpha$ and $T_C\underline{\chi}^\alpha = \pm T(R)\underline{\chi}^\alpha \rightarrow T(R)\Pi^-\underline{\chi}^\alpha = \mp\Pi^-\underline{\chi}^\alpha$
- $T(R)\underline{\chi}^\alpha = \pm\underline{\chi}^\alpha$ and $T_C\underline{\chi}^\alpha \neq \pm T(R)\underline{\chi}^\alpha \rightarrow T(R)\Pi^-\underline{\chi}^\alpha = \pm\Pi^-\underline{\chi}^\alpha$
- $T(R)\underline{\chi}^\alpha = \underline{\chi}^\alpha$ and $T_C\underline{\chi}^\alpha = \pm T(R)\underline{\chi}^\alpha \rightarrow T(R)\Pi^-\underline{\chi}^\alpha = \begin{cases} 0 \\ \Pi^-\underline{\chi}^\alpha \end{cases} = \begin{cases} 0 \\ \underline{\chi}^\alpha \end{cases}$
- $T(R)\underline{\chi}^\alpha = -\underline{\chi}^\alpha$ and $T_C\underline{\chi}^\alpha = \pm T(R)\underline{\chi}^\alpha \rightarrow T(R)\Pi^-\underline{\chi}^\alpha = \begin{cases} -\Pi^-\underline{\chi}^\alpha \\ 0 \end{cases} = \begin{cases} -\underline{\chi}^\alpha \\ 0 \end{cases}$.

These internal symmetries under rotation and reflection of $\Pi^\pm\underline{\chi}^\alpha$ can be generally classified.

Classification of the internal rotation/reflection symmetries

The basis elements $\Pi^\pm_C\underline{\chi}^\alpha$ may have such internal symmetries that they are irreducible basis vectors of the IRs of the subgroups of G_{lr}.

There are ten subgroups of G_{lr}, which we will list in appendix C together with their IRs. Here we illustrate the classification of the internal symmetries concerning the subgroup $G^{4b} : \{R_0, R_1, R_2, R_3\}$ and we refer for the other subgroups to the appendix C.

Table 3.4: The characters c^{4b} of the IRs of the subgroup G^{4b} of the group G_{lr}.

	1st class: $\{R_0\}$	2nd class: $\{R_1\}$	3rd class: $\{R_2\}$	4th class: $\{R_3\}$
$j_{4b}=0$	1	1	1	1
$j_{4b}=1$	1	1	-1	-1
$j_{4b}=2$	1	-1	1	-1
$j_{4b}=3$	1	-1	-1	1

The subgroup G^{4b} corresponds to the dihedral group D_2, which has four one-dimensional IRs (see ref. [16]) which we label with $j_{4b}=0,1,2,3$. Table 3.4 gives the characters of these IRs.

An element of the loop space basis projected onto charge parity can have an internal symmetry concerning this subgroup, i.e. it is an irreducible basis vector:

$$T(R)\Pi^{\pm}\underline{\chi}^{\alpha} = D^{j_{4b}}(R)\Pi^{\pm}\underline{\chi}^{\alpha}\,.$$

The basis element $\Pi_C^{\pm}\underline{\chi}^4$, for example, has such an internal symmetry. To show this we proceed as follows:

First we check the symmetries of $\underline{\chi}^4$ with respect to rotation/reflections and charge conjugation, as we did above for the plaquette function. The basis element χ^4 has the form

$\chi^4 =$ 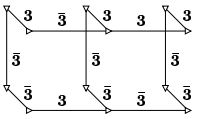

and we get the following symmetries:

$$\begin{aligned} T(R_0)\underline{\chi}^4 &= \underline{\chi}^4 & T(R_0)\underline{\chi}^4 &\neq T_C\underline{\chi}^4 \\ T(R_1)\underline{\chi}^4 &= \underline{\chi}^4 & T(R_1)\underline{\chi}^4 &\neq T_C\underline{\chi}^4 \\ T(R_2)\underline{\chi}^4 &= T_C\underline{\chi}^4 & T(R_2)\underline{\chi}^4 &\neq \underline{\chi}^4 \\ T(R_3)\underline{\chi}^4 &= T_C\underline{\chi}^4 & T(R_3)\underline{\chi}^4 &\neq \underline{\chi}^4\,. \end{aligned}$$

Then we check the cases presented at the end of the last section and get the internal symmetries of the basis $\Pi_C^{\pm}\underline{\chi}^4$ projected onto charge parity. For positive charge parity we have

$$T(R_i)\Pi_C^{+}\underline{\chi}^4 \;=\; \Pi_C^{+}\underline{\chi}^4\,,\; i=0,1,2,3$$

and we see, that $\Pi_C^{+}\underline{\chi}^4$ is an irreducible basis vector of the IR labelled with $j_{4b}=0$ (see table 3.4).

For negative charge parity we get

$$\begin{aligned} T(R_i)\Pi_C^{-}\underline{\chi}^4 &= \Pi_C^{+}\underline{\chi}^4\,,\; i=0,1 \\ T(R_i)\Pi_C^{-}\underline{\chi}^4 &= -\Pi_C^{+}\underline{\chi}^4\,,\; i=2,3\,, \end{aligned}$$

Table 3.5: The number of occurrence $m_{j_{4b}}^{J^P}$ of the IRs of the group G_{lr} in the induced representation $D^{j_{4b}} \uparrow G_{lr}$ of the subgroup G^{4b}.

	$j_{4b}=0$	$j_{4b}=1$	$j_{4b}=2$	$j_{4b}=3$
$J^P=0^+$	1	0	0	0
$J^P=0^-$	0	0	0	1
$J^P=1^\pm$	0	1	1	0
$J^P=2^+$	1	0	0	0
$J^P=2^-$	0	0	0	1

and $\Pi_C^- \underline{\chi}^4$ is an irreducible basis vector of the IR labelled with $j_{4b}=1$ (see table 3.4).

As we want to classify the basis elements $\Pi^\pm \underline{\chi}^\alpha$ according to the IRs of the large group G_{lr} labelled with $J^P = 0^+, 0^-, 1^\pm, 2^+, 2^-$, we need to apply the concept of induced representations. This is the reverse process of the subduction we presented in section 3.2.2. An induced representation means the construction of a representation of the larger group (here G_{lr}) from the IRs of its subgroup (here G^{4b}). We denote it (as in ref. [10]) by

$$D^{j_{4b}} \uparrow G_{lr} = \sum_{J^P} \oplus m_{j_{4b}}^{J^P} D^{J^P}(G_{lr}) \,,$$

where $m_{j_{4b}}^{J^P}$ is the number of the occurrence of the IR J^P of G_{lr} in the induced representation.

Frobenius reciprocity theorem (see e.g. ref. [10]) states, that the number of times $D^{J^P}(G_{lr})$ occurs in $D^{j_{4b}} \uparrow G_{lr}$ is equal to the number of times the IR of the subgroup $D^{j_{4b}}(G^{4b})$ appears in the subduced representation $D^{J^P} \downarrow G^{4b}$, i.e.

$$m_{j_{4b}}^{J^P} = m_{J^P}^{j_{4b}} \,.$$

Thus we can calculate these multiplicities as given in formula (3.8). In table 3.5 we present the results.

We have seen above that $\Pi_C^+ \underline{\chi}^4$ is an irreducible vector of the IR of G^{4b} labelled with $j_{4b}=0$ and we deduce from table 3.5, that it will not contribute to lattice angular momentum/parity $J^P = 0^-, 1^\pm, 2^-$. The element $\Pi_C^- \underline{\chi}^4$ will not contribute to lattice angular momentum/parity $J^P = 0^+, 0^-, 2^+, 2^-$, as it is an irreducible vector of the IR of G^{4b} labelled with $j_{4b}=1$. For the other subgroups we will list the multiplicity tables in appendix C. Altogether we get 25 possible internal symmetries. Table 3.6 and table 3.7 give the number of basis elements $\Pi_C^+ \underline{\chi}^\alpha$ and $\Pi_C^- \underline{\chi}^\alpha$ with these internal symmetries.

Considering all IRs of the subgroups we have a classification of all internal symmetries with an information about the contributions a basis element has to certain lattice angular momentum and parity states.

We finally want to mention the plaquette function again. Projected onto charge parity + (see eq. (3.11)) it has an internal symmetry corresponding to the IR of the subgroup

$G^{8a} = G_{lr}$ labelled with $j_{8a} = 0^+$ (see appendix C). We see from the multiplicities that it contributes only to $J^P = 0^+$, as it should. Projected onto charge parity $-$ (see eq. (3.12)) it has an internal symmetry corresponding to the IR of G^{8a} labelled with $j_{8a} = 0^-$. It contributes only to lattice angular-momentum parity $J^P = 0^-$.

Table 3.6: The number of basis elements $\Pi_C^+ \underline{\chi}^\alpha$ with positive charge parity with internal symmetries, according to the irreducible representations of the subgroups of the lattice rotation/reflection group G_{lr}. The order δ of a basis element is defined in chapter 2. Together with the number of basis elements $n(\Pi_C^+ \underline{\chi}^\alpha = 0)$, which are projected via Π_c^+ onto zero (next to last line), we get the total number of basis elements (last line) (see as well table 2.3).

subgroups	IR	$\delta \leq 0$	$\delta \leq 1$	$\delta \leq 2$	$\delta \leq 3$	$\delta \leq 4$	$\delta \leq 5$	$\delta \leq 6$
G^{1a}	$j_{1a} = 0$	0	0	0	16	544	15499	366864
G^{2a}	$j_{2a} = 0$	0	0	0	0	35	291	2646
	$j_{2a} = 1$	0	0	0	0	2	2	143
G^{2b}	$j_{2b} = 0$	0	0	0	13	93	688	5568
	$j_{2b} = 1$	0	0	0	0	0	0	181
G^{2c}	$j_{2c} = 0$	0	0	0	0	24	80	1207
	$j_{2c} = 1$	0	0	0	0	0	0	24
G^{2d}	$j_{2d} = 0$	0	0	0	3	20	91	709
	$j_{2d} = 1$	0	0	0	2	13	79	584
G^{2e}	$j_{2e} = 0$	0	0	0	1	3	68	431
	$j_{2e} = 1$	0	0	0	2	6	76	315
G^{4a}	$j_{4a} = 0$	0	0	0	0	0	0	0
	$j_{4a} = 1$	0	0	0	0	0	0	0
G^{4b}	$j_{4b} = 0$	0	0	4	8	53	94	393
	$j_{4b} = 1$	0	0	0	0	0	0	0
	$j_{4b} = 2$	0	0	0	0	1	1	1
	$j_{4b} = 3$	0	0	0	0	2	2	2
G^{4c}	$j_{4c} = 0$	0	0	0	0	3	8	71
	$j_{4c} = 1$	0	0	0	0	2	2	20
	$j_{4c} = 2$	0	0	0	0	0	0	0
	$j_{4c} = 3$	0	0	0	0	0	0	0
G^{8a}	$j_{8a} = 0^+$	1	2	4	6	16	27	43
	$j_{8a} = 0^-$	0	0	0	0	2	2	2
	$j_{8a} = 2^+$	0	0	0	0	0	0	0
	$j_{8a} = 2^-$	0	0	0	0	1	1	1
$n(\Pi_C^+ \underline{\chi}^\alpha = 0)$		0	0	0	0	1	1	21
total		1	2	8	51	821	17012	379226

Table 3.7: The number of basis elements $\Pi_C^- \underline{\chi}^\alpha$ with negative charge parity with internal symmetries, according to the irreducible representations of the subgroups of the lattice rotation/reflection group G_{lr}. The order δ of a basis element is defined in chapter 2. Together with the number of basis elements $n(\Pi_C^- \underline{\chi}^\alpha = 0)$, which are projected via Π_c^- onto zero (next to last line), we get the total number of basis elements (last line) (see as well table 2.3).

subgroup	IR	$\delta \leq 0$	$\delta \leq 1$	$\delta \leq 2$	$\delta \leq 3$	$\delta \leq 4$	$\delta \leq 5$	$\delta \leq 6$
G^{1a}	$j_{1a} = 0$	0	0	0	16	544	15499	366874
G^{2a}	$j_{2a} = 0$	0	0	0	0	6	5	444
	$j_{2a} = 1$	0	0	0	0	32	289	2343
G^{2b}	$j_{2b} = 0$	0	0	0	0	4	4	278
	$j_{2b} = 1$	0	0	0	13	89	684	5461
G^{2c}	$j_{2c} = 0$	0	0	0	0	12	64	629
	$j_{2c} = 1$	0	0	0	0	12	16	602
G^{2d}	$j_{2d} = 0$	0	0	0	2	18	84	659
	$j_{2d} = 1$	0	0	0	3	15	86	626
G^{2e}	$j_{2e} = 0$	0	0	0	2	6	76	454
	$j_{2e} = 1$	0	0	0	1	3	68	287
G^{4a}	$j_{4a} = 0$	0	0	0	0	0	0	0
	$j_{4a} = 1$	0	0	0	0	0	0	0
G^{4b}	$j_{4b} = 0$	0	0	0	0	2	2	8
	$j_{4b} = 1$	0	0	2	2	26	26	145
	$j_{4b} = 2$	0	0	0	0	2	2	28
	$j_{4b} = 3$	0	0	2	6	22	63	206
G^{4c}	$j_{4c} = 0$	0	0	0	0	2	2	22
	$j_{4c} = 1$	0	0	0	0	1	6	37
	$j_{4c} = 2$	0	0	0	0	0	0	23
	$j_{4c} = 3$	0	0	0	0	2	2	5
G^{8a}	$j_{8a} = 0^+$	0	0	0	0	0	0	0
	$j_{8a} = 0^-$	0	1	2	4	10	21	36
	$j_{8a} = 2^+$	0	0	0	0	2	2	2
	$j_{8a} = 2^-$	0	0	0	0	4	4	4
$n(\Pi_C^- \underline{\chi}^\alpha = 0)$		1	1	2	2	7	7	53
total		1	2	8	51	821	17012	379226

3.4.2 Normalisation

Now that we have all properties of the action of the symmetry transformations on the loop space basis we can derive the norm $||\Pi^0\Pi^{J^P}\Pi^{\pm}_C\chi^\alpha(U)||$ of the symmetry projected basis η (see eq. (1.19)):

$$\eta^\alpha_{J^{PC},\nu\sigma}(U) \;=\; \frac{\Pi^0\Pi^{J^P}_{\nu\sigma}\Pi^{\pm}_C\chi^\alpha(U)}{||\Pi^0\Pi^{J^P}_{\nu\sigma}\Pi^{\pm}_C\chi^\alpha(U)||}\,. \tag{3.13}$$

For the vacuum state (see eq. (1.18)) we have $J^{PC}=0^{++}$.

We first determine the norm of the basis elements $\Pi^{\pm}_C\chi^\alpha$ projected onto charge parity. The scalar product between states with different charge parity vanishes

$$\langle\Pi^{\pm}_C\chi^\alpha|\Pi^{\mp}_C\chi^\alpha\rangle = 0$$

and we are left with the following norm:

$$\begin{aligned} ||\Pi^{\pm}_C\chi^\alpha||^2 &= \int DU\big(\frac{1}{2}(\chi^\alpha \pm (\chi^\alpha)^*)\big)\big(\frac{1}{2}((\chi^\alpha)^* \pm \chi^\alpha)\big) \\ &= \begin{cases} 1\,, & \text{if } T_C\chi^\alpha = (\chi^\alpha)^* = \chi^\alpha \\ \frac{1}{2}\,, & \text{else} \end{cases}\,, \end{aligned} \tag{3.14}$$

where the Haar measure DU is defined in eq. (1.14) and we have used the fact that the loop space basis constructed in chapter 2 is orthonormal.

Now we check if η is orthonormal, as we demanded in chapter 1. We explain the different steps of the computation below:

$$\begin{aligned} &\langle\Pi^0\Pi^{J^P}_{\nu\sigma}\Pi^{\pm}_C\chi^\alpha(U)|\Pi^0\Pi^{J^{P'}}_{\nu'\sigma'}\Pi^{\pm}_C\chi^\beta(U)\rangle \\ &= \int DU\frac{(\dim J^P)(\dim J^{P'})}{|G_{lr}|^2}\sum_{R_1,R_2\in G_{lr}} D^{J^P}_{\nu\sigma}{}^*(R_1^{-1})D^{J^{P'}}_{\nu'\sigma'}(R_2^{-1}) \\ &\quad\times\big(T(R_1)\Pi^{\pm}_C\Pi^0(\chi^\alpha)^*(U)\big)\big(T(R_2)\Pi^{\pm}_C\Pi^0\chi^\beta(U)\big) \qquad (3.15) \\ &= \int DU\frac{(\dim J^P)(\dim J^{P'})}{|G_{lr}|^2}\sum_{R_1,R_3\in G_{lr}} D^{J^P}_{\nu\sigma}{}^*(R_1^{-1})D^{J^{P'}}_{\nu'\sigma'}(R_3^{-1}R_1^{-1}) \\ &\quad\times T(R_1)\left[\big(\Pi^{\pm}_C\Pi^0(\chi^\alpha)^*(U)\big)\big(T(R_3)\Pi^{\pm}_C\Pi^0\chi^\beta(U)\big)\right]\,,\text{where } R_3 = R_1^{-1}R_2 \\ &= \int DU\frac{(\dim J^P)(\dim J^{P'})}{|G_{lr}|^2}\sum_{t_{\mathbf{a}_1},t_{\mathbf{a}_2}\in G_{lt}}\sum_{\substack{R_1\in G_{lr},\\ R_3\in G_{\chi^\beta}}} p(R_3)D^{J^P}_{\nu\sigma}{}^*(R_1^{-1})D^{J^{P'}}_{\nu'\sigma'}(R_3^{-1}R_1^{-1}) \\ &\quad\times T_{\mathbf{a}_1}T(R_1)\left[\big(\Pi^{\pm}_C(\chi^\alpha)^*(U)\big)T_{\mathbf{a}_2}\big(\Pi^{\pm}_C\chi^\beta(U)\big)\right]\,,\text{where } p(R_3)=\pm1 \qquad (3.16) \\ &= |G_{lt}|\frac{(\dim J^P)(\dim J^{P'})}{|G_{lr}|^2}\sum_{R_1\in G_{lr},R_3\in G_{\chi^\beta}} p(R_3)D^{J^P}_{\nu\sigma}{}^*(R_1^{-1})D^{J^{P'}}_{\nu'\sigma'}(R_3^{-1}R_1^{-1}) \\ &\quad\times\delta_{\alpha\beta}\begin{cases} 1\,, & \text{if } T_C\chi^\alpha = \chi^\alpha \\ \frac{1}{2}\,, & \text{else} \end{cases}\,. \end{aligned}$$

In the first step we have used that the projection operators commute (see eq. (3.4)).

In the step to eq. (3.16) we have used that, only if $T(R_3)\Pi_C^{\pm}\Pi^0\chi^\beta = p(R_3)\Pi_C^{\pm}\Pi^0\chi^\beta$, we get a contribution. Thus R_3 has to be an element of the internal symmetry group of $\Pi_C^{\pm}\Pi^0\chi^\beta$, which we denote here with G_{χ^β}. The phase $p(R_3) = \pm 1$ is then fixed.

In the step to eq. (3.17) we inserted the norm of eq. (3.14) and used that the projection onto momentum $\mathbf{p} = 0$ provides the translation $T_{\mathbf{a}_2}$, which has to be the identity, and the translation $T_{\mathbf{a}_1}$, which gives a factor $|G_{lt}|$.

The factor $|G_{lt}|$ is a volume factor. It will be omitted from now on. This corresponds to the fact that we want to get well-defined coefficients S_α in the exp$S$-Ansatz (see eq. (1.15) and eq. (1.16)), which are independent of the lattice volume.

Now with the representation property of the IRs of G_{lr}

$$D^{J^P}_{\nu'\sigma'}(R_3^{-1}R_1^{-1}) \;=\; \sum_{\sigma''} D^{J^P}_{\nu'\sigma''}(R_3^{-1}) D^{J^P}_{\sigma''\sigma'}(R_1^{-1})$$

and with the orthonormality condition

$$\frac{\dim J^P}{|G_{lr}|} \sum_{R_1 \in G_{lr}} D^{J^P *}_{\nu\sigma}(R_1^{-1}) D^{(J^P)'}_{\sigma''\sigma'}(R_1^{-1}) \;=\; \delta_{J^P (J^P)'} \delta_{\nu\sigma''} \delta_{\sigma\sigma'}$$

we get for the scalar product of the basis η:

$$\begin{aligned} &\langle \Pi^0 \Pi^{J^P}_{\nu\sigma} \Pi_C^{\pm} \chi^\alpha | \Pi^0 \Pi^{(J^P)'}_{\nu'\sigma'} \Pi_C^{\pm} \chi^\beta \rangle \\ &= \frac{(\dim J^P)}{|G_{lr}|} \sum_{R_3 \in G_{\chi^\beta}} p(R_3) D^{J^P}_{\nu'\nu}(R_3^{-1}) \delta_{J^P (J^P)'} \delta_{\sigma\sigma'} \delta_{\alpha\beta} \begin{cases} 1 \,, & \text{if } T_C \chi^\alpha = \chi^\alpha \\ \frac{1}{2} \,, & \text{else} \end{cases} . \end{aligned} \tag{3.17}$$

The norm matrix $\sum_{R_3 \in G_{\chi^\beta}} p(R_3) D^{J^P}_{\nu'\nu}(R_3^{-1})$ is for the one-dimensional IRs $J^P = 0^+, 0^-, 2^+$ and 2^- of course diagonal. As will be shown in appendix C for the two-dimensional IR $J^P = 1^\pm$ it is either diagonal and we have one or two basis elements labelled with $\nu = 0$ and/or $\nu = 1$, or it can be diagonalised in a trivial way and we get only one basis element labelled with $\nu = 0$ or $\nu = 1$.

Thus with the following norm

$$||\Pi^0 \Pi^{J^P}_{\nu\sigma} \Pi_C^{\pm} \chi^\alpha||^2 \;=\; \frac{(\dim J^P)}{|G_{lr}|} \sum_{R_3 \in G_{\chi^\alpha}} p(R_3) D^{J^P}_{\nu\nu}(R_3^{-1}) \begin{cases} 1 \,, & \text{if } T_C \chi^\alpha = \chi^\alpha \\ \frac{1}{2} \,, & \text{else} \end{cases} ,$$

our symmetry projected basis η is orthonormal:

$$\langle \eta^\alpha_{J^{PC},\nu\sigma} | \eta^\beta_{(J^{PC})',\nu'\sigma'} \rangle \;=\; \delta_{J^{PC}(J^{PC})'} \delta_{\nu\nu'} \delta_{\sigma\sigma'} \delta_{\alpha\beta} \,.$$

Chapter 4 **Results**

In this chapter we will present the results for the calculation of SU(3) glueballs up to 5th order. At first we give the size of the basis used and define the truncation scheme needed for the numerical calculations. Then we show the method of solving the ground state and excited state equations. The results for the vacuum energy and the glueball states both for the unimproved and the improved Hamiltonian will be given. Our data will be compared to the results of other computations done in the Hamiltonian approach of lattice gauge field theories (see ref. [9, 18, 27]) and to the analytic studies of ref. [53]. Furthermore a comparison to results of standard lattice Monte Carlo calculations (see ref. [60]) will be shown. We will also discuss the various contributions of the basis functions to the vacuum and the glueball wave functions.

4.1 Number of basis functions

In chapter 2 we constructed the loop space basis χ by first generating subspaces Λ from geometrically inequivalent plaquette products and then by constructing an orthogonal basis χ in these subspaces. The order δ is the number of plaquette products the subspaces Λ are built of. It defines the truncation scheme we have to introduce for the concrete calculations of the vacuum energy and the glueball states presented below. The truncation prescription we use follows the proposal of Guo *et al.* (see ref. [20]):

The coupled cluster matrix element (see eq. (A.3)) is defined to be the coefficient in the expansion of the product of two basis elements η^{α_1} and η^{α_2} in the symmetry projected basis η (see chapter 3). For calculations in the order δ we truncate this matrix element by

$$C^{\alpha_1\alpha_2}_{\alpha_3,\nu\kappa}(J^{PC}) = 0 \;\text{ for }\; \delta(\eta^{\alpha_1}) + \delta(\eta^{\alpha_2}) > \delta + 1\,, \tag{4.1}$$

demanding that the resulting basis element η^{α_3} has an order $\delta(\eta^{\alpha_3}) \leq \delta$.

Alternative truncations were studied in ref. [64], but we could not find any prescription which provides a better continuum limit than eq. (4.1).

Table 4.1 gives the number of geometrical subspaces Λ and the number of the elements of the loop space basis χ up to a given order δ (see as well section 2.2.2). The table also lists the number of elements of the basis η. As it is the symmetry projected basis the elements have the correct quantum numbers, i.e. vanishing (lattice) momentum $\mathbf{p} = 0$ and angular momentum/parity and charge parity:

$$J^{PC} = 0^{++}, 0^{-+}, 1^{\pm+}, 2^{++}, 2^{-+}, 0^{+-}, 0^{--}, 1^{\pm-}, 2^{+-}, 2^{--}\,.$$

Table 4.1: The number of geometrical subspaces Λ, of loop space basis elements χ and of functions η with lattice angular momentum/parity and charge parity up to the order $\delta = 6$.

order	$\delta \leq 0$	$\delta \leq 1$	$\delta \leq 2$	$\delta \leq 3$	$\delta \leq 4$	$\delta \leq 5$	$\delta \leq 6$
Λ	1	2	6	18	103	685	5400
χ	1	2	8	51	821	17012	379226
$\eta_{0^{++}}$	1	2	8	47	791	16846	377932
$\eta_{0^{-+}}$	0	0	0	20	595	15742	369318
$\eta_{1^{\pm+}}$	0	0	0	53	1261	32294	744354
$\eta_{2^{++}}$	0	0	4	41	770	16809	377597
$\eta_{2^{-+}}$	0	0	0	20	599	15751	369609
$\eta_{0^{+-}}$	0	0	0	20	594	15736	369368
$\eta_{0^{--}}$	0	1	4	43	728	16780	376499
$\eta_{1^{\pm-}}$	0	0	2	55	1315	32356	745705
$\eta_{2^{+-}}$	0	0	0	20	591	15738	369187
$\eta_{2^{--}}$	0	0	2	39	727	16763	376650

4.2 Vacuum state

For the vacuum state we derived in chapter 1 the following set of coupled cluster equations (see eq. (1.31)):

$$\epsilon_{\alpha_3} S_{\alpha_3} + \sum_{\alpha_1>0,\alpha_2>0} S_{\alpha_1} S_{\alpha_2} C^{\alpha_1,\alpha_2}_{\alpha_3}(0^{++}) \;=\; \frac{||\tilde{\Pi}^0 \chi^1||\beta^2}{N_c^2}\delta_{\alpha_3 1} + \frac{E_0}{N}\delta_{\alpha_3 0}\,,$$

where in the order under consideration α_3 ranges from 1 up the corresponding dimension presented in table 4.1 for $\eta_{0^{++}}$. Its solution provides both the vacuum energy density $\frac{E_0}{N}$ and the vacuum wave function $\Psi_0 = \exp(\sum_{\alpha>0} S_\alpha \eta^\alpha)$.

Here we first present the method to solve the vacuum equation and then we discuss our results for the energy density and the wave function in the unimproved and improved case. There exist other computations in the Hamiltonian formulation of lattice gauge field theories based on an analytic variational approach [9] and on the application of random phase approximation to the coupled cluster expansion [27]. We will compare our data with the results.

4.2.1 Solving the vacuum equation

The vacuum equation (4.2) can be solved by iteration: We rewrite the equation as a set of quadratic equations:

$$\begin{aligned} 0 = & \left[\sum_{\substack{\alpha_1>0,\alpha_2>0 \\ \alpha_1\neq\alpha_3,\alpha_2\neq\alpha_3}} C_{\alpha_3}^{\alpha_1,\alpha_2}(0^{++})\ S_{\alpha_1}S_{\alpha_2} - \frac{||\tilde{\Pi}^0\chi^1||\beta^2}{N_c^2}\delta_{\alpha_3 1} - \frac{E_0}{N}\delta_{\alpha_3 0} \right] \\ & + \left[\epsilon_{\alpha_3} + \sum_{\substack{\alpha_1>0 \\ \alpha_1\neq\alpha_3}} C_{\alpha_3}^{\alpha_1,\alpha_3}(0^{++})\ S_{\alpha_1} + \sum_{\substack{\alpha_2>0 \\ \alpha_1\neq\alpha_3}} C_{\alpha_3}^{\alpha_3,\alpha_2}(0^{++})\ S_{\alpha_2} \right] S_{\alpha_3} \\ & + C_{\alpha_3}^{\alpha_3,\alpha_3}(0^{++})\ S_{\alpha_3}S_{\alpha_3}. \end{aligned} \tag{4.2}$$

We start the iteration with $\alpha_3 = 1, S_{\alpha_3>1} = 0$:

$$\epsilon_1 S_1 = \frac{||\tilde{\Pi}^0\chi^1||}{N_c^2}\,.$$

Then we use S_1 to calculate S_2 with $S_{\alpha_3>2} = 0$ and so on. We get a preliminary result for all S_{α_3} as a function of the S_{α_3} calculated before:

$$S_{\alpha_3} = f(S_1, \ldots, S_{\alpha_3-1})\,.$$

This result is used to determine a new set of S_{α_3} component by component:

$$\begin{aligned} S_1' &= f(S_2, \ldots, S_{\alpha_3,\max}) \\ S_{\alpha_3}' &= f(S_1', \ldots, S_{\alpha_3-1}', S_{\alpha_3+1}, \ldots, S_{\alpha_3,\max})\,. \end{aligned}$$

If the last (quadratic) term in eq. (4.2) occurs, we select of the two solutions the root which is nearest to the corresponding value of the previous iteration step. This iteration procedure is repeated until one gets convergence in the energy E_0 which is included in the process via

$$S_0 = \frac{E_0}{N}\,.$$

It can be calculated from the other S_{α_3} using the coupled cluster matrix element $C_0^{\alpha_1,\alpha_2}(0^{++})$.

Our iteration process incorporates a relaxation by determining $S_{\alpha_3}^{\text{new}}$ via

$$S_{\alpha_3}^{\text{new}} \to (1-R)S_{\alpha_3}^{\text{new}} + RS_{\alpha_3}^{\text{old}}\,,$$

with $0 < R \leq 1$.

We use this procedure for the SU(3) vacuum state. In ref. [64] other iteration schemes were tried and discussed for the SU(2) case.

4.2.2 Vacuum energy

In fig. 4.1 and fig. 4.2 we present our results for the vacuum energy density. We compare the energy density $\frac{E_0}{N} = a\langle H\rangle$ of the dimensionless Hamiltonian $H = \sum_{l,a} E_l^a E_l^a - \sum_p \frac{\beta^2}{2N_c^2}\mathrm{Tr}(\square + \square)$ of eq. (1.13) with the corresponding results of refs. [9, 27] in the first figure. As was done in ref. [9] we can re-include the constant part of the Kogut-Susskind Hamiltonian $H_{KS} = \frac{g^2}{2}\left(\sum_{l,a} E_l^a E_l^a + \sum_p \frac{2}{g^4 a^2}\mathrm{Tr}\left(2 - \square - \square\right)\right)$ of eq. (1.11) and the right pre-factor to get the energy density $\frac{\epsilon_0}{N} = a\langle H_{KS}\rangle$. The second figure shows our results for $\frac{\epsilon_0}{N}$ compared with that of ref. [9]. Note that in ref. [9] a different definition of β was used ($2\tilde{\beta} = \beta$).

In section 4.3 we will see that at $\beta = \frac{2N_c}{g^2 a} \approx 6$ we get an approximate scaling window. In this region of coupling we obtain a satisfactory agreement with refs. [9, 27] and up to $\beta \approx 7$ we have a good convergence. As was already the case for the SU(2) results in ref. [64] the convergence of the energy density seems to be alternating at best.

Our iteration procedure breaks down for larger β, e.g. in the order $\delta = 5$ already at $\beta \approx 11.5$. The analytic variational approach of ref. [9], with a ground state which is approximated by a one plaquette trial state only, reaches much larger β. They present results up to $\beta \approx 40$ ($\tilde{\beta} \approx 20$). Below we shall try to implement their data for the vacuum wave function in our calculations to investigate whether such simple, but stable vacuum state provides a better starting point for calculating glueball masses.

4.2.3 Vacuum wave function

Solving the vacuum equation we automatically get all components of the vacuum wave function $\Psi_0 = \exp(\sum_{\alpha>0} S_\alpha \eta^\alpha)$. In table 4.2 we present the most important amplitudes S_α of the components in the symmetry projected basis η at $\beta = 6$, where we assume our scaling window. We also depict the corresponding loop space basis elements χ^α.

We show the basis elements up to the order $\delta = 3$, but the calculations are done in the order $\delta = 5$. The most important amplitude of the 4th order basis states has the value

$$10^3 \cdot S_{57} = 0.11$$

and in the 5th order the largest amplitude is:

$$10^3 \cdot S_{827} = -0.02\,.$$

These values are more than one order of magnitude smaller than the values of the 3rd order basis states. Though the number of basis elements (see table 4.1) is growing rapidly with increasing order, we see that the components are very small. Thus we have a good convergence with the order.

The most important component is the plaquette function with the amplitude S_1. This holds for all β also for calculations in orders $\delta < 5$. The weight of S_1, i.e. the square of the amplitude in the basis η, is nearly 99% for all orders up to $\beta \approx 7$. Therefore in fig. 4.3 we present the amplitude S_1 as a function of β for the different orders and compare it with the vacuum wave function of ref. [9], which is approximated by the plaquette term only. Up to $\beta \approx 6$ the amplitude S_1, which mostly determines our vacuum wave function, does not differ much from the coefficient of the plaquette of ref. [9]. At higher β other components than the plaquette function become more important in our method and a comparison is no longer possible.

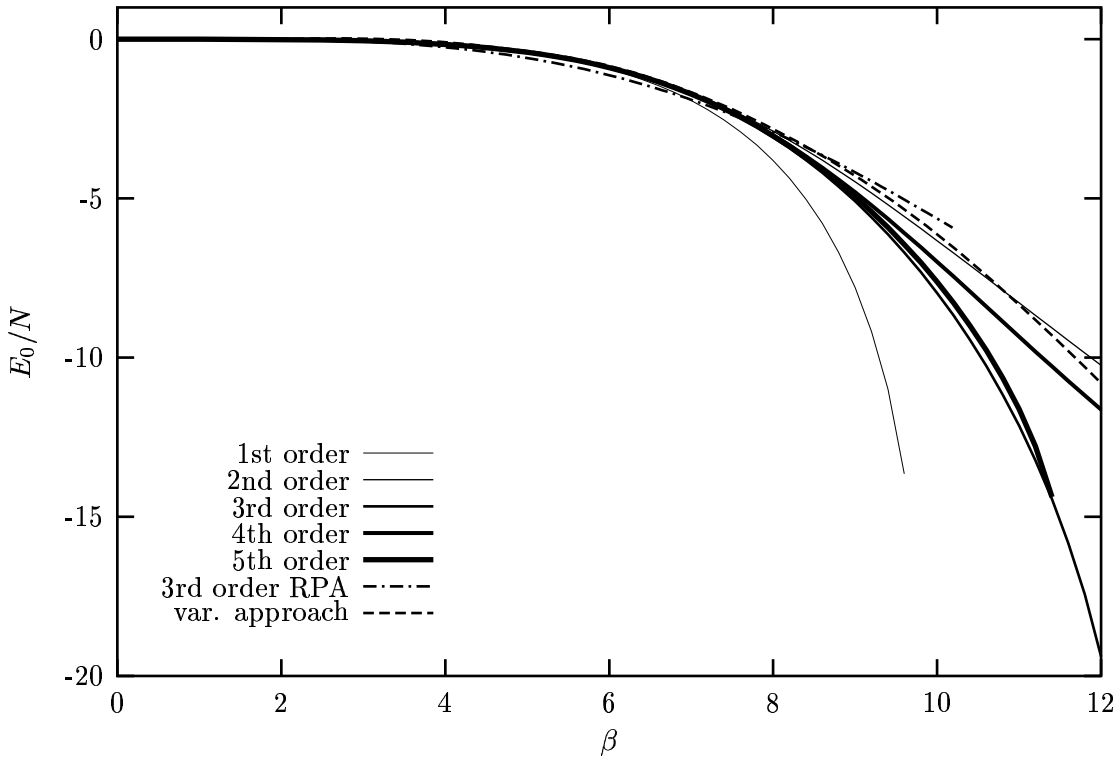

Figure 4.1: Vacuum energy density of the dimensionless Hamiltonian as a function of the inverse coupling $\beta = \frac{2N_c}{g^2 a}$ up to 5th order. For comparison: Analytic variational approach (var. approach) [9] and application of the random phase approximation (3rd order RPA) to the coupled cluster expansion [27].

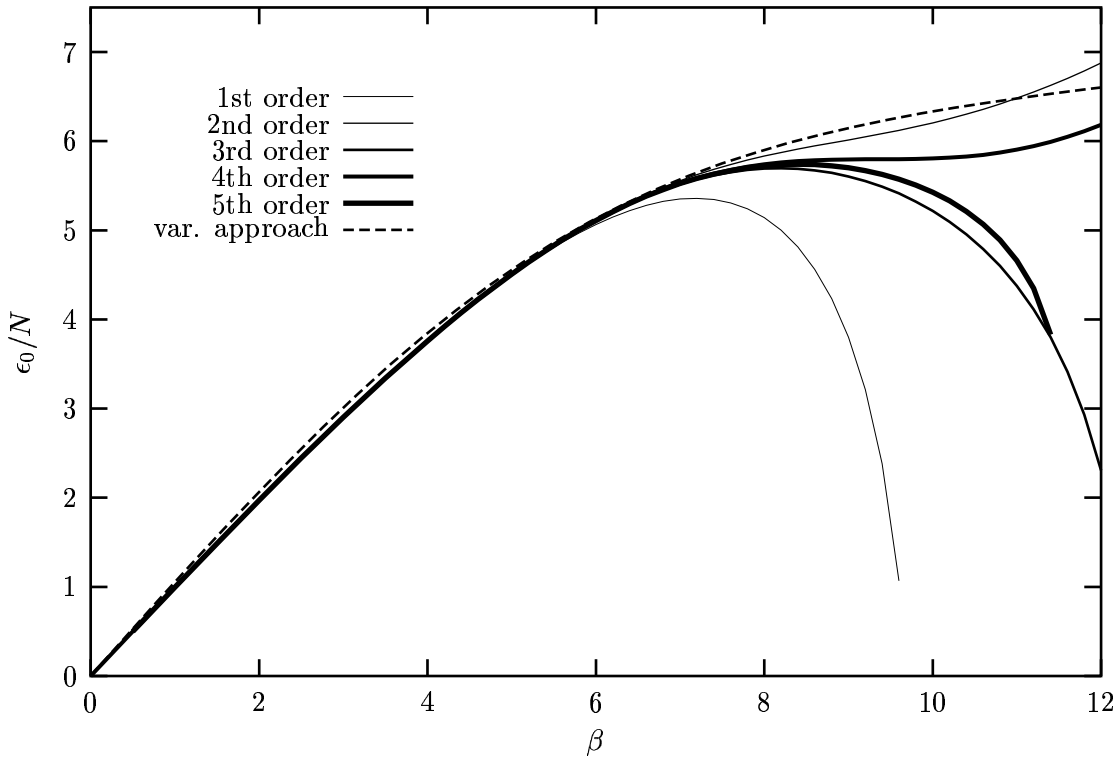

Figure 4.2: Vacuum energy density including the constant part in the Kogut-Susskind Hamiltonian as a function of the inverse coupling $\beta = \frac{2N_c}{g^2 a}$ up to 5th order. For comparison: Analytic variational approach (var. approach) [9].

Table 4.2: The largest components of the vacuum correlation function S and their amplitudes for $\beta = 6$.

δ	χ^α	$10^3 \cdot S_\alpha$
1	$\chi^1 =$ 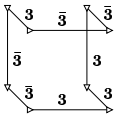	$10^3 \cdot S_1 = 575.92$
2	$\chi^6 =$ 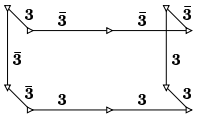	$10^3 \cdot S_6 = 20.57$
	$\chi^4 =$ 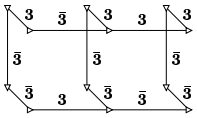	$10^3 \cdot S_4 = -14.35$
	$\chi^2 =$ 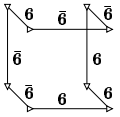	$10^3 \cdot S_2 = -12.22$
	$\chi^3 =$ 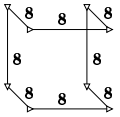	$10^3 \cdot S_3 = -10.61$
	$\chi^5 =$ 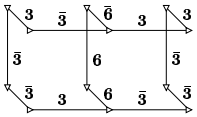	$10^3 \cdot S_5 = -8.46$
	$\chi^7 =$ 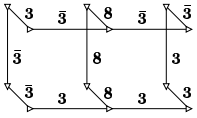	$10^3 \cdot S_7 = -5.31$
3	$\chi^9 =$ 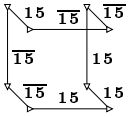	$10^3 \cdot S_9 = 1.19$
	$\chi^{12} =$ 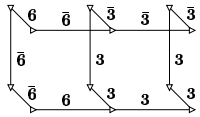	$10^3 \cdot S_{12} = -1.17$
	$\chi^{39} =$ 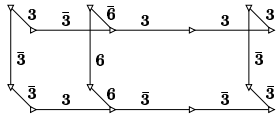	$10^3 \cdot S_{39} = -1.07$
	$\chi^{14} =$ 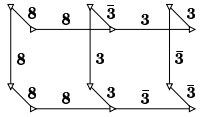	$10^3 \cdot S_{14} = -1.05$
	$\chi^{10} =$ 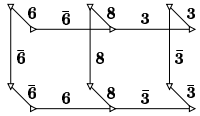	$10^3 \cdot S_{10} = 0.82$

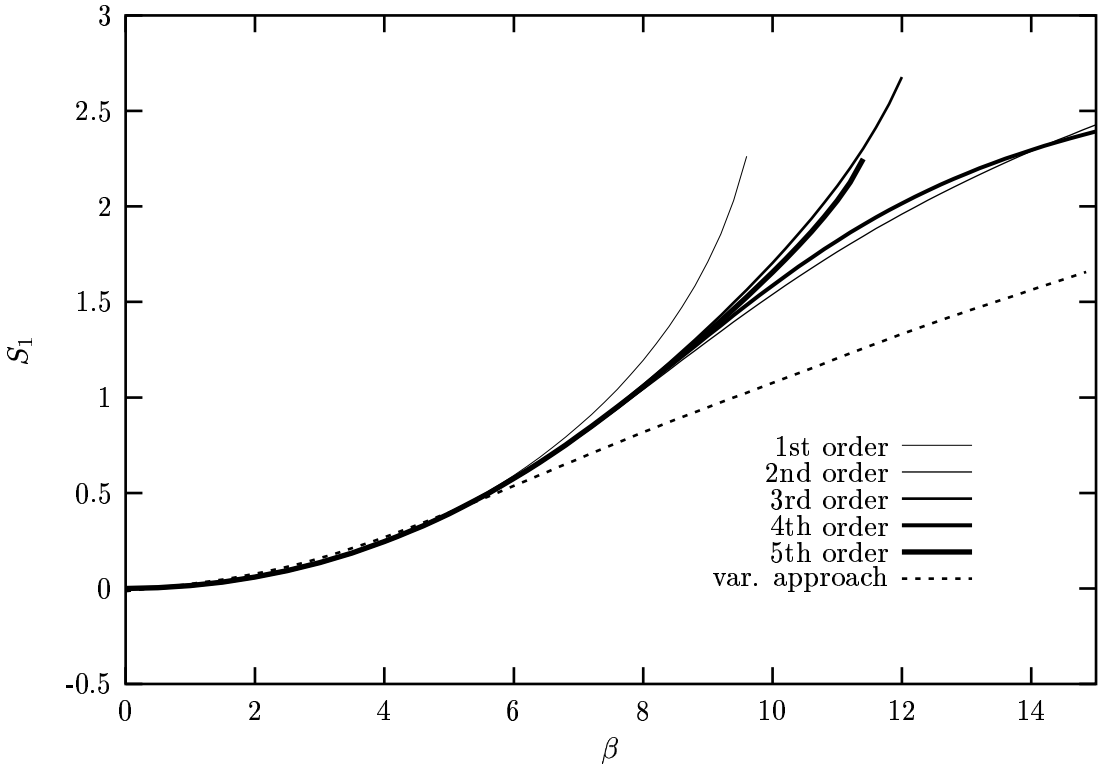

Figure 4.3: The amplitude S_1 of the plaquette function as function of the inverse coupling $\beta = \frac{2N_c}{g^2 a}$ up to 5th order. For comparison: Analytic calculation of the variational parameter of the vacuum wave function of ref. [9], which is approximated by a one plaquette term.

4.2.4 Improvement

As described in section 1.3 for the implementation of classical improvement and tadpole improvement in the Hamiltonian formulation we have to perform the substitution of eq. (1.33) and calculate the mean value u_0 of the link variable via the plaquette expectation value

$$u_0 = \langle 0| \frac{1}{2N_c} \mathrm{Tr} \left(\square + \square \right) |0\rangle^{\frac{1}{4}} .$$

Fig. 4.4 gives the result for u_0 as a function of β and fig. 4.5 shows the improved vacuum energy density.

With an improved Hamiltonian one implements an alternative regularisation scheme with the same continuum limit as in the unimproved case. This is the reason for the different weak coupling behaviour of the improved vacuum and the unimproved one (see fig. 4.5) and for the change of the scales of β. As we will see below in section 4.3 we assume that the scaling region is shifted from $\beta \approx 6$ in the unimproved case to $\beta \approx 3$ in the improved one. Up to this region we find similar convergence properties as before for both the mean link value u_0 and the vacuum energy density. At larger β our method again breaks down.

For the mean link value we get the following value in 5th order at $\beta = 3$:

$$u_0 \approx 0.77 .$$

The improved vacuum wave function is very similar to the unimproved one and we refer to the discussion in the previous section.

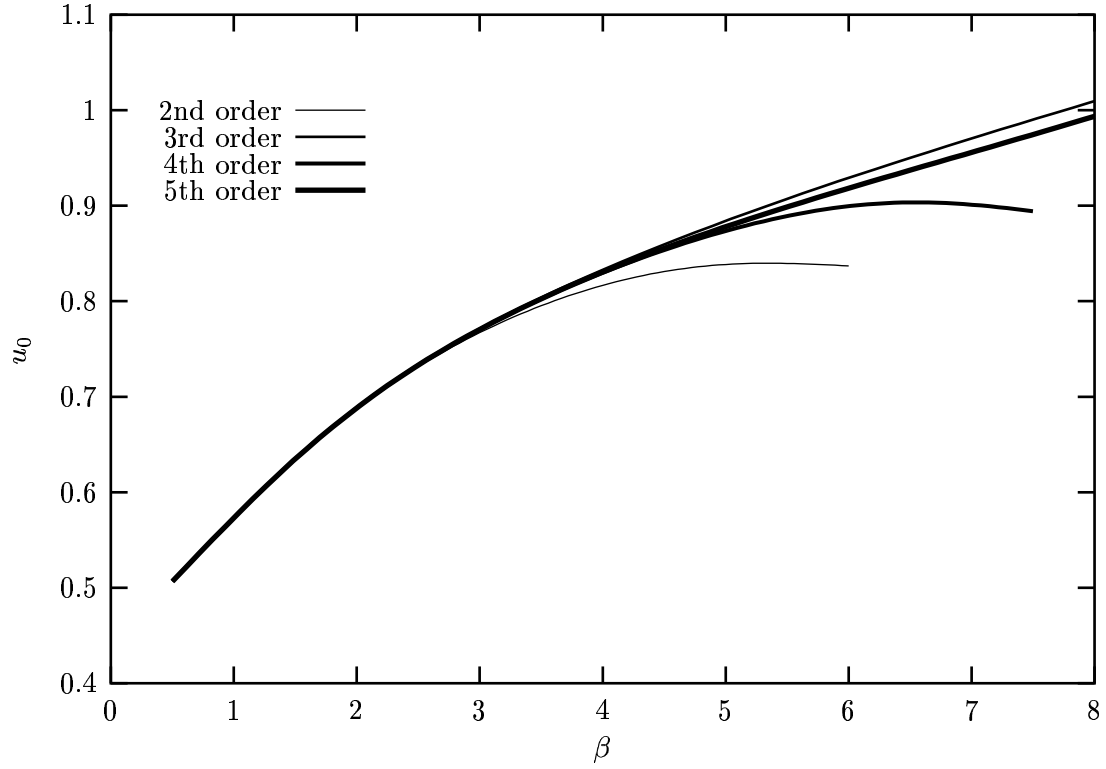

Figure 4.4: Mean link value u_0 as function of the inverse coupling $\beta = \frac{2N_c}{g^2 a}$ up to 5th order.

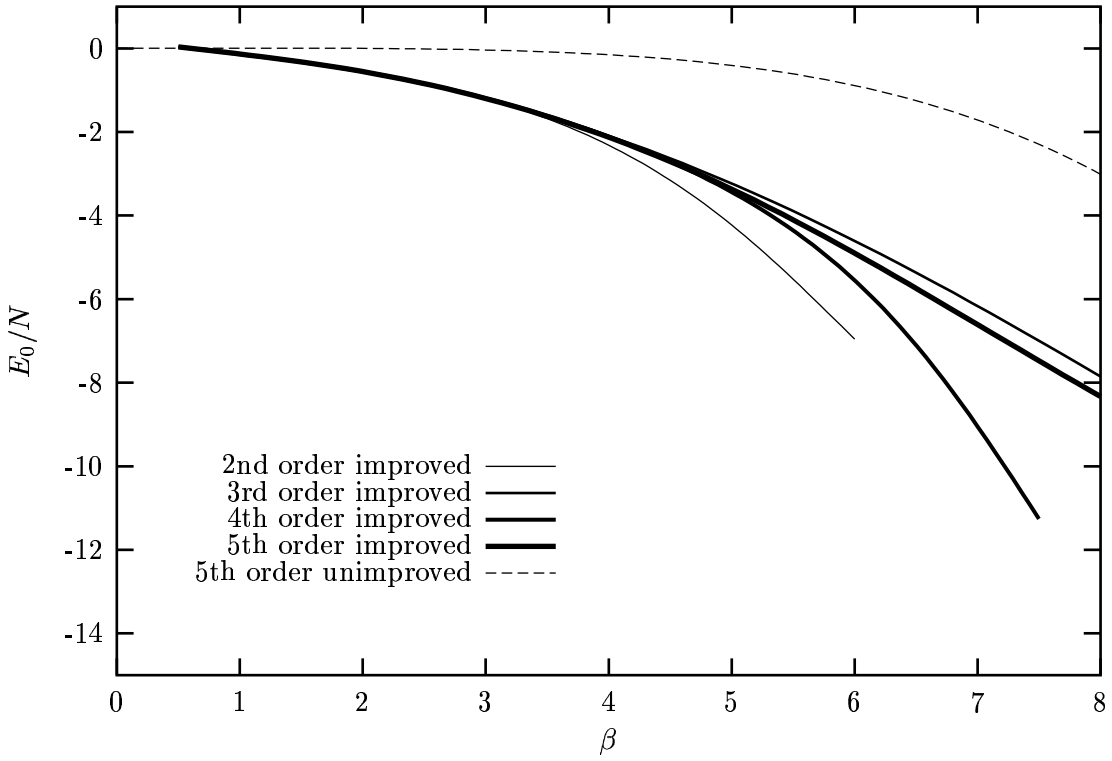

Figure 4.5: Improved vacuum energy density as a function of the inverse coupling $\beta = \frac{2N_c}{g^2 a}$ up to 5th order. For comparison: Unimproved vacuum energy density in 5th order.

4.3 Glueball states

We start this section by presenting the method of solving the coupled cluster equations for the excited (glueball) states. Then we will discuss the strong coupling spectra, because they already show properties of the whole glueball spectra, which will be given afterwards for the improved and the unimproved case. In particular we will emphasise the 0^{++} glueball. Then we will discuss the most important components of the glueball wave functions. To infer the scaling region we will present mass ratios, i.e. quantities which should be independent of the lattice spacing in the scaling region. At the end of this section we will calculate mean values of data of various orders and of the improved and the unimproved lattice to get a final estimate for our glueball spectrum.

We will compare our results to standard lattice Monte Carlo calculations of ref. [60], to results of the analytic variational approach of ref. [9], to the analytic studies of ref. [53] and to the application of random phase approximation to the coupled cluster expansion in ref. [18].

4.3.1 Solving the excited state equations

The equation for the glueball states (1.32) is a simple eigenvalue equation for the excitation operator $F^{J^{PC}}$:

$$\begin{aligned} \epsilon_{\alpha_3} F^{J^{PC}}_{\alpha_3} + 2 \sum_{\alpha_1>0,\alpha_2} S_{\alpha_1} F^{J^{PC}}_{\alpha_2} C^{\alpha_1,\alpha_2}_{\alpha_3,\nu_2\nu_3}(J^{PC}) &= (E-E_0) F^{J^{PC}}_{\alpha_3}\,, \\ \text{or} \sum_{\alpha_2} A_{\alpha_3\alpha_2} F^{J^{PC}}_{\alpha_2} &= (E-E_0) F^{J^{PC}}_{\alpha_3}\,, \end{aligned}$$

where ν_2 and ν_3 denote the indices of the coupled cluster matrix element. The matrix A has the following form:

$$A_{\alpha_3\alpha_2} = \epsilon_{\alpha_3} + 2 \sum_{\alpha_1>0} S_{\alpha_1} C^{\alpha_1,\alpha_2}_{\alpha_3,\nu_2\nu_3}(J^{PC})\,.$$

It is a huge, non-symmetric, sparse matrix. The Arnoldi method is used to find extreme eigenvalues of A by successive transformation to smaller matrices H. It has already been implemented for SU(2) glueballs (see ref. [64]) via the Meschach package (see ref. [55]).

The size of the matrices A occurring in the calculations of SU(3) glueball masses is given by the number of elements of the symmetry projected basis η for the quantum number under consideration (see table 4.1). The largest matrix in 5th order we have to handle has the size 745705×745705 and occurs in the $1^{\pm-}$ sector.

For the size of the matrix H we have checked that the results do not vary any more, if we choose in 4th order a 100×100 matrix and in 5th order a 150×150 matrix.

4.3.2 Strong coupling spectra

In the strong coupling limit $g \to \infty, \beta = \frac{2N_c}{g^2 a} \to 0$ the Hamiltonian has the form $H \to \sum_{l,a} E^a_l E^a_l$. The loop space basis vectors χ^α and therefore as well the vectors

η^α of the symmetry projected basis are via construction (see eq. (2.5)) strong coupling eigenfunctions

$$\sum_{l,a} E_l^a E_l^a \chi^\alpha = \epsilon_\alpha \chi^\alpha \,.$$

Below we will present the glueball masses in the assumed scaling region $\beta \approx 6$ and we will see that they do not differ much from the eigenvalues in the strong coupling limit $\beta \to 0$.

Table 4.3 on the following two pages gives the nine lowest strong coupling eigenvalues up to the 3rd order, the corresponding vectors χ^α, and their internal symmetries under symmetry transformations on the lattice (see chapter 3) in the charge parity plus and the charge party minus sector.

Note that here we present the strong coupling eigenvalues $\frac{1}{2}\epsilon_\alpha$. We include the factor $\frac{1}{2}$ of the Kogut-Susskind Hamiltonian (see eq. (1.11)).

The upper index at an eigenvalue in the table represents the multiplicity, i.e. that there are more than one eigenstates, which are degenerate. This can occur in the $1^{\pm+}$ and the $1^{\pm-}$ sectors, which are represented by two-dimensional irreducible representations of the group G_{lr} of lattice rotations and reflections (see section 3.2).

As discussed in section 3.4.1 the internal symmetries of a basis element determine the contribution of this element to a certain lattice angular momentum/parity and charge parity sector. The plaquette function χ^1 for example does only contribute for positive charge parity to the 0^{++} sector and for negative charge parity to the 0^{--} sector (see the discussion at the end of section 3.4.1) and it has an eigenvalue $\frac{1}{2}\epsilon_1 = \frac{8}{3}$ (see eq. (2.2)).

Therefore also the number of basis elements contributing to a certain sector depends on the internal symmetries (see table 4.1). In the 2nd order we have for example no basis element in the $0^{-+}, 1^{\pm+}, 2^{-+}, 0^{+-}$, and the 2^{+-} sectors and thus have no results for the corresponding glueballs. Not until the 3rd order where basis elements without any internal symmetry occur, e.g. χ^{23}, there are contributions in all sectors.

Up to the 3rd order the lowest strong coupling eigenvalues EV in the different angular momentum/parity and charge parity sectors are:

J^{PC}	0^{++}	0^{-+}	$1^{\pm+}$	2^{++}	2^{-+}	0^{+-}	0^{--}	$1^{\pm-}$	2^{+-}	2^{--}
EV up to 3rd order	$\frac{8}{3}$	6	$\frac{16}{3}$	4	$\frac{16}{3}$	6	$\frac{8}{3}$	$\frac{14}{3}$	$\frac{16}{3}$	4
lower lying EV in 4th order		$\frac{16}{3}$				$\frac{16}{3}$				

In the 4th order a new basis element

$\chi^{199} =$ 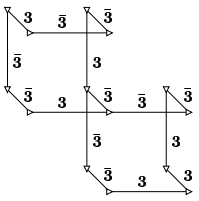

occurs, which has the eigenvalue $\frac{1}{2}\epsilon_{199} = \frac{16}{3}$. This is twice the eigenvalue of the plaquette function. It contributes to the 0^{-+}, 2^{++}, 0^{+-} and 2^{--} sectors. This changes the lowest lying eigenvalues in the 0^{-+} and the 0^{+-} sector (see the table above). This new state, which is a two-plaquette state, is called a two-cluster state. Other similar states also occur in 4th order. In some sectors they have a large contribution not only in the strong coupling limit, but also in the scaling region. Therefore these states will be discussed in some detail in section 4.3.4.

In the complete eigenvalue spectra given in the next section we can identify the strong coupling properties as the lowest eigenvalues and the two-cluster states discussed above.

Table 4.3: The nine lowest strong coupling eigenvalues, the corresponding loop space basis elements χ^α, and their internal symmetries (int. sym.) under symmetry transformations on the lattice in the charge parity plus $C = +$ and the charge party minus sector $C = -$.

δ	χ^α		$C=+$ int. sym.	0^{++}	0^{-+}	$1^{\pm+}$	2^{++}	2^{-+}	$C=-$ int. sym.	0^{+-}	0^{--}	$1^{\pm-}$	2^{+-}	2^{--}
1	χ^1	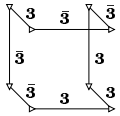	$G^{8a}, j_{8a}=0^+$	$\frac{8}{3}$	-	-	-	-	$G^{8a}, j_{8a}=0^-$	-	$\frac{8}{3}$	-	-	-
2	χ^6	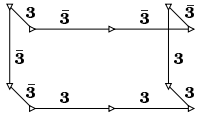	$G^{4b}, j_{4b}=0$	4	-	-	4	-	$G^{4b}, j_{4b}=3$	-	4	-	-	4
2	χ^4	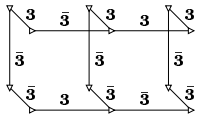	$G^{4b}, j_{4b}=0$	$\frac{14}{3}$	-	-	$\frac{14}{3}$	-	$G^{4b}, j_{4b}=1$	-	-	$\frac{14}{3}$	-	-
3	χ^{42}	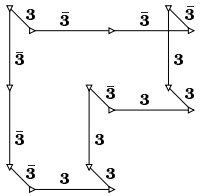	$G^{2e}, j_{2e}=0$	$\frac{16}{3}$	-	$\frac{16}{3}$	-	$\frac{16}{3}$	$G^{2e}, j_{2e}=1$	-	$\frac{16}{3}$	$\frac{16}{3}$	$\frac{16}{3}$	-
3	χ^{48}	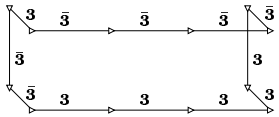	$G^{4b}, j_{4b}=0$	$\frac{16}{3}$	-	-	$\frac{16}{3}$	-	$G^{4b}, j_{4b}=3$	-	$\frac{16}{3}$	-	-	$\frac{16}{3}$
2	χ^7	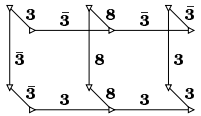	$G^{4b}, j_{4b}=0$	$\frac{11}{2}$	-	-	$\frac{11}{2}$	-	$G^{4b}, j_{4b}=3$	-	$\frac{11}{2}$	-	-	$\frac{11}{2}$
2	χ^5	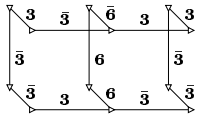	$G^{4b}, j_{4b}=0$	$\frac{17}{3}$	-	-	$\frac{17}{3}$	-	$G^{4b}, j_{4b}=1$	-	-	$\frac{17}{3}$	-	-
2	χ^3	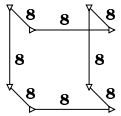	$G^{8a}, j_{8a}=0^+$	6	-	-	-	-	-	-	-	-	-	-

3	χ^{23}	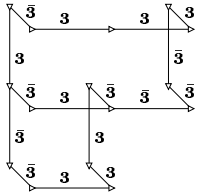	$G^{1a}, j_{1a}=0$	6	6	6^2	6	6	$G^{1a}, j_{1a}=0$	6	6	6^2	6	6
3	χ^{29}	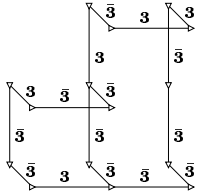	$G^{1a}, j_{1a}=0$	6	6	6^2	6	6	$G^{1a}, j_{1a}=0$	6	6	6^2	6	6
3	χ^{38}	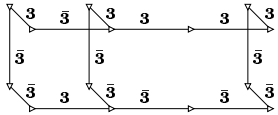	$G^{2b}, j_{2b}=0$	6	-	6	6	-	$G^{2b}, j_{2b}=1$	-	6	6	-	6
2	χ^{2}	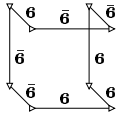	$G^{8a}, j_{8a}=0^+$	$\frac{20}{3}$	-	-	-	-	$G^{8a}, j_{8a}=0^-$	-	$\frac{20}{3}$	-	-	-
3	χ^{17}	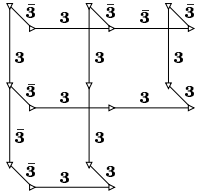	$G^{2e}, j_{2e}=1$	-	$\frac{20}{3}$	$\frac{20}{3}$	$\frac{20}{3}$	-	$G^{2e}, j_{2e}=0$	$\frac{20}{3}$	-	$\frac{20}{3}$	-	$\frac{20}{3}$
3	χ^{18}	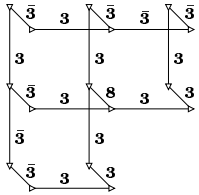	$G^{2e}, j_{2e}=1$	-	$\frac{20}{3}$	$\frac{20}{3}$	$\frac{20}{3}$	-	$G^{2e}, j_{2e}=0$	$\frac{20}{3}$	-	$\frac{20}{3}$	-	$\frac{20}{3}$
3	χ^{35}	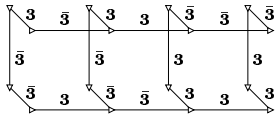	$G^{4b}, j_4 b=0$	$\frac{20}{3}$	-	-	$\frac{20}{3}$	-	$G^{4b}, j_{4b}=3$	-	$\frac{20}{3}$	-	-	$\frac{20}{3}$

4.3.3 Eigenvalue spectra

Here we first present the eigenvalue spectra for all possible glueballs and then discuss in particular the lowest 0^{++} glueball.

The energy spectra of all glueballs

In figs. 4.6, 4.7, 4.8 and 4.9 we show the energy eigenvalues $M = \frac{1}{2}(E - E_0)$ for the unimproved and the improved Hamiltonian as a function of the inverse coupling $\beta = \frac{2N_c}{g^2 a}$. In the 0^{++} and the 0^{--} sectors we show the lowest three and in the other sectors the lowest two eigenvalues. The different lines denote the different orders:

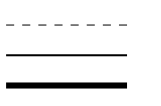

For the data with improvement calculations for $\beta \approx 0$ are difficult as $u_0(\beta = 0) = 0$ and the Hamiltonian contains $\frac{1}{u_0^4}$. Thus the plots start at $\beta = 0.5$. Comparing the results of the unimproved Hamiltonian with the improved ones we again see the change of the scale, but no real effect of improvement in reaching the continuum limit. This was already the case for the SU(2) glueballs (see ref. [64]), where we chose a similar improvement. To get a better continuum limit involves a very delicate choice of the parameters which we are not able to calculate. In our formulation "improvement" is essentially an alternative regularisation scheme with the same continuum limit, as we will also see when we examine mass ratios in section 4.3.5.

Comparing the 3rd order results with the ones in the 4th order we see, that in the higher order new lower lying states appear. This effect is due to two-cluster states and was already seen in the strong coupling spectra (see section 4.3.2). It occurs in the 0^{+-}, 0^{-+}, 2^{-+}, 2^{+-} and the $1^{\pm-}$ sectors. We will discuss it when examining the glueball wave functions in the next section.

The plots show that in some sectors we have problems with complex eigenvalues. This is due to the non-symmetric structure of the eigenvalue equations of the excitation operator expanded in a truncated basis (see section 4.3.1). Complex eigenvalues occur in complex conjugate pairs, are real for $\beta = 0$. There is a point at which two curves unite to a third curve representing the (common) real part of the two complex eigenvalues. We can find this effect for example in the 0^{++} sector in the 4th order. These complex eigenvalues mostly appear at $\beta > 6$ in the unimproved and at $\beta > 3$ in the improved case. After inspecting our data we will omit these values for the final result, when they occur in our scaling region. For this reason we will in the following not present results for the 2^{++*} and the $1^{\pm+*}$ glueball any more.

In addition to complex eigenvalues there occur level-crossings, e.g. in the $1^{\pm-}$ sector and also in the 2^{+-} sector, where, because we only give the lowest curve, the sharp bend reflects the point of level-crossing.

At higher β the effect of the break down of iteration procedure for the vacuum is seen, but altogether we can state that up to $\beta \approx 6$ ($\beta \approx 3$ with improvement) the results in most sectors are reliable.

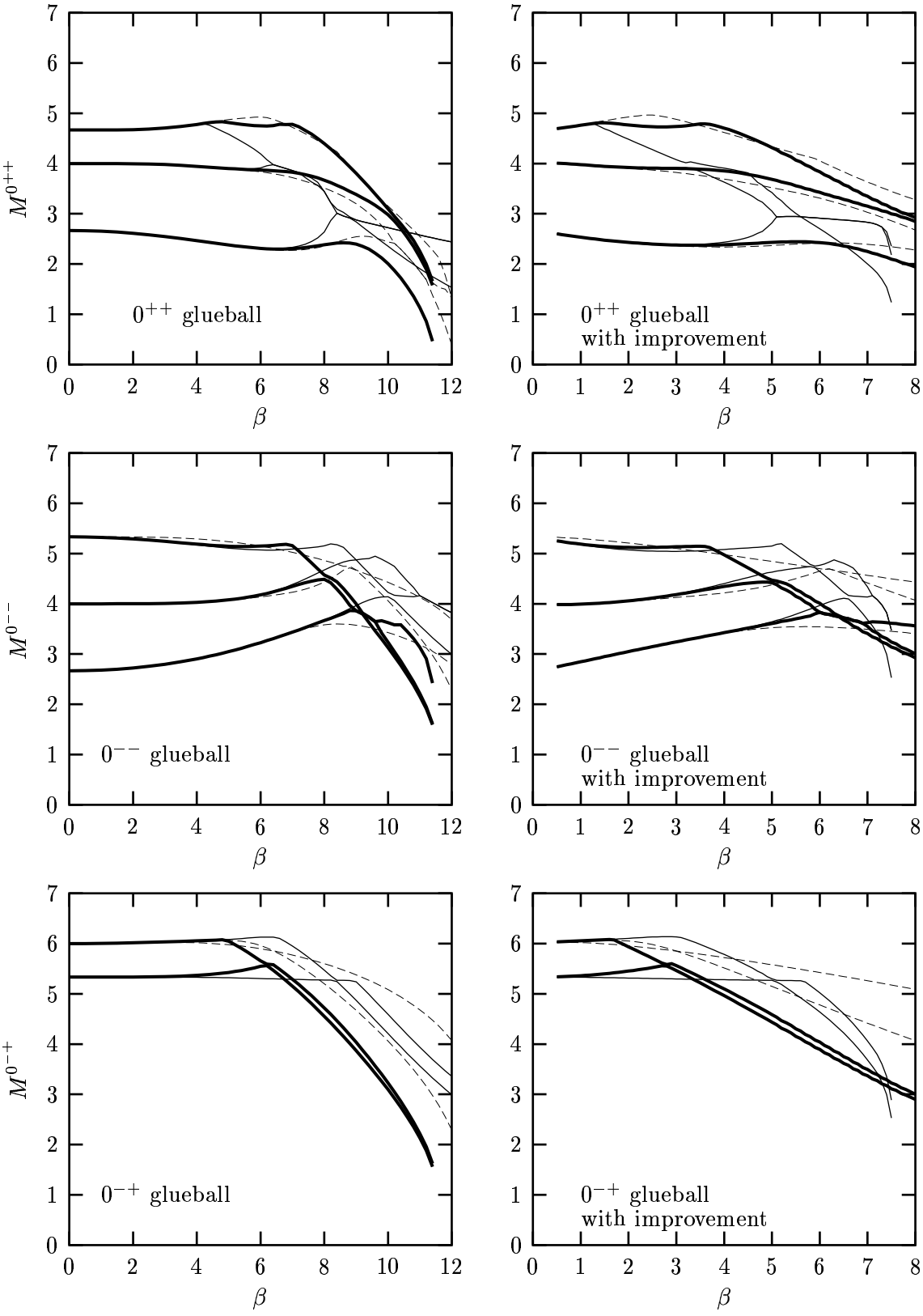

Figure 4.6: Excited $0^{++}, 0^{--}, 0^{-+}$ state energy as a function of the inverse coupling $\beta = \frac{2N_c}{g^2 a}$ up to 5th order without and with improvement.

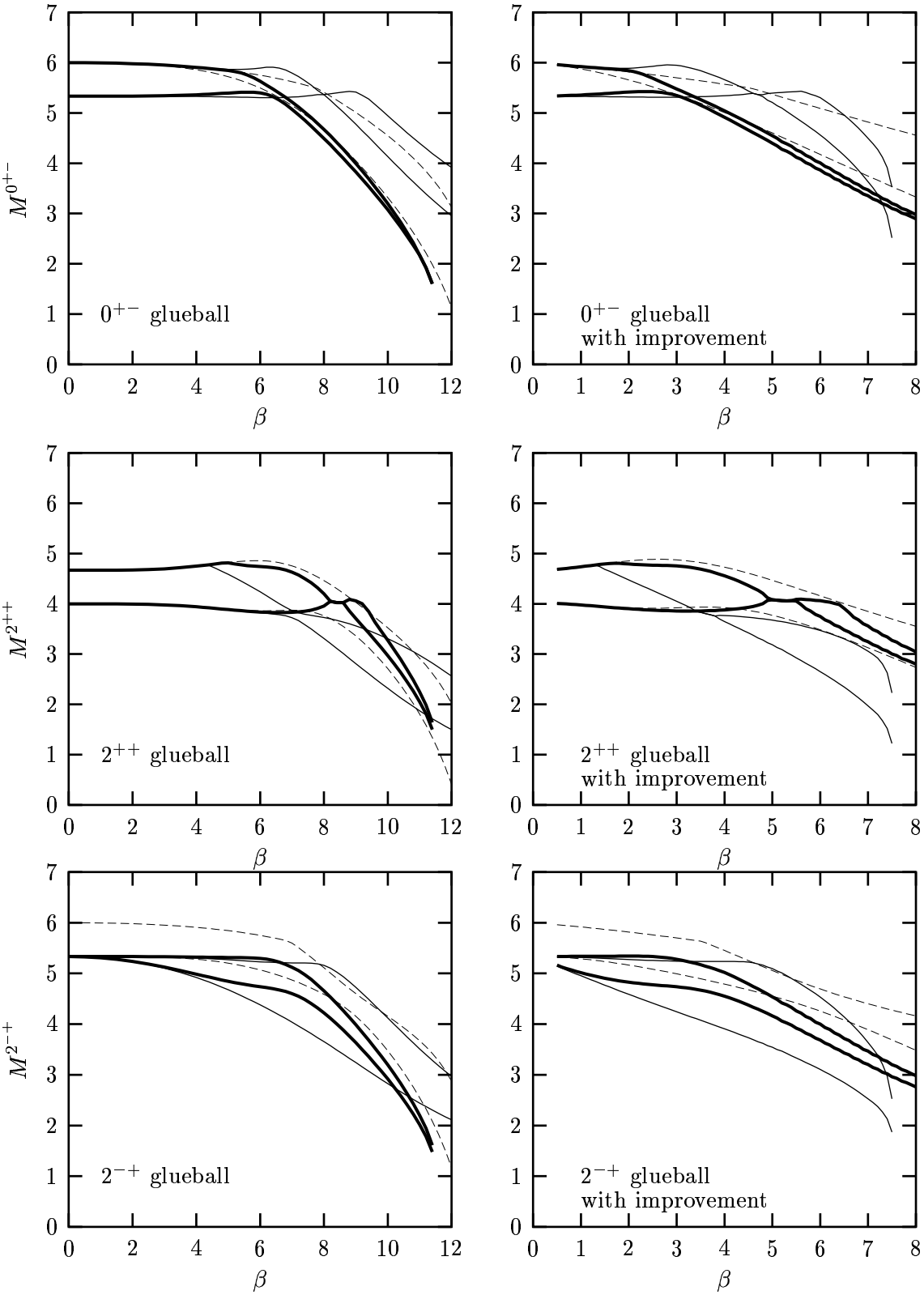

Figure 4.7: Excited $0^{+-}, 2^{++}, 2^{-+}$ state energy as a function of the inverse coupling $\beta = \frac{2N_c}{g^2 a}$ up to 5th order without and with improvement.

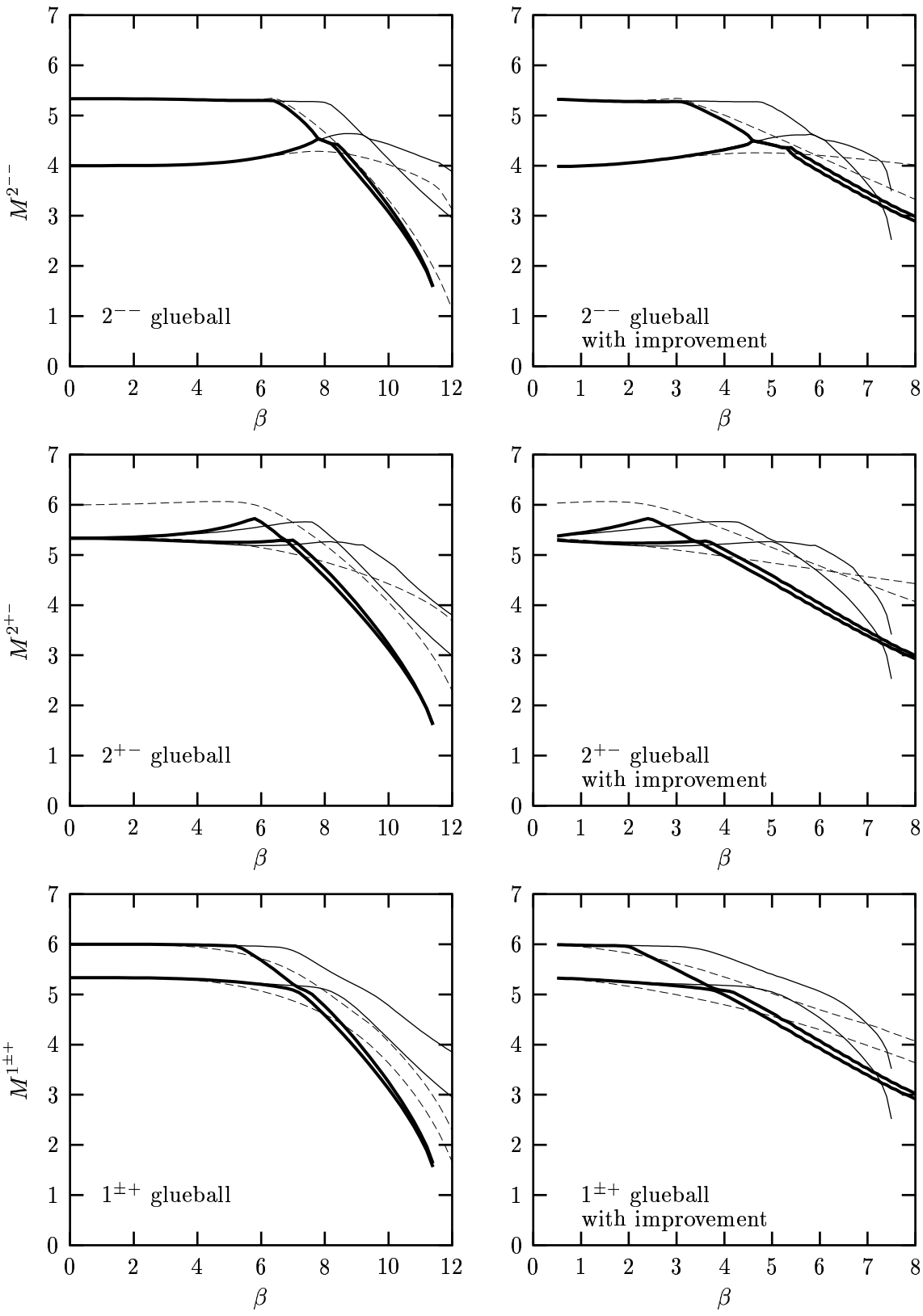

Figure 4.8: Excited 2^{--} 2^{+-}, $1^{\pm+}$ state energy as a function of the inverse coupling $\beta = \frac{2N_c}{g^2 a}$ up to 5th order without and with improvement.

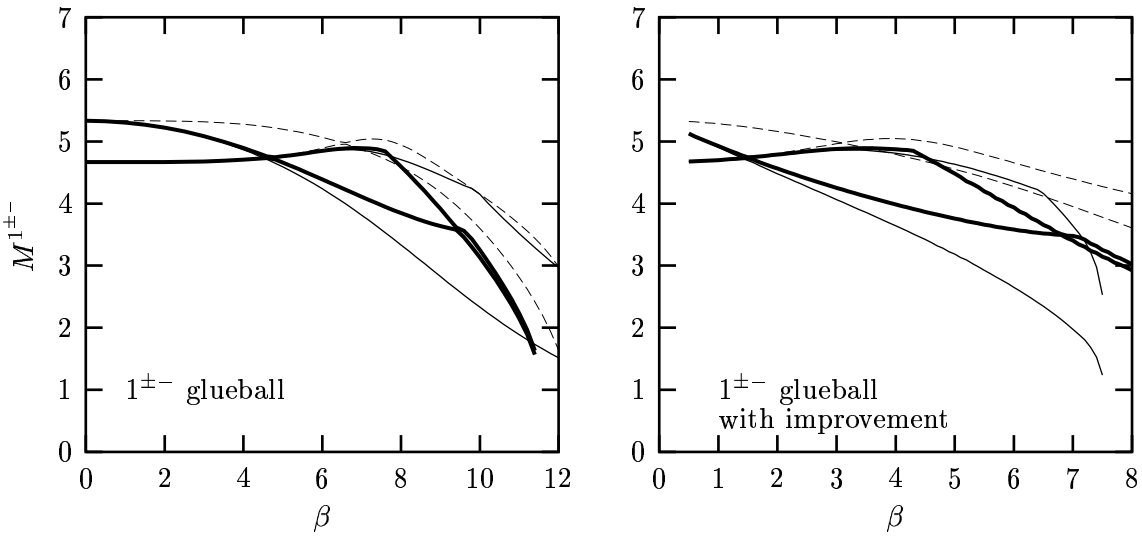

Figure 4.9: Excited $1^{\pm-}$ state energy as a function of the inverse coupling $\beta = \frac{2N_c}{g^2 a}$ up to 5th order without and with improvement.

Lowest 0^{++} glueball

In fig. 4.10 we present the lowest 0^{++} glueball separately without and with improvement.

We see, that up to $\beta \approx 7$ ($\beta \approx 4$ with improvement) the results are reliable and we are able to estimate the mass values within errors. In section 4.3.5 we show that our scaling region is at $\beta \approx 6$ ($\beta \approx 3$ with improvement). At this coupling we get the following values for the 0^{++} glueball mass:

$$\begin{aligned} M^{0^{++}}(\beta = 6) &= 2.31 \text{ (without improvement)} \\ M^{0^{++}}(\beta = 3) &= 2.38 \text{ (with improvement)}\,. \end{aligned}$$

This is a reasonable result compared to the corresponding value of Fang *et al.* [18] 2.13 ± 0.10, the value of Teper [60] 2.39 ± 0.02 and the value of Samuel [53] 1.84 ± 0.46. Carlsson *et al.* [9] gives an upper limit of 3.26520 ± 0.00009 for the mass value.

As we have already mentioned the analytic variational approach of ref. [9], where the vacuum wave function is approximated by the one plaquette term only, provides data at very high β, where our method breaks down. In fig. 4.11 we compare the 0^{++} mass calculated with our vacuum (see section 4.2) and with the coefficient given in ref. [9] for the one plaquette vacuum.

The calculation of the 0^{++} mass with our coupled cluster Ansatz for the vacuum breaks down at $\beta \approx 11.5$ in 5th order (see section 4.2.2). This does not happen if we implement the stable vacuum of ref. [9]. With respect to the behaviour with the orders the "new" 0^{++} glueball behaves in a similar way as the "old" one, but is shifted to a higher β. Later we calculate mass ratios with the same method and obtain a "new" scaling region at $\beta \approx 9$ in contrast to $\beta \approx 6$ for the "old" results. In this "new" scaling region the 0^{++} glueball mass has the value $M^{0^{++}}_{\text{new}}(\beta = 6) = 2.17$ and thus clearly lies below the values given above.

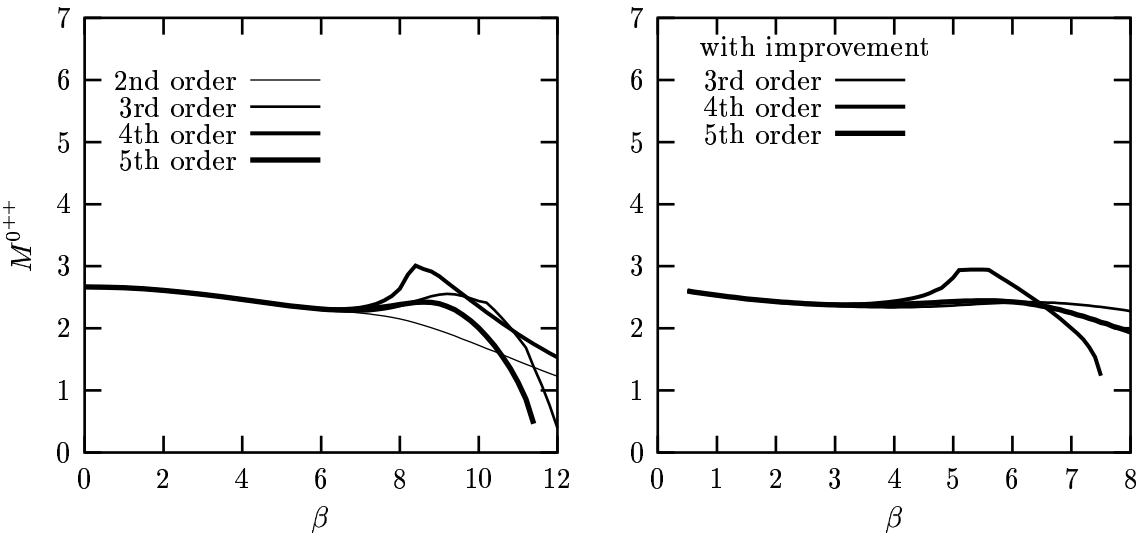

Figure 4.10: Excited 0^{++} state energy as a function of the inverse coupling $\beta = \frac{2N_c}{g^2 a}$ up to 5th order without and with improvement.

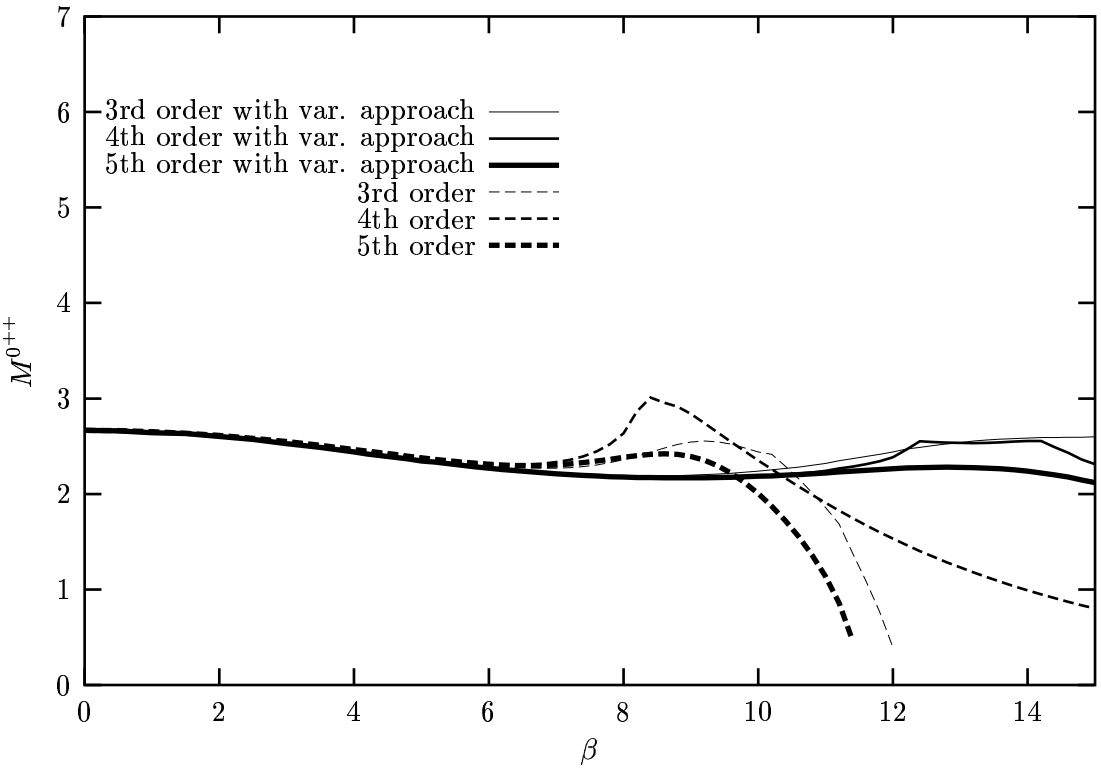

Figure 4.11: Excited 0^{++} state energy as a function of the inverse coupling $\beta = \frac{2N_c}{g^2 a}$ up to 5th order calculated with our coupled cluster vacuum and with the vacuum of the analytic variational approach (var.approach)[9].

4.3.4 Glueball wave functions

In this section we list the most important components of the glueball wave functions in the different angular momentum, parity and charge parity sectors. We will show components for calculations in 5th order at $\beta = 6$, where we see an approximate scaling window (see section 4.3.5) for the unimproved Hamiltonian. With improvement this region is shifted to $\beta \approx 3$. There the corresponding wave functions show a behaviour, which hardly differs from the unimproved case. Thus the discussion presented here is also applicable to the results with improvement.

In contrast to the vacuum state, where the plaquette function provides the dominant contribution, for the excited states also elements of higher orders play an important role.

Having a closer look at the different sectors (see the following three pages) we can roughly distinguish two different types of elements:

One type are components looking like "plaquettes" or "rectangles". They contribute to the 0^{++}, 0^{--}, 2^{++}, 2^{--} and the $1^{\pm+}$ sectors. For the 0^{++} and the 0^{--} glueball wave functions the plaquette function itself is the dominant part, but also a 1×2 rectangle element and even a larger plaquette play a role. In the 2^{++} and the 2^{--} sector we find 1×2 and 1×3 rectangles and in the $1^{\pm-}$ sector a more complicate "plaquette". Altogether the components looking like "plaquettes" and "rectangles" might give evidence for a sensible behaviour with the lattice size. The variational approach of ref. [9] uses only such rectangular states and for the 0^{++} and the 0^{--} glueball they find a perfect scaling behaviour. This suggests to choose a different basis, but we see below that in our calculations not only "rectangle"-like elements have a significant contribution to the wave functions.

The other type of components are called two-cluster states. They are dominant in the 0^{-+}, 0^{+-}, 2^{-+}, 2^{+-} and the $1^{\pm-}$ sectors. These states are two-plaquette states and have the following form

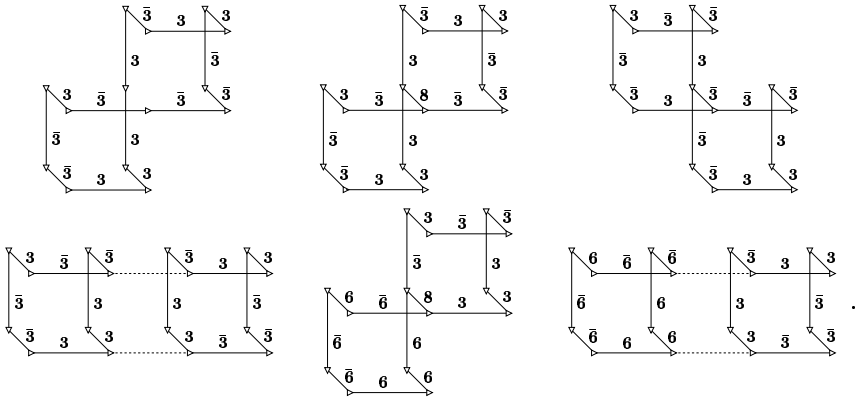

They already occurred (see section 4.3.2) in the strong coupling spectra when we extended the calculations from the 3rd to the 4th order. Trivially they have exactly twice the eigenvalue of the 0^{++} glueball, which is given here by the simple plaquette function. We can identify them in this limit with two-glueball states. In the orders where we are able to calculate these components do not seem to interact much with other elements at higher β. We find often up to $\beta > 6$ ($\beta > 3$ with improvement) straight lines at a value of twice the eigenvalue of the plaquette function (see figs. 4.6, 4.7, 4.8). The occurrence of these two-cluster states we already know from the SU(2) glueball wave functions discussed in

ref. [64]. We assume that in the corresponding sectors the glueball in question lies in the continuum of two (lowest) 0^{++} glueball states.

0^{++} **glueball wave function at** $\beta = 6$

$F^{0^{++}}$:

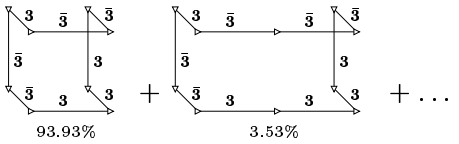

$F^{0^{++*}}$:

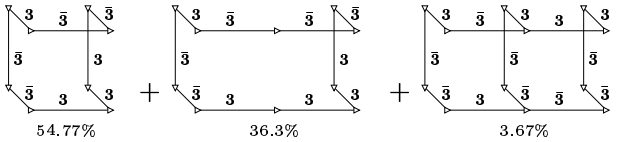

$F^{0^{++**}}$:

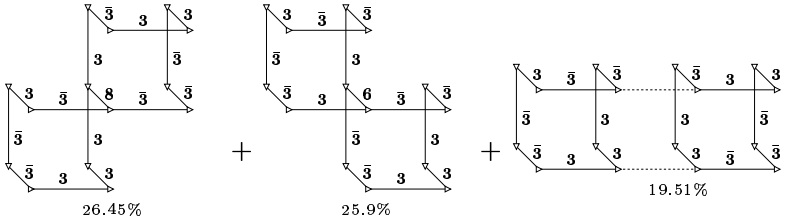

0^{--} **glueball wave function at** $\beta = 6$

$F^{0^{--}}$:

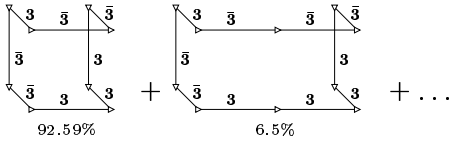

$F^{0^{--*}}$:

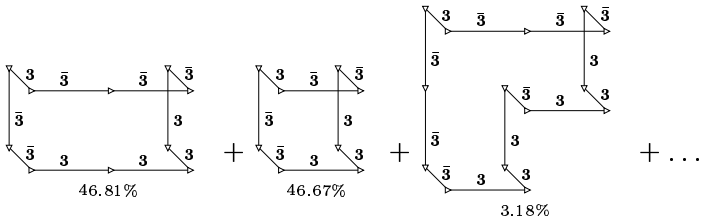

$F^{0^{--**}}$:

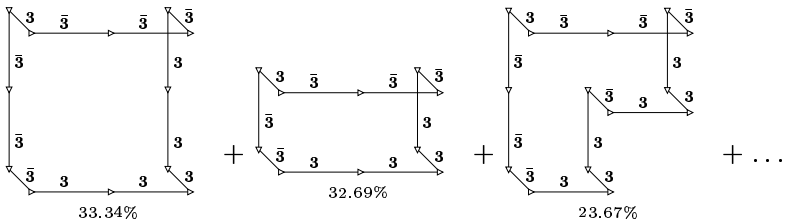

0^{-+} **glueball wave function at** $\beta = 6$

$F^{0^{-+}}$:

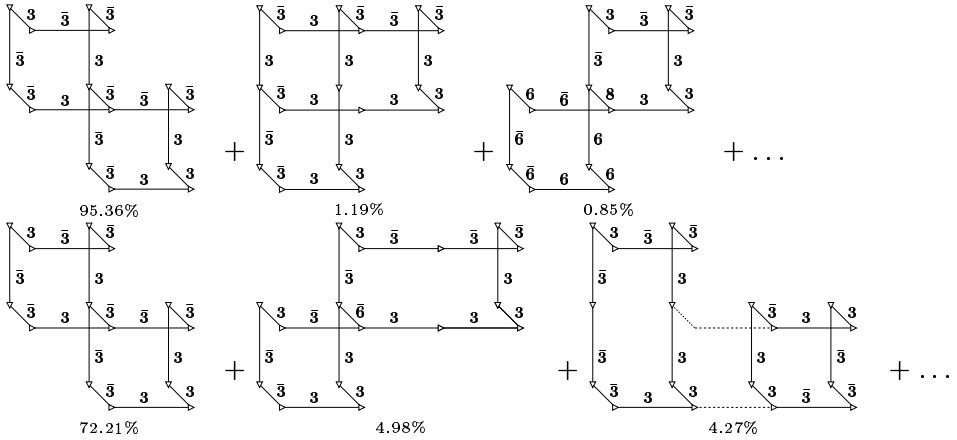

0^{+-} **glueball wave function at** $\beta = 6$

$F^{0^{+-}}$:

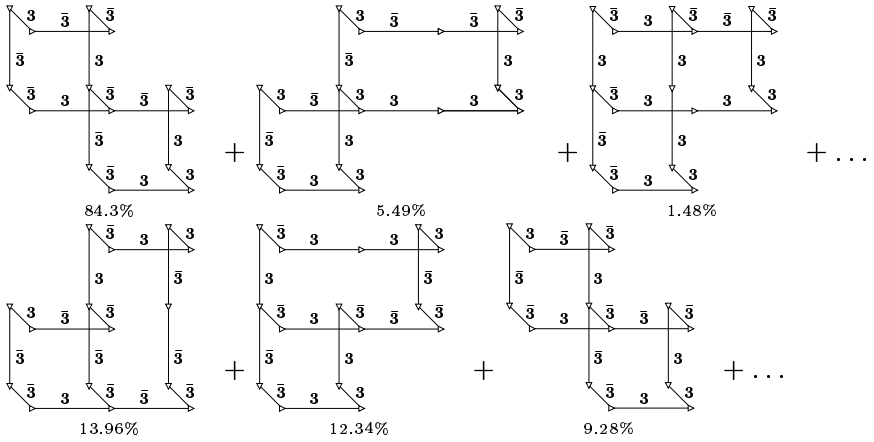

2^{++} **glueball wave function at** $\beta = 6$

$F^{2^{++}}$:

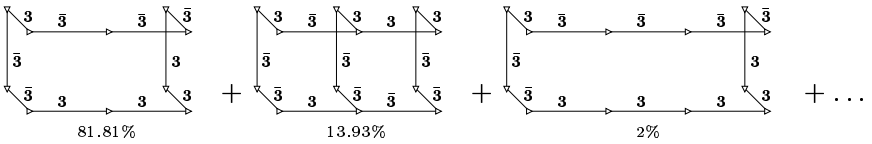

2^{-+} **glueball wave function at** $\beta = 6$

$F^{2^{-+}}$:

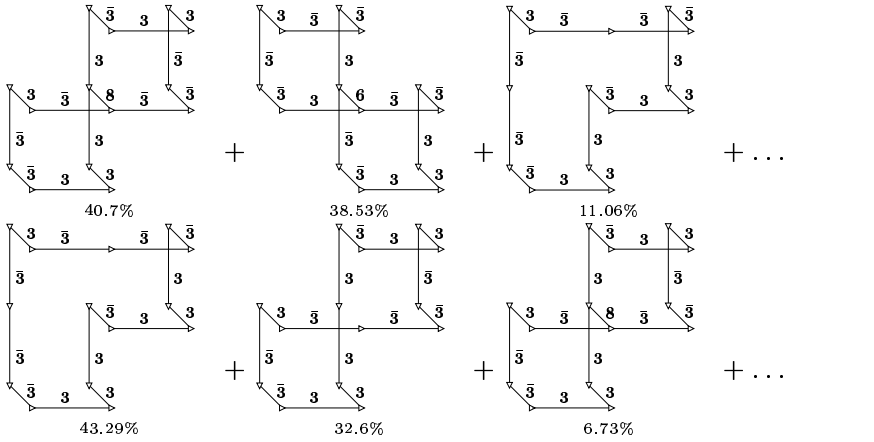

2^{--} **glueball wave function at** $\beta = 6$

$F^{2^{--}}$:

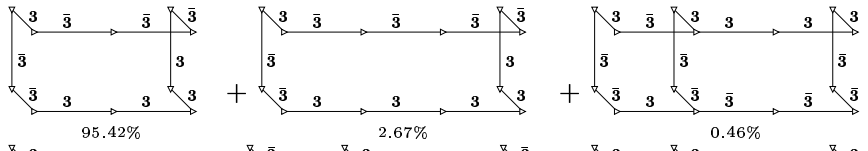

$F^{2^{--*}}$:

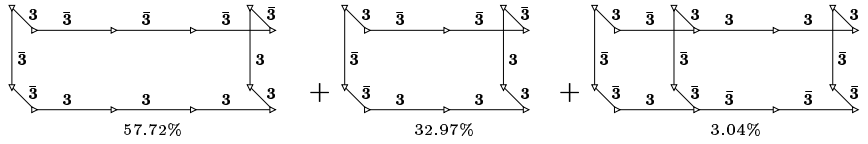

2^{+-} **glueball wave function at** $\beta = 6$

$F^{2^{+-}}$:

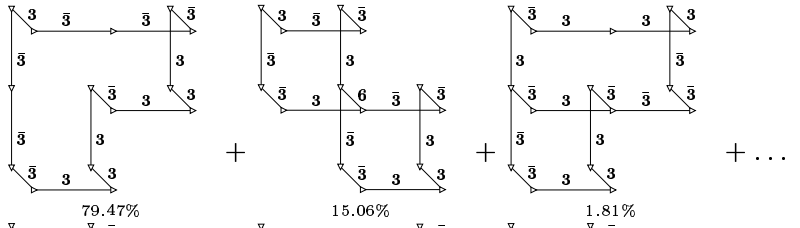

$F^{2^{+-*}}$:

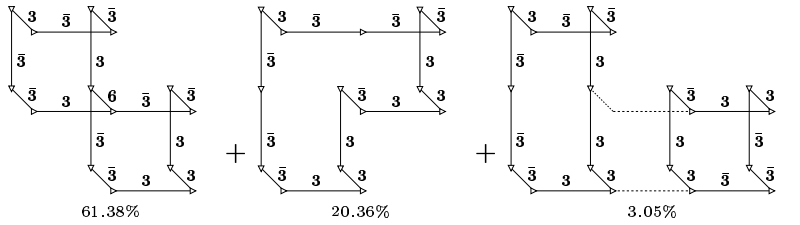

$1^{\pm+}$ **glueball wave function at** $\beta = 6$

$F^{1^{\pm+}}$:

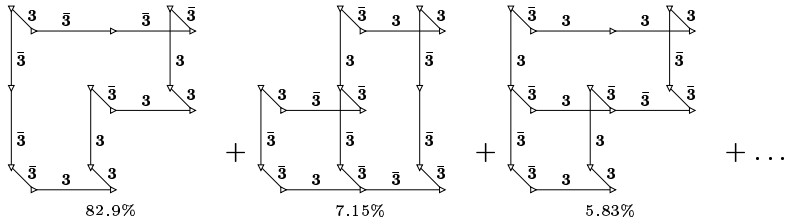

$1^{\pm-}$ **glueball wave function at** $\beta = 6$

$F^{1^{\pm-}}$:

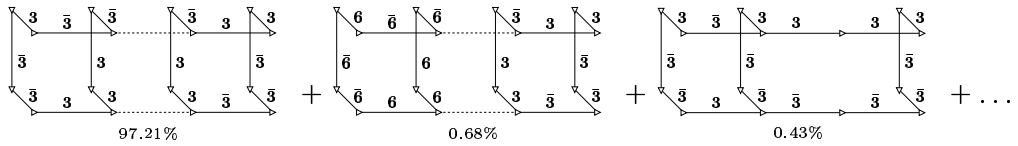

$F^{1^{\pm-*}}$:

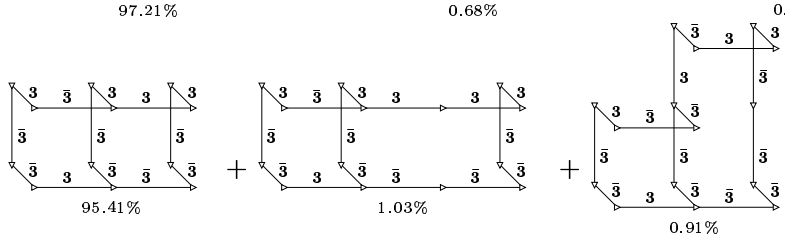

4.3.5 Mass ratios

In this section we first present mass ratios of all excited states relative to the 0^{++} state and then discuss the 0^{--} and the 2^{++} mass gap ratio as special examples.

Mass ratios of the excited states

Mass ratios are dimensionless quantities and should be independent of β in the scaling window. As we mentioned in the introduction this region of coupling contains already continuum physics.

In figs. 4.12, 4.13, 4.14 and 4.15 we show the mass ratios for the different glueballs as a function of the inverse coupling β. We always calculated ratios of data of the same order. In the 0^{++} and the 0^{--} sector we give the lowest three glueballs and in the other sectors the lowest two ones. As the 2^{++*} and the $1^{\pm+*}$ have complex eigenvalues we omit them. The different lines denote the different orders:

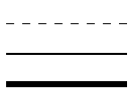

.

For most of the mass ratios we find a stationary region at $\beta \approx 6$ and at this coupling we assume an approximate scaling window. For the results with improvement the scaling region is at $\beta \approx 3$. In our calculations the "improved" lattice has no better continuum limit, but is important as it provides an alternative regularisation scheme we can compare the unimproved results with.

We compare our data to the scaling window results of standard Monte Carlo calculations (straight lines) of ref. [60]. For the different scaling behaviour of the Hamiltonian and the Lagrangian lattice see ref. [21].

In the sectors where we have two-cluster states (see section 4.3.4) the interpretation of the spectra is not straightforward. This occurs in the 0^{-+}, 0^{+-}, 2^{-+}, 2^{+-} and the $1^{\pm-}$ sectors.

In the 0^{++}, 0^{--}, 2^{++}, 2^{--} and the $1^{\pm+}$ sectors, which are not spoiled with two-cluster states our results show a satisfactory agreement with ref. [60]. The mass gap between the lowest state and the next excitation (see the 0^{++} and the 2^{--} sectors) is similar to that of ref. [60] and in most sectors (0^{--}, the 2^{++} and the $1^{\pm+}$ sector) we even get a similar value in the scaling region.

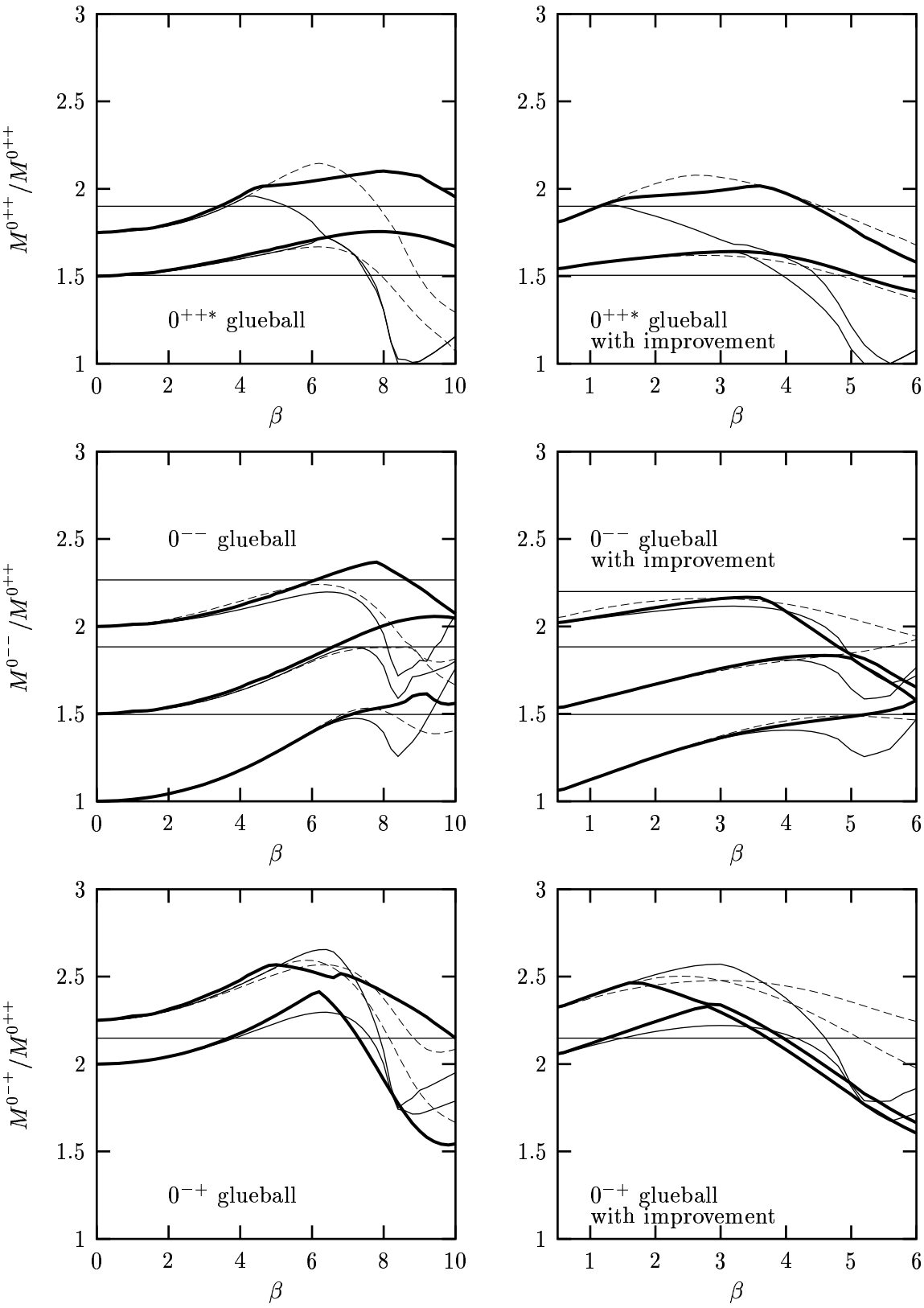

Figure 4.12: Mass ratio in the 0^{++}, the 0^{--} and the 0^{-+} sector relative to the lowest 0^{++} state as a function of the inverse coupling $\beta = \frac{2N_c}{g^2 a}$ up to 5th order without and with improvement. For comparison: Scaling window result of standard Monte Carlo calculations (straight lines) [60].

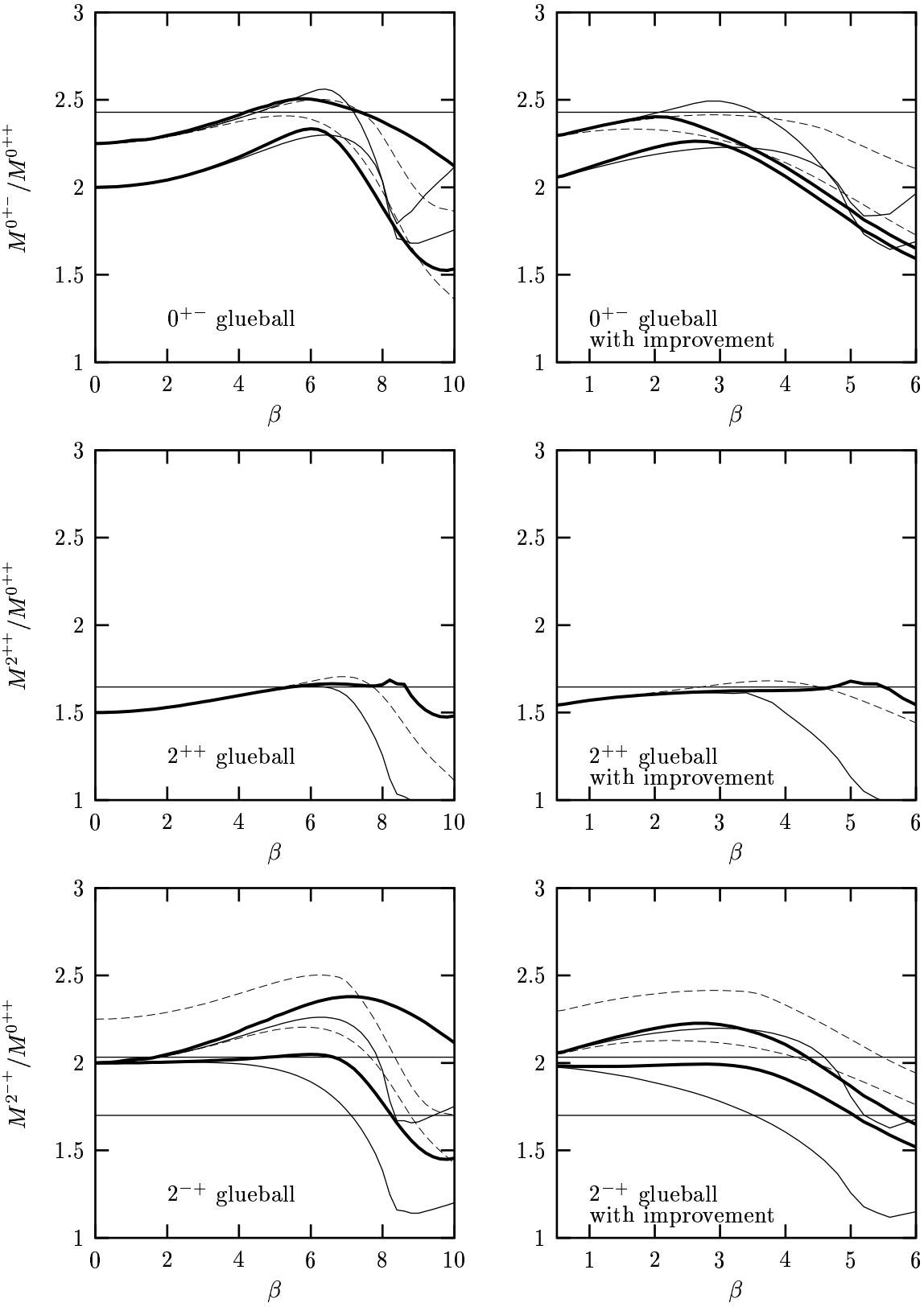

Figure 4.13: Mass ratio in the 0^{+-}, the 2^{++} and the 2^{-+} sector relative to the lowest 0^{++} state as a function of the inverse coupling $\beta = \frac{2N_c}{g^2 a}$ up to 5th order without and with improvement. For comparison: Scaling window result of standard Monte Carlo calculations (straight lines) [60].

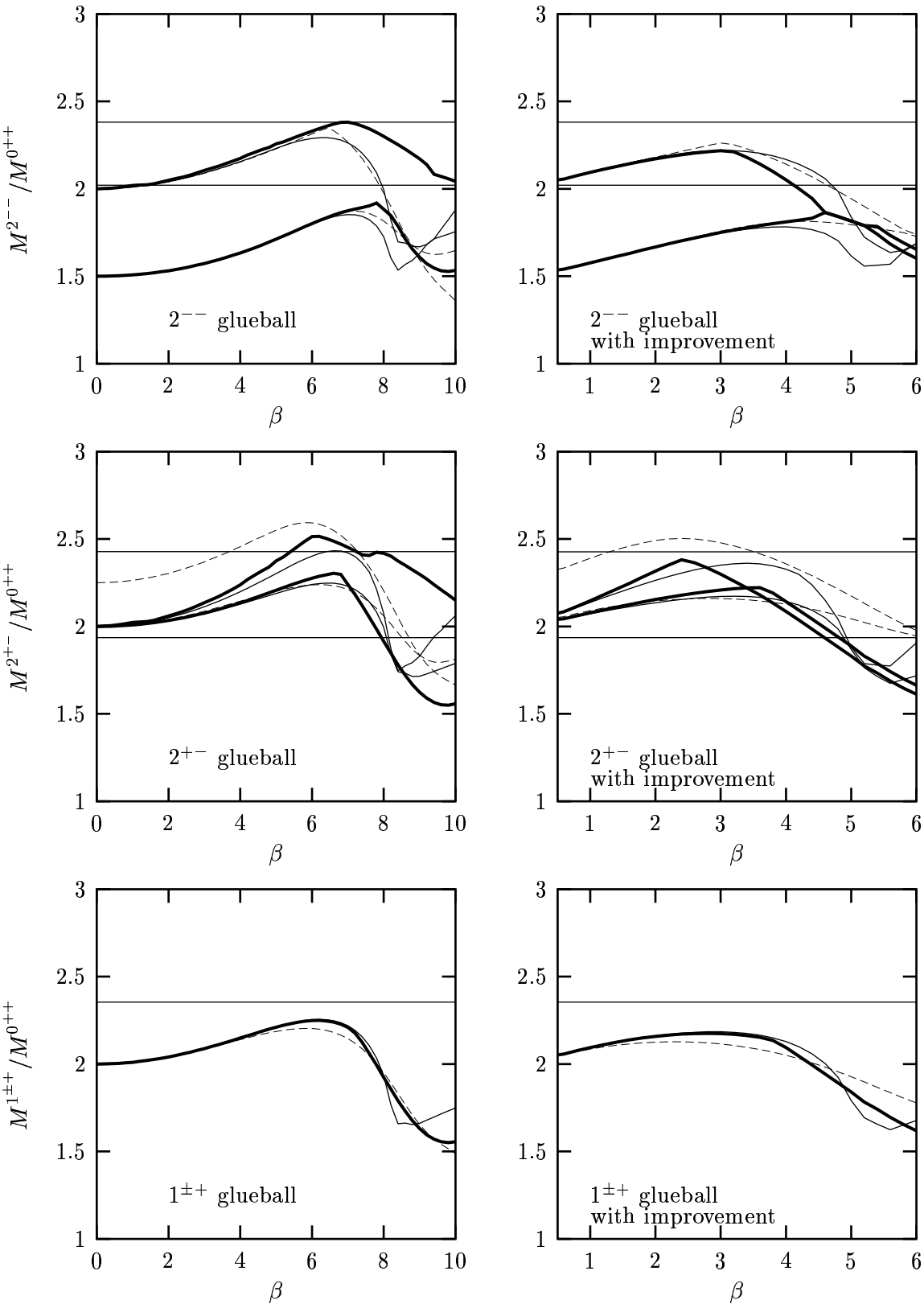

Figure 4.14: Mass ratio in the 2^{--}, the 2^{+-} and the $1^{\pm+}$ sector relative to the lowest 0^{++} state as a function of the inverse coupling $\beta = \frac{2N_c}{g^2 a}$ up to 5th order without and with improvement. For comparison: Scaling window result of standard Monte Carlo calculations (straight lines) [60].

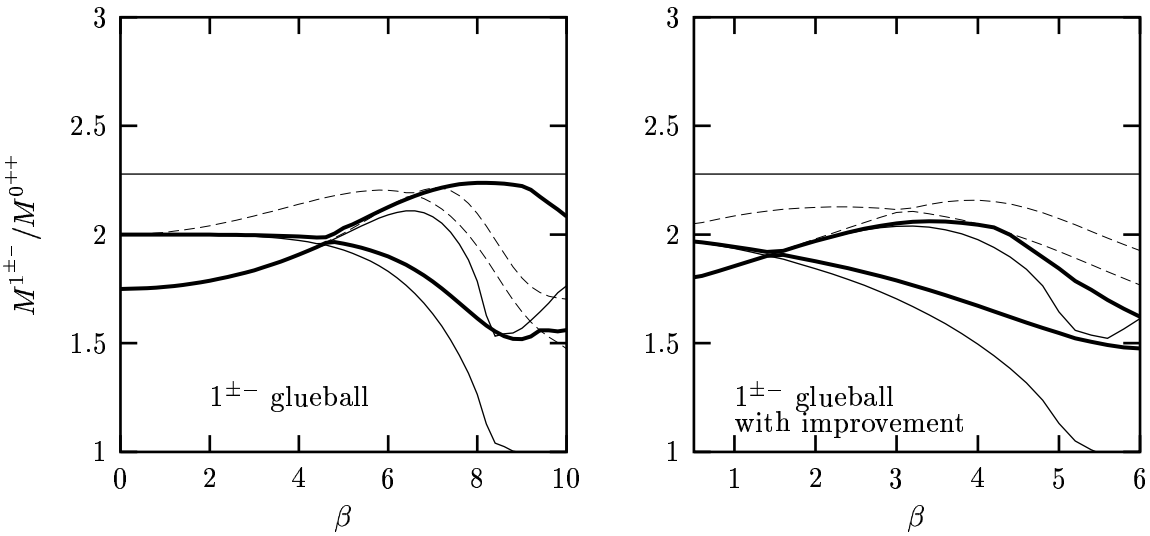

Figure 4.15: Mass ratio in the $1^{\pm-}$ sector relative to the lowest 0^{++} state as a function of the inverse coupling $\beta = \frac{2N_c}{g^2 a}$ up to 5th order without and with improvement. For comparison: Scaling window result of standard Monte Carlo calculations (straight lines) [60].

Lowest 0^{--} mass gap ratio

If we assume our scaling region to be at $\beta \approx 6$ ($\beta \approx 3$ with improvement), we get the following mass gap ratio for the 0^{--} glueball (see fig. 4.16):

$$\begin{aligned} \frac{M^{0^{--}}}{M^{0^{++}}}(\beta = 6) &= 1.40 \text{ (without improvement)} \\ \frac{M^{0^{--}}}{M^{0^{++}}}(\beta = 3) &= 1.36 \text{ (with improvement)} \end{aligned}$$

We can not only compare to the results of Teper [60] with a value of 1.5 ± 0.02 (see fig. 4.16), but also to the results of Carlsson *et al.* [9] with a corresponding value of 1.6173 ± 0.0008 and with the value 1.6989 of Chen *et al.* [11]. Our mass ratio has a smaller value, but fig. 4.16 suggests that the scaling window for the 0^{--} glueball is at a higher coupling $\beta \approx 7$ in the unimproved case. For this coupling we get a value of ≈ 1.5 in 5th order, which agrees with the one of Teper.

As we did for the 0^{++} glueball (see section 4.3.3) we can again implement the data for the vacuum state given in ref. [9] to calculate a "new" mass ratio of the 0^{--} state energy relative to the 0^{++} state. The vacuum of ref. [9] is approximated by a one plaquette term only and a very good scaling for the 0^{++} and the 0^{--} glueball is seen.

Fig. 4.17 presents the result compared to the "old" mass ratio. At higher β where our results with the coupled cluster Ansatz for the vacuum state breaks down, the results with the vacuum of ref. [9] is still valid. We can assume a "new" scaling region at $\beta \approx 9$ and get a value of 1.60 for 0^{--} mass ratio relative to the 0^{++} state, which lies between the results of Teper [60] and Carlsson *et al.* [9].

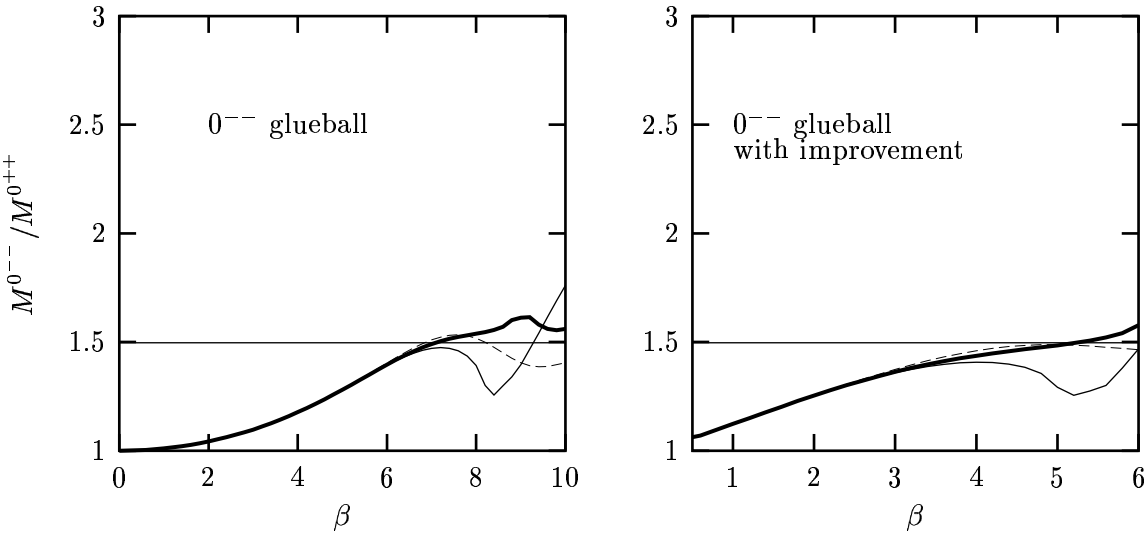

Figure 4.16: Mass ratio of the 0^{--} glueball relative to the lowest 0^{++} state as a function of the inverse coupling $\beta = \frac{2N_c}{g^2 a}$ up to 5th order without and with improvement. For comparison: Scaling window result of standard Monte Carlo calculations (straight lines) [60].

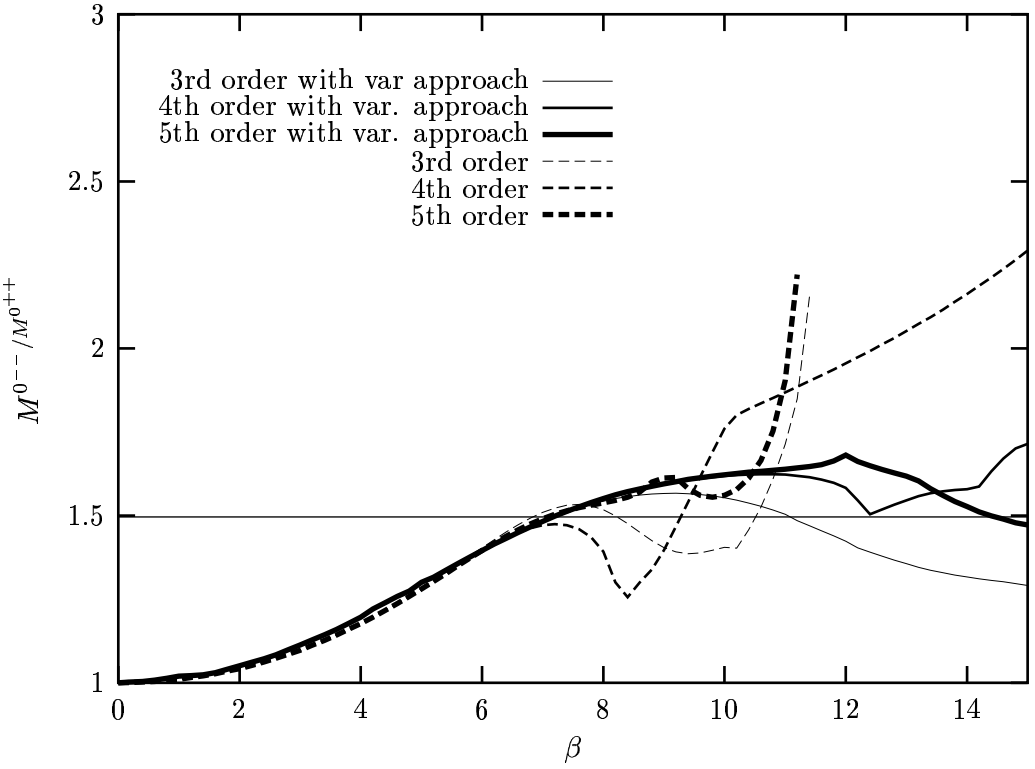

Figure 4.17: Mass ratio of the 0^{--} glueball relative to the lowest 0^{++} state as a function of the inverse coupling $\beta = \frac{2N_c}{g^2 a}$ up to 5th order calculated with our coupled cluster vacuum and with the vacuum of the analytic variational approach (var.approach)[9]. For comparison: Scaling window result of standard Monte Carlo calculations (straight lines) [60].

Lowest 2^{++} mass gap ratio

In the corresponding sector in fig. 4.13 we presented the 2^{++} mass gap ratio. In our scaling region at $\beta \approx 6$ ($\beta \approx 3$ with improvement), we get the following values for this excited state:

$$\begin{aligned} \frac{M^{2^{++}}}{M^{0^{++}}}(\beta = 6) &= 1.66 \text{ (without improvement)} \\ \frac{M^{2^{++}}}{M^{0^{++}}}(\beta = 3) &= 1.62 \text{ (with improvement)} \end{aligned}$$

We get a very good agreement with the value of 1.65 ± 0.04 given by Teper [60] .

4.3.6 Summary

At the end of this chapter we present a final estimate of our glueball spectrum in units of the 0^{++} glueball mass. In the following table we give the values for the glueball mass ratios for various states J^{PC} in the scaling region at $\beta = 6$ (at $\beta = 3$ with improvement). We show the data of calculations in the 4th and the 5th order.

J^{PC}	unimproved $\beta = 6$		improved $\beta = 3$		
	$\delta = 4$	$\delta = 5$	$\delta = 4$	$\delta = 5$	
0^{++}	1	1	1	1	
0^{++*}	1.69	1.71	1.64	1.64	
0^{++**}	1.81	2.04	1.71	1.99	level-crossing,two-cluster states
0^{--}	1.39	1.40	1.36	1.36	
0^{--*}	1.81	1.83	1.76	1.76	
0^{--**}	2.19	2.26	2.11	2.17	
0^{-+}	2.29	2.40	2.22	2.30	two-cluster states
0^{-+*}	2.65	2.53	2.57	2.34	two-cluster states
0^{+-}	2.29	2.34	2.23	2.25	two-cluster states
0^{+-*}	2.55	2.50	2.49	2.30	
2^{++}	1.65	1.66	1.61	1.62	
2^{-+}	1.89	2.05	1.78	1.99	two-cluster states
2^{-+*}	2.26	2.34	2.20	2.22	two-cluster states
2^{--}	1.80	1.80	1.75	1.75	
2^{--*}	2.29	2.33	2.22	2.22	
2^{+-}	2.24	2.28	2.17	2.21	two-cluster states
2^{+-*}	2.40	2.51	2.35	2.30	two-cluster states
$1^{\pm+}$	2.25	2.25	2.18	2.17	
$1^{\pm-}$	1.83	1.89	–	1.79	level-crossing, two-cluster states
$1^{\pm-}$	2.09	2.13	–	2.05	level-crossing

Our final glueball spectrum in fig. 4.18 presents mean values of the numbers of the table above. The errors are deviations of the mean values. We also show Standard Monte Carlo results of Teper [60]. In the sectors where two-cluster states occur we cannot really compare the data, but the others are quite consistent with the results of Teper.

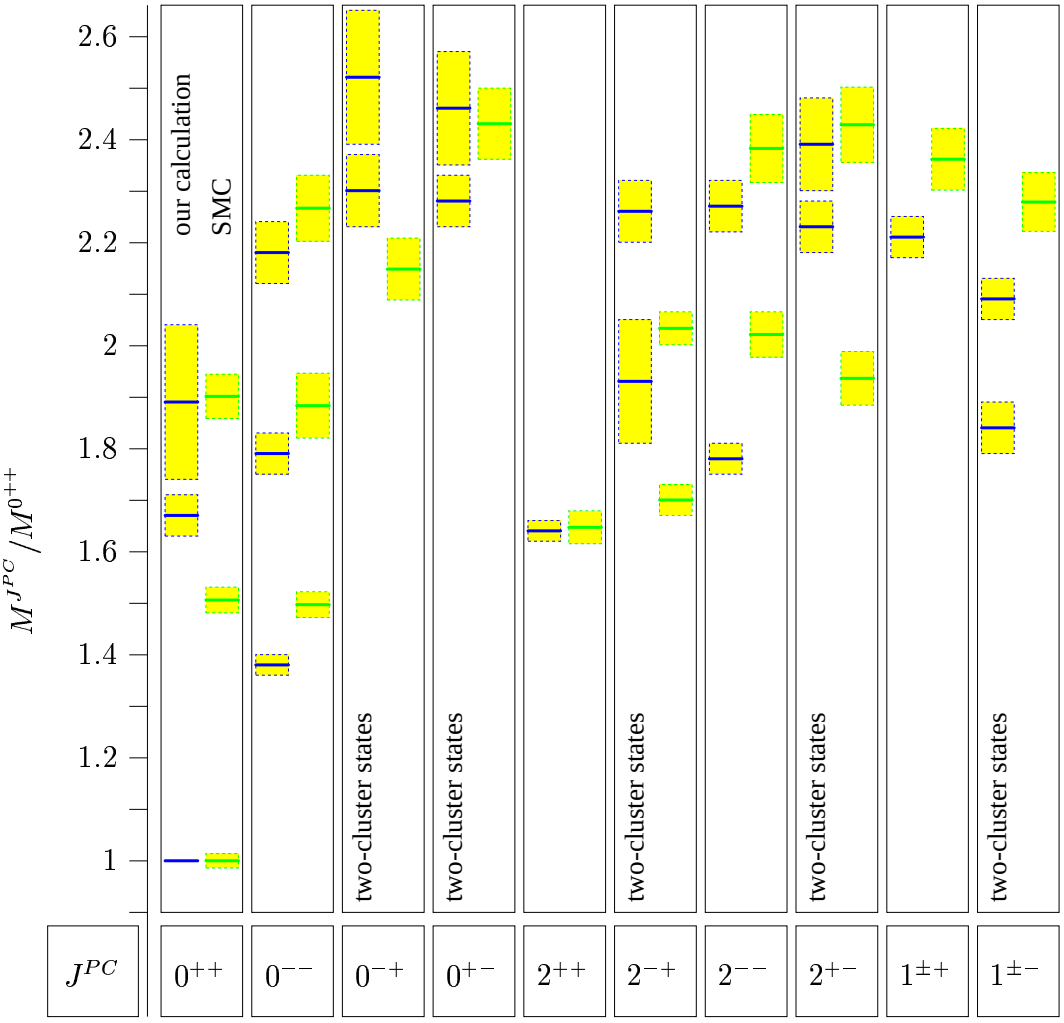

Figure 4.18: Final estimate of the glueball spectrum in units of the 0^{++} glueball. The bars in the left column are mean values of the numbers in table in section 4.3.6. The shaded area reflects the estimated error. For comparison: Scaling window result of standard Monte Carlo calculations SMC [60] on the right side of the column.

Summary and outlook

In this thesis calculations on the pure SU(3) glueball spectrum in two spatial dimensions using the coupled cluster method in the Hamiltonian lattice gauge field theory were presented.

The special features of this study, i.e. its problems and possibilities, were very similar to the ones of the computations for SU(2) glueballs within the same approach (see ref. [64]).

The main problem that occurred is the break-down of the iteration procedure for the SU(3) vacuum state at inverse couplings β even smaller than for the SU(2) calculations.

Nevertheless, up to $\beta \approx 6$, where we saw an approximate scaling window for the SU(3) calculations without improvement, our results were reliable. As was already detected in ref. [64] in our approach improvement provides an alternative regularisation scheme and the scaling window is shifted to smaller inverse couplings, i.e. to $\beta \approx 3$ for the SU(3) glueballs.

For the vacuum state we got satisfactory convergence and a good agreement with results of refs. [9, 27].

Fig. 4.18 summarised our final estimate of the glueball spectrum in units of the lowest 0^{++} glueball mass. Special glueball mass ratios, e.g. in the 0^{++}, the 0^{--} and the 2^{++} sector, showed a satisfactory agreement with the results of ref. [60]. Other ratios could not be compared to literature values because they were found to be two-cluster states. The value for the 0^{++} glueball itself agreed with the corresponding value of refs. [18, 60].

We are convinced that our results point into the right direction, but only a restricted interpretation of the spectrum and of the wave functions is up to now possible because of the truncation of the basis we work with.

Thus the next step to be done for the calculations in two spatial dimensions would be the extension to higher orders. In this work we were restricted for the construction of the basis to the order $\delta = 6$ and for the solution of the coupled cluster equations to an order $\delta = 5$ because of memory limitations. To extend the SU(2) calculations of ref. [64] to higher orders would also be useful, as the similar structure of the results of the SU(2) theory to the SU(3) data supposes it to be a good test case.

Of more physical interest would be to employ the case of SU(3) glueballs in three space dimensions. For the corresponding SU(2) calculations we had serious problems with the iteration procedure of the vacuum state (see ref. [64]). Thus SU(3) calculations in three dimensions would be an important test for the Ansatz of our vacuum state.

The Hamiltonian formulation of lattice gauge field theory has the advantage that it provides direct access to the mass spectrum and to the wave functions and as the numerical effort in this formalism is much smaller than in the Lagrangian formulation of lattice gauge field theory it stays an alternative method to study non-perturbative aspects of QCD.

Appendix A The coupled cluster matrix element

In this appendix we calculate the coupled cluster matrix element, which was defined in chapter 1 to be the coefficient in the expansion of the product of two elements of the basis η. As η is the loop space basis χ after projection on states of zero momentum, angular momentum J^P and charge parity C, we have to consider the contribution of these projectors to the coupled cluster matrix element. The determination follows the one for SU($N_c = 2$)-glueballs done in refs. [63, 64], but in addition we have to consider charge conjugation. The products of elements of the loop space basis were determined at the end of chapter 2. The corrects coefficients are called c-coefficients.

We start with the calculation of products of loop space basis elements, then we compute the corresponding products including the projection on charge parity and finally we also consider zero momentum, angular momentum and parity projection.

A.1 Products of the loop space elements

The products of loop space basis elements were calculated in chapter 2. The corresponding coefficients are defined in eq. (2.19) and eq. (2.19) as:

$$\begin{aligned}
\chi^{\alpha_1} T_{\mathbf{a}_2} T(R_2) \chi^{\alpha_2} &= \sum_{\substack{t_{\mathbf{a}_3} \in G_{lt}, \\ R_3 \in G_{lr}}} \sum_{\alpha_3} c^{\alpha_1 \alpha_2}_{\alpha_3, \mathbf{a}_2, \mathbf{a}_3, R_2, R_3} T_{\mathbf{a}_3} T(R_3) \Pi^{\pm}_C \chi^{\alpha_3} \,, \\
(T_C \chi^{\alpha_1}) T_{\mathbf{a}_2} T(R_2) \chi^{\alpha_2} &= \sum_{\substack{t_{\mathbf{a}_3} \in G_{lt}, \\ R_3 \in G_{lr}}} \sum_{\alpha_3} c^{\bar{\alpha}_1 \alpha_2}_{\alpha_3, \mathbf{a}_2, \mathbf{a}_3, R_2, R_3} T_{\mathbf{a}_3} T(R_3) \Pi^{\pm}_C \chi^{\alpha_3} \,.
\end{aligned}$$

These c-coefficients were determined at the end of section 2.3.5.

A.2 Projection on momentum and angular momentum, parity and charge parity

As defined in eq. (1.19) the basis η has the form:

$$\eta^{\alpha}_{J^{PC},\nu\sigma} = \frac{\Pi^0 \Pi^{J^P}_{\nu\sigma} \Pi^{\pm}_C(\chi^{\alpha})}{||\Pi^0 \Pi^{J^P}_{\nu\sigma} \Pi^{\pm}_C(\chi^{\alpha})||} \,.$$

The operator $\Pi^0 \Pi^{J^P}_{\nu\sigma} \Pi^{\pm}_C$ projects onto states with momentum $\mathbf{p} = 0$ and angular momentum, parity and charge parity J^{PC}, with magnetic quantum numbers ν and σ. For the ground state we have $J^{PC} = 0^{++}$. These projectors were discussed in detail in chapter

3. The calculation of the coupled cluster matrix element involves the computation of the following product (see eq. (1.29) and eq. (1.30)):

$$\sum_{\mu}[\eta^{\alpha_1}_{0^{++}}]_\mu[\eta^{\alpha_2}_{J^{PC},\nu\sigma}]_\mu = \sum_{\mu}\frac{[\Pi^0\Pi^{0^+}\Pi^+_C(\chi^{\alpha_1})_\mu]}{||\tilde{\Pi}^0\chi^{\alpha_1}||}\frac{[\Pi^0\Pi^{J^P}_{\nu\sigma}\Pi^\pm_C(\chi^{\alpha_2})_\mu]}{||\tilde{\Pi}^K\chi^{\alpha_2}||} \tag{A.1}$$

The index μ is an abbreviation for the action of the conjugate momenta $E^a_l, a = 1,\dots N_c^2$, on the link variables U_l:

$$\begin{aligned} f_{(l,a)} &:= [E^a_l, f] \\ f_{(l,a)(l,a)} &:= [E^a_l, f_{(l,a)}] \\ \mu &:= (l,a)\,. \end{aligned}$$

Projection on charge parity

Here we calculate the product $\sum_\mu \Pi^+_c(\chi^{\alpha_1})_\mu(T_{\mathbf{a}_2}T(R_2)\Pi^\pm_c\chi^{\alpha_2})_\mu$, which we need for the calculation of the product of eq. (A.1). We use the definition of the c-coefficients (see section A.1). As mentioned before μ denotes the action of the canonical momenta. This corresponds to a differential operator acting on the lattice gauge fields. With the product rule for derivatives we get:

$$\begin{aligned} \textstyle\sum_\mu\ & \Pi^+_c(\chi^{\alpha_1})_\mu(T_{\mathbf{a}_2}T(R_2)\Pi^\pm_c\chi^{\alpha_2})_\mu \\ = & \sum_\mu\frac{1}{2}\Big([\Pi^+_c\chi^{\alpha_1}T_{\mathbf{a}_2}T(R_2)\Pi^\pm_c\chi^{\alpha_2}]_{\mu\mu} \\ & -\Pi^+_c(\chi^{\alpha_1})_{\mu\mu}T_{\mathbf{a}_2}T(R_2)\Pi^\pm_c\chi^{\alpha_2} - \Pi^+_c\chi^{\alpha_1}(T_{\mathbf{a}_2}T(R_2)\Pi^\pm_c\chi^{\alpha_2})_{\mu\mu}\Big) \\ = & \sum_{\substack{t_{\mathbf{a}_3}\in G_{lt},\\ R_3\in G_{lr}}}\sum_{\alpha_3}\frac{1}{2}(\epsilon_{\alpha_3}-\epsilon_{\alpha_1}-\epsilon_{\alpha_2})\frac{1}{2}(c^{\alpha_1\alpha_2}_{\alpha_3,\mathbf{a}_2,\mathbf{a}_3,R_2,R_3}+c^{\bar{\alpha}_1\alpha_2}_{\alpha_3,\mathbf{a}_2,\mathbf{a}_3,R_2,R_3})T_{\mathbf{a}_3}T(R_3)\Pi^\pm_c\chi^{\alpha_3} \\ = & \sum_{\substack{t_{\mathbf{a}_3}\in G_{lt},\\ R_3\in G_{lr}}}\sum_{\alpha_3}\tilde{C}^{\alpha_1\alpha_2}_{\alpha_3,\mathbf{a}_2,\mathbf{a}_3,R_2,R_3}T_{\mathbf{a}_3}T(R_3)\Pi^\pm_c\chi^{\alpha_3} \end{aligned} \tag{A.2}$$

In the last steps we used the fact that the localised basis χ consists of strong coupling eigenfunctions (see eq. (2.5)) and we have defined the coefficient $\tilde{C}$ as abbreviation. The projector on charge parity is given by (see eq. (3.10)):

$$\Pi^\pm_c\chi^\alpha = \frac{1}{2}(1\pm T_c)\chi^\alpha\,,$$

and for the product $\Pi^+_C\chi^{\alpha_1}(T_{\mathbf{a}_2}T(R_2)\Pi^\pm_C\chi^{\alpha_2})$ we get:

$$\begin{aligned} \Pi^+_C\chi^{\alpha_1}(T_{\mathbf{a}_2}T(R_2)\Pi^\pm_C\chi^{\alpha_2}) &= \frac{1}{2}(1+T_C)\chi^{\alpha_1}(T_{\mathbf{a}_2}T(R_2)\frac{1}{2}(1\pm T_C)\chi^{\alpha_2}) \\ &= \frac{1}{4}\big((\chi^{\alpha_1}T_{\mathbf{a}_2}T(R_2)\chi^{\alpha_2}+(T_C\chi^{\alpha_1})T_{\mathbf{a}_2}T(R_2)\chi^{\alpha_2}) \\ &\quad \pm T_C\big((T_C\chi^{\alpha_1})T_{\mathbf{a}_2}T(R_2)\chi^{\alpha_2}+\chi^{\alpha_1}T_{\mathbf{a}_2}T(R_2)\chi^{\alpha_2}\big)\big) \\ &= \frac{1}{2}\Pi^\pm_C\big(\chi^{\alpha_1}T_{\mathbf{a}_2}T(R_2)\chi^{\alpha_2}+(T_C\chi^{\alpha_1})T_{\mathbf{a}_2}T(R_2)\chi^{\alpha_2}\big) \\ &= \frac{1}{2}\sum_{\substack{t_{\mathbf{a}_3}\in G_{lt},\\ R_3\in G_{lr}}}\sum_{\alpha_3}(c^{\alpha_1\alpha_2}_{\alpha_3,\mathbf{a}_2,\mathbf{a}_3,R_2,R_3}+c^{\bar{\alpha}_1\alpha_2}_{\alpha_3,\mathbf{a}_2,\mathbf{a}_3,R_2,R_3})T_{\mathbf{a}_3}T(R_3)\Pi^\pm\chi^{\alpha_3} \end{aligned}$$

We have used the fact that charge conjugation commutes with all translations, rotations and reflections (see eq. (2.16) and eq. (2.18)).

Projection on momentum and angular momentum and parity

The projection operators on definite momentum and angular momentum/parity are given by (see eq. (3.3) and eq. (3.5)):

$$\begin{aligned}
\Pi^0 &= \sum_{t_{\mathbf{a}} \in G_{lt}} T_{\mathbf{a}} \,, \\
\Pi^{JP}_{\nu\sigma} &= \frac{\dim J^P}{|G_{lr}|} \sum_{R \in G_{lr}} D^{JP}_{\nu\sigma}(R^{-1}) T(R) = \sum_{R \in G_{lr}} d^{JP}_{\nu\sigma}(R^{-1}) T(R) \,, \\
\text{where } \Pi^{0^+} &= \sum_{R \in G_{lr}} d_0 T(R) \;, d_0 = \frac{1}{|G_{lr}|} \,.
\end{aligned}$$

With the properties of translations $t_{\mathbf{a}} \in G_{lt}$ and rotation/reflections $R \in G_{lr}$ and of the corresponding transformations $T_{\mathbf{a}}$ and $T(R)$ of the loop space basis discussed in chapter 3, we can now calculate the product of eq. (A.1):

$$\begin{aligned}
&\textstyle\sum_\mu \quad [\Pi^0 \Pi^{0^+} \Pi^+_C(\chi^{\alpha_1})_\mu][\Pi^0 \Pi^{JP}_{\nu\sigma} \Pi^\pm_C(\chi^{\alpha_2})_\mu] \\
&= \sum_\mu \Big(\sum_{t_{\mathbf{a}_1} \in G_{lt}} T_{\mathbf{a}_1} \sum_{R_1 \in G_{lr}} d_0 T(R_1) \Pi^+_C(\chi^{\alpha_1})_\mu \Big) \Big(\sum_{t_{\mathbf{a}} \in G_{lt}} T_{\mathbf{a}} \sum_{R \in G_{lr}} d^{JP}_{\nu\sigma}(R^{-1}) T(R) \Pi^\pm_C(\chi^{\alpha_2})_\mu \Big) \\
&= \sum_\mu \sum_{\substack{t_{\mathbf{a}_1}, t_{\mathbf{a}} \in G_{lt} \\ R_1, R \in G_{lr}}} d_0 T_{\mathbf{a}_1} T(R_1) \Pi^+_C(\chi^{\alpha_1})_\mu \Big(T(R_1^{-1}) T_{-\mathbf{a}_1} T_{\mathbf{a}} d^{JP}_{\nu\sigma}(R^{-1}) T(R) \Pi^\pm_C(\chi^{\alpha_2})_\mu \Big) \\
&= \sum_\mu \sum_{\substack{t_{\mathbf{a}_1}, t_{\mathbf{a}} \in G_{lt} \\ R_1, R \in G_{lr}}} d_0 d^{JP}_{\nu\sigma}(R^{-1}) T_{\mathbf{a}_1} T(R_1) \Big(\Pi^+_C(\chi^{\alpha_1})_\mu T_{R_1^{-1}(\mathbf{a}-\mathbf{a}_1)} T(R_1^{-1} R) \Pi^\pm_C(\chi^{\alpha_2})_\mu \Big) \\
&= \sum_\mu \sum_{\substack{t_{\mathbf{a}_1}, t_{\mathbf{a}_2} \in G_{lt} \\ R_1, R_2 \in G_{lr}}} d_0 d^{JP}_{\nu\sigma}(R_2^{-1} R_1^{-1}) T_{\mathbf{a}_1} T(R_1) \Big(\Pi^+_C(\chi^{\alpha_1})_\mu T_{\mathbf{a}_2} T(R_2) \Pi^\pm_C(\chi^{\alpha_2})_\mu \Big), \\
&\qquad \text{where } \mathbf{a}_2 = (R_1^{-1}(\mathbf{a} - \mathbf{a}_1)) \text{ and } R_2 = (R_1^{-1} R) \,.
\end{aligned}$$

The calculation of the product $\sum_\mu \Pi^+_c(\chi^{\alpha_1})_\mu (T_{\mathbf{a}_2} T(R_2) \Pi^\pm_c \chi^{\alpha_2})_\mu$, which involves charge conjugation and the c-coefficients of the products of loop space basis elements, as presented above. With this result and with the definition of $\tilde{C}$ of eq. (A.2) we can proceed:

$$\begin{aligned}
&= \sum_{\substack{t_{\mathbf{a}_1}, t_{\mathbf{a}_2}, t_{\mathbf{a}_3} \in G_{lt} \\ R_1, R_2, R_3 \in G_{lr}}} \sum_{\alpha_3} d_0 d^{JP}_{\nu\sigma}(R_2^{-1} R_1^{-1}) T_{\mathbf{a}_1} T(R_1) \tilde{C}^{\alpha_1 \alpha_2}_{\alpha_3, \mathbf{a}_2, \mathbf{a}_3, R_2, R_3} T_{\mathbf{a}_3} T(R_3) \Pi^\pm_C \chi^{\alpha_3} \\
&= \sum_{\substack{t_{\mathbf{a}_1}, t_{\mathbf{a}_2}, t_{\mathbf{a}_3} \in G_{lt} \\ R_1, R_2, R_3 \in G_{lr}}} \sum_{\alpha_3} d_0 d^{JP}_{\nu\sigma}(R_2^{-1} R_1^{-1}) \tilde{C}^{\alpha_1 \alpha_2}_{\alpha_3, \mathbf{a}_2, \mathbf{a}_3, R_2, R_3} T_{\mathbf{a}_1 + R_1 \mathbf{a}_3} T(R_1 R_3) \Pi^\pm_C \chi^{\alpha_3} \\
&= \sum_{\substack{t_{\mathbf{a}}, t_{\mathbf{a}_2}, t_{\mathbf{a}_3} \in G_{lt} \\ R, R_2, R_3 \in G_{lr}}} \sum_{\alpha_3} d_0 d^{JP}_{\nu\sigma}(R_2^{-1} R_3 R^{-1}) \tilde{C}^{\alpha_1 \alpha_2}_{\alpha_3, \mathbf{a}_2, \mathbf{a}_3, R_2, R_3} T_{\mathbf{a}} T(R) \Pi^\pm_C \chi^{\alpha_3} \,, \\
&\qquad \text{where } \mathbf{a} = (\mathbf{a}_1 + R_1 \mathbf{a}_3) \text{ and } R = (R_1 R_3) \\
&= \frac{1}{|G_{lr}|} \sum_{\substack{t_{\mathbf{a}_2}, t_{\mathbf{a}_3} \in G_{lt} \\ R_2, R_3 \in G_{lr}}} \sum_{\alpha_3} \sum_{\kappa} D^{JP}_{\nu_2 \kappa}(R_2^{-1} R_3) \tilde{C}^{\alpha_1 \alpha_2}_{\alpha_3, \mathbf{a}_2, \mathbf{a}_3, R_2, R_3} \Pi^0 \Pi^{JP}_{\kappa\sigma_2} \Pi^\pm_C \chi^{\alpha_3} \,.
\end{aligned}$$

In the last step we have used the representation property:

$$\begin{aligned}\sum_{R_1,R_2\in G_{lr}} d^{J^P}_{\nu\sigma}(R_1R_2) &= \frac{\dim J^P}{|G_{lr}|}\sum_{R_1,R_2\in G_{lr}} D^{J^P}_{\nu\sigma}(R_1R_2)\\ &= \frac{\dim J^P}{|G_{lr}|}\sum_{R_1,R_2\in G_{lr}}\sum_{\kappa} D^{J^P}_{\nu\kappa}(R_1)D^{J^P}_{\kappa\sigma}(R_2)\,.\end{aligned}$$

We can now define the coupled cluster matrix elements by

$$C^{\alpha_1\alpha_2}_{\alpha_3,\nu\kappa}(J^{PC}) = \frac{1}{|G_{lr}|}\frac{||\tilde{\Pi}^K\chi^{\alpha_3}||}{||\tilde{\Pi}^0\chi^{\alpha_1}||\,||\tilde{\Pi}^K\chi^{\alpha_2}||}\sum_{\substack{t_{\mathbf{a}_2},t_{\mathbf{a}_3}\in G_{lt}\\ R_2,R_3\in G_{lr}}} D^{J^P}_{\nu\kappa}(R_2^{-1}R_3)\tilde{C}^{\alpha_1\alpha_2}_{\alpha_3,\mathbf{a}_2,\mathbf{a}_3,R_2,R_3}\,, \qquad \text{(A.3)}$$

where $\tilde{\Pi}^K$ abbreviates the projectors on momentum, angular momentum, parity and charge parity.

Altogether for the products of the η's we get:

$$\sum_{\mu}[\eta^{\alpha_1}_{0^{++}}]_\mu[\eta^{\alpha_2}_{J^{PC},\nu\sigma}]_\mu = \sum_{\alpha_3}\sum_{\kappa} C^{\alpha_1\alpha_2}_{\alpha_3,\nu\kappa}(J^{PC})\;\eta^{\alpha_3}_{J^{PC},\kappa\sigma}\,.$$

Appendix B Irreducible representations of SU(3)

In this appendix we present the notations and definitions for the irreducible representations (IRs) of SU(3) and the corresponding Clebsch-Gordan-coefficients CGC used in this thesis.

The SU(3)-CGC were calculated with an adaption of a program of ref. [29] and therefore we follow their conventions.

B.1 Irreducible representations

The matrix elements of the IRs, which are denoted by

$$D^{\Gamma}_{\gamma\gamma'}(U), \;\; U \in \mathrm{SU}(3)\,,$$

are labelled by $\Gamma := (p,q)$, where $p,q \in \mathbb{Z}^+$. The dimension of the IR (p,q) is given by

$$\dim(\Gamma) = \dim(p,q) = \frac{1}{2}(p+1)(q+1)(p+q+2)\,.$$

We will often use the abbreviation

$$\hat{\Gamma} = \sqrt{\dim(\Gamma)}\,.$$

For the eigenvalue of the quadratic Casimir operator $\sum_{a=1}^{8} E^a E^a$ for SU(3), which is defined in eq. (1.12) for the link variables $U_l \in \mathrm{SU}(3)$, we get:

$$\epsilon(\Gamma) = \frac{1}{3}\left(p^2+q^2+3(p+q)+pq\right)\,. \tag{B.1}$$

The states $|\Gamma\gamma\rangle$ in an IR are labelled by $\gamma := (k,l,m)$, $k,l,m \in \mathbb{Z}$, where these subspace labels fulfil the inbetweenness conditions:

$$0 \le l \le q \le k \le p+q; \qquad l \le m \le k\,.$$

Alternatively we shall use as subspace labels $\gamma = (y,I,i)$:

$$\begin{aligned} I &:= \frac{k-l}{2} \\ i &= I_3 := m - \frac{k+l}{2} \\ y &:= k+l-\frac{2}{3}(p+2q)\,. \end{aligned}$$

which in the case of $SU(3)_{\text{flavor}}$ have the meaning of isospin, its third component and hypercharge, respectively. The inverse relations are:

$$\begin{aligned} k &= \frac{1}{2}y + I + \frac{1}{3}(p+2q) \\ l &= \frac{1}{2}y - I + \frac{1}{3}(p+2q) \\ m &= \frac{1}{2}y + i + \frac{1}{3}(p+2q) \end{aligned}$$

The conjugated IR

$$D^{\bar{\Gamma}}_{\bar{\gamma}\bar{\gamma}'}(U), \;\; U \in \mathrm{SU}(3)$$

is labelled by $\bar{\Gamma} = (q,p)$ and the subspace labels of the conjugated IR are given by $\bar{\gamma} = (\bar{k},\bar{l},\bar{m}) = (\bar{y},\bar{I},\bar{i})$, where

$$\begin{aligned} \bar{k} = p+q-l; \quad \bar{l} = p+q-k; \quad \bar{m} = p+q-m \qquad \Leftrightarrow \\ \bar{y} = -y; \qquad \bar{I} = I; \qquad \bar{i} = -i\,. \end{aligned}$$

Thus we have a relation between the quantum numbers of $\bar{\Gamma}$ and Γ. This and the properties of the IRs which are given now were discussed in detail in ref. [58].

The matrices of the IRs are normalised

$$\int \mathrm{D}U \, (D^{\Gamma_1}_{\gamma_1\gamma_1'})^*(U) \; D^{\Gamma_2}_{\gamma_2\gamma_2'}(U) = \frac{\delta_{\Gamma_1\Gamma_2}\delta_{\gamma_1\gamma_2}\delta_{\gamma_1'\gamma_2'}}{\hat{\Gamma}^2} \tag{B.2}$$

$$D^{\Gamma}_{\gamma\gamma'}(\mathbf{1}) = \delta_{\gamma\gamma'}\,, \tag{B.3}$$

and they are unitary

$$(D^{\Gamma}_{\gamma\gamma'})^*(U) = \binom{\Gamma}{\gamma}\binom{\Gamma}{\gamma'} D^{\bar{\Gamma}}_{\bar{\gamma},\bar{\gamma}'}(U) = D^{\Gamma}_{\gamma'\gamma}(U^{-1})\,. \tag{B.4}$$

Here the $1\Gamma\gamma$-symbol is defined by $\binom{\Gamma}{\gamma} = (-1)^{-\frac{1}{3}(2p+q)+i+\frac{1}{2}y}$. For products of the IRs we get:

$$D^{\Gamma_1}_{\gamma_1\gamma_1'}(U) D^{\Gamma_2}_{\gamma_2\gamma_2'}(U) = \sum_{\Gamma_3} \sum_{\gamma_3,\gamma_3'} \sum_{n} D^{\Gamma_3}_{\gamma_3\gamma_3'}(U) \, \langle \Gamma_1\gamma_1;\Gamma_2\gamma_2 \, | \Gamma_3\gamma_3 \rangle_n \, \langle \Gamma_1\gamma_1';\Gamma_2\gamma_2' \, | \Gamma_3\gamma_3' \rangle_n$$

$\langle \Gamma_1\gamma_1;\Gamma_2\gamma_2 \, | \Gamma_3\gamma_3 \rangle_n$ are the Clebsch-Gordan-coefficients defined in the next section.

B.2 The Clebsch-Gordan-coefficients

Definition of the Clebsch-Gordan-coefficients

The Clebsch-Gordan-coefficients (CGC) are the coefficients in the expansion of the composite SU(3)-state into product states:

$$|[\Gamma_1\Gamma_2]\Gamma_3\gamma_3\rangle = \sum_{\gamma_1\gamma_2 n} |\Gamma_1\gamma_1\rangle \, |\Gamma_2\gamma_2\rangle \, \langle \Gamma_1\gamma_1 \, ; \Gamma_2\gamma_2 \, | \Gamma_3\gamma_3 \rangle_n \;,$$

where $n = 1, 2, \ldots$ enumerates the outer degeneracy, i.e. the multiplicity with which Γ_3 occurs in the Clebsch-Gordan series of $\Gamma_1 \otimes \Gamma_2$. A formula to calculate n is given in ref. [49]. If $n = 1$ we omit it from the CGC.

With the subspace labelling given above, the CGC can be factorised into SU(2)-CGC for the SU(2) subgroup and an isoscalar factor:

$$\begin{aligned} &\langle (p_1,q_1)k_1,l_1,m_1;(p_2,q_2)k_2,l_2,m_2 \,|(p_3,q_3)k_3,l_3,m_3\rangle_n \\ &\quad = \langle (p_1,q_1)k_1,l_1;(p_2,q_2)k_2,l_2 \| (p_3,q_3)k_3,l_3\rangle_n \,\langle I_1 i_1 I_2 i_2 \,|I_3 i_3\rangle \end{aligned} \tag{B.5}$$

Orthonormality of the Clebsch-Gordan-coefficients

The CGC obey the orthonormality relations:

$$\begin{aligned} \sum_{\Gamma_3,\gamma_3,n} \langle \Gamma_1\gamma_1;\Gamma_2\gamma_2 \,|\Gamma_3\gamma_3\rangle_n \,\langle \Gamma_1\gamma_1';\Gamma_2\gamma_2' \,|\Gamma_3\gamma_3\rangle_n &= \delta_{\gamma_1\gamma_1'}\delta_{\gamma_2\gamma_2'} \\ \sum_{\gamma_1,\gamma_2} \langle \Gamma_1\gamma_1;\Gamma_2\gamma_2 \,|\Gamma_3\gamma_3\rangle_n \,\langle \Gamma_1\gamma_1;\Gamma_2\gamma_2 \,\left|\Gamma_3'\gamma_3'\right\rangle_{n'} &= \delta_{\Gamma_3\Gamma_3'}\delta_{\gamma_3\gamma_3'}\delta_{nn'} \end{aligned} \tag{B.6}$$

Phase conventions and symmetries

The phases of the CGC are chosen in such a way that

$$\left\langle (p_1,q_1)k_1^h,l_1^h;(p_2,q_2)k_2^m,l_2^m \middle\| (p_3,q_3)k_3^h,l_3^h \right\rangle > 0\,,$$

where the subspace labels of the highest weight state: (k^h, l^h, m^h) of the IR (p,q) are given by

$$\begin{aligned} k^h = p+q; \qquad l^h = 0; \qquad m^h = p+q \qquad &\Leftrightarrow \\ y^h = \frac{1}{3}(p-q); \quad I^h = \tfrac{1}{2}(p+q); \quad i^h = \frac{1}{2}(p+q)\,. \end{aligned}$$

and $y_2^m = y_3^h - y_1^h$ and I_2^m is the highest isospin in the coupling.

This implies the following symmetry relations (see ref. [66]):

$$\langle \Gamma_1\gamma_1\Gamma_2\gamma_2 \,|\Gamma_3\gamma_3\rangle_n = (-1)^{\tau+\sigma+\max(\tau,\sigma)+n} \,\langle \Gamma_2\gamma_2\Gamma_1\gamma_1 \,|\Gamma_3\gamma_3\rangle_n\,,$$

for interchanging $(1 \leftrightarrow 2)$. Furthermore we have for interchanging $(1 \leftrightarrow 3)$

$$\langle \Gamma_1\gamma_1\Gamma_2\gamma_2 \,|\Gamma_3\gamma_3\rangle_n = \binom{\bar\Gamma_2}{\bar\gamma_2} (-1)^{n-\min(0,\tau-\sigma)} \frac{\hat\Gamma_3}{\hat\Gamma_1} \,\langle \bar\Gamma_3\bar\gamma_3\Gamma_2\gamma_2 \,\left|\bar\Gamma_1\bar\gamma_1\right\rangle_n\,. \tag{B.7}$$

For conjugation of a CGC we find

$$\langle \Gamma_1\gamma_1\Gamma_2\gamma_2 \,|\Gamma_3\gamma_3\rangle_n = (-1)^{\tau+\sigma+\min(\tau,\sigma)+n} \,\langle \bar\Gamma_1\bar\gamma_1\bar\Gamma_2\bar\gamma_2 \,\left|\bar\Gamma_3\bar\gamma_3\right\rangle_n\,.$$

Here

$$\tau := \frac{1}{3}(p_1+p_2-p_3); \qquad \sigma := \frac{1}{3}(q_1+q_2-q_3)\,. \tag{B.8}$$

and

$$\binom{\bar\Gamma}{\bar\gamma} = (-1)^{p+q}\binom{\Gamma}{\gamma}\,.$$

Clebsch-Gordan-coefficients coupling to a singlet

The singlet IR is given by $\Gamma = (p,q) = \mathbf{1} = (0,0)$. Because

$$\langle \mathbf{10}; \Gamma\gamma \,|\Gamma\gamma\rangle = +1\,,$$

we have, according to eq. (B.7):

$$\begin{aligned}\langle \Gamma_1\gamma_1; \Gamma_2\gamma_2 \,|\mathbf{10}\rangle &= \binom{\bar\Gamma_2}{\bar\gamma_2}(-1)^{-\min(0,\tau-\sigma)}\frac{1}{\hat\Gamma_1}\,\langle \mathbf{10}; \Gamma_2\gamma_2 \,\big|\bar\Gamma_1\bar\gamma_1\big\rangle \\ &= \binom{\bar\Gamma_2}{\bar\gamma_2}(-1)^{-\min(0,\tau-\sigma)}\frac{1}{\hat\Gamma_1}\,\delta_{\Gamma_2\bar\Gamma_1}\delta_{\gamma_2\bar\gamma_1}\,.\end{aligned}$$

Now for this coupling

$$(\tau-\sigma) = \frac{1}{3}(p_1+q_1-p_2-q_2) = 0\,.$$

Therefore the Clebsch-Gordan-coefficient for the coupling to a singlet is given by

$$\langle \Gamma_1\gamma_1; \Gamma_2\gamma_2 \,|\mathbf{10}\rangle = \binom{\Gamma_1}{\gamma_1}\frac{1}{\hat\Gamma_1}\,\delta_{\Gamma_2\bar\Gamma_1}\delta_{\gamma_2\bar\gamma_1}\,. \tag{B.9}$$

Definition of the 9Γ-symbols

The $X9\Gamma$-symbol and 9Γ-symbol are defined as the recoupling coefficient

$$\begin{aligned}\sum_{\gamma_i,\gamma_{ij}} & \langle \Gamma_1\gamma_1\Gamma_2\gamma_2 \,|\Gamma_{12}\gamma_{12}\rangle_{n_{12}}\,\langle \Gamma_3\gamma_3\Gamma_4\gamma_4 \,|\Gamma_{34}\gamma_{34}\rangle_{n_{34}}\,\langle \Gamma_{12}\gamma_{12}\Gamma_{34}\gamma_{34} \,|\Gamma\gamma\rangle_{n_{12,34}} \\ & \langle \Gamma_1\gamma_1\Gamma_3\gamma_3 \,|\Gamma_{13}\gamma_{13}\rangle_{n_{13}}\,\langle \Gamma_2\gamma_2\Gamma_4\gamma_4 \,|\Gamma_{24}\gamma_{24}\rangle_{n_{24}}\,\langle \Gamma_{13}\gamma_{13}\Gamma_{24}\gamma_{24} \,\big|\Gamma'\gamma'\big\rangle_{n_{13,24}} \\ =: \quad & \delta_{\Gamma,\Gamma'}\,\delta_{\gamma,\gamma'} \\ & \Big\langle [[\Gamma_1,\Gamma_2]\,\Gamma_{12,n_{12}},[\Gamma_3,\Gamma_4]\,\Gamma_{34,n_{34}}]\,\Gamma_{n_{12,34}} \,\Big|[[\Gamma_1,\Gamma_3]\,\Gamma_{13,n_{13}},[\Gamma_2,\Gamma_4]\,\Gamma_{24,n_{24}}]\,\Gamma_{n_{13,24}}\Big\rangle \\ =: \quad & \delta_{\Gamma,\Gamma'}\,\delta_{\gamma,\gamma'}\;X\begin{pmatrix}\Gamma_1 & \Gamma_2 & \Gamma_{12,n_{12}}\\ \Gamma_3 & \Gamma_4 & \Gamma_{34,n_{34}}\\ \Gamma_{13,n_{13}} & \Gamma_{24,n_{24}} & \Gamma_{n_{12,34},n_{13,24}}\end{pmatrix} \\ =: \quad & \delta_{\Gamma,\Gamma'}\,\delta_{\gamma,\gamma'}\;\hat\Gamma_{12}\hat\Gamma_{34}\hat\Gamma_{13}\hat\Gamma_{24}\begin{Bmatrix}\Gamma_1 & \Gamma_2 & \Gamma_{12,n_{12}}\\ \Gamma_3 & \Gamma_4 & \Gamma_{34,n_{34}}\\ \Gamma_{13,n_{13}} & \Gamma_{24,n_{24}} & \Gamma_{n_{12,34},n_{13,24}}\end{Bmatrix}\,.\end{aligned} \tag{B.10}$$

They are independent of γ. Orthonormality implies that

$$\sum_{\substack{\Gamma_{13},\Gamma_{24},\\ n_{13},n_{24},n_{13,24}}} X\begin{pmatrix}\Gamma_1 & \Gamma_2 & \Gamma_{12,n_{12}}\\ \Gamma_3 & \Gamma_4 & \Gamma_{34,n_{34}}\\ \Gamma_{13,n_{13}} & \Gamma_{24,n_{24}} & \Gamma_{n_{12,34},n_{13,24}}\end{pmatrix} X\begin{pmatrix}\Gamma_1 & \Gamma_2 & \Gamma'_{12,n'_{12}}\\ \Gamma_3 & \Gamma_4 & \Gamma'_{34,n'_{34}}\\ \Gamma_{13,n_{13}} & \Gamma_{24,n_{24}} & \Gamma_{n'_{12,34},n_{13,24}}\end{pmatrix}$$

$$= \delta_{\Gamma_{12},\Gamma'_{12}}\delta_{\Gamma_{34},\Gamma'_{34}}\delta_{n_{12},n'_{12}}\delta_{n_{34},n'_{34}}\delta_{n_{12,34},n'_{12,34}}\,.$$

Appendix C The group of lattice rotations and reflections

C.1 Irreducible representations

As we have already mentioned in chapter 3 there are four one-dimensional and one two-dimensional irreducible representations (IRs) of the group of lattice rotations and reflections G_{lr}, which corresponds to the crystal group C_{4v}. We list them here.

One-dimensional representations

Angular momentum/parity 0^+:

$$\begin{aligned} D^{0^+}(R_0) &= 1 & D^{0^+}(R_4) &= 1 \\ D^{0^+}(R_1) &= 1 & D^{0^+}(R_5) &= 1 \\ D^{0^+}(R_2) &= 1 & D^{0^+}(R_6) &= 1 \\ D^{0^+}(R_3) &= 1 & D^{0^+}(R_7) &= 1\,. \end{aligned}$$

Angular momentum/parity 0^-:

$$\begin{aligned} D^{0^-}(R_0) &= 1 & D^{0^-}(R_4) &= -1 \\ D^{0^-}(R_1) &= -1 & D^{0^-}(R_5) &= 1 \\ D^{0^-}(R_2) &= -1 & D^{0^-}(R_6) &= 1 \\ D^{0^-}(R_3) &= 1 & D^{0^-}(R_7) &= -1 \end{aligned}$$

Angular momentum/parity 2^+:

$$\begin{aligned} D^{2^+}(R_0) &= 1 & D^{2^+}(R_4) &= -1 \\ D^{2^+}(R_1) &= 1 & D^{2^+}(R_5) &= -1 \\ D^{2^+}(R_2) &= 1 & D^{2^+}(R_6) &= -1 \\ D^{2^+}(R_3) &= 1 & D^{2^+}(R_7) &= -1 \end{aligned}$$

Angular momentum/parity 2^-:

$$\begin{aligned} D^{2^-}(R_0) &= 1 & D^{2^-}(R_4) &= 1 \\ D^{2^-}(R_1) &= -1 & D^{2^-}(R_5) &= -1 \\ D^{2^-}(R_2) &= -1 & D^{2^-}(R_6) &= -1 \\ D^{2^-}(R_3) &= 1 & D^{2^-}(R_7) &= 1 \end{aligned}$$

Two-dimensional representation

Angular momentum/parity $1^{\pm}$:

$$D^{1^{\pm}}(R_0) = \begin{pmatrix} 1 & 0 \\ 0 & 1 \end{pmatrix} \qquad D^{1^{\pm}}(R_4) = \begin{pmatrix} 0 & 1 \\ 1 & 0 \end{pmatrix}$$
$$D^{1^{\pm}}(R_1) = \begin{pmatrix} -1 & 0 \\ 0 & 1 \end{pmatrix} \qquad D^{1^{\pm}}(R_5) = \begin{pmatrix} 0 & 1 \\ -1 & 0 \end{pmatrix}$$
$$D^{1^{\pm}}(R_2) = \begin{pmatrix} 1 & 0 \\ 0 & -1 \end{pmatrix} \qquad D^{1^{\pm}}(R_6) = \begin{pmatrix} 0 & -1 \\ 1 & 0 \end{pmatrix}$$
$$D^{1^{\pm}}(R_3) = \begin{pmatrix} -1 & 0 \\ 0 & -1 \end{pmatrix} \qquad D^{1^{\pm}}(R_7) = \begin{pmatrix} 0 & -1 \\ -1 & 0 \end{pmatrix}$$

C.2 Subgroups

We list here the ten subgroups of G_{lr}:

1. $G^{1a} = \{R_0\}$
2. $G^{2a} = \{R_0, R_1\}$
3. $G^{2b} = \{R_0, R_2\}$
4. $G^{2c} = \{R_0, R_3\}$
5. $G^{2d} = \{R_0, R_4\}$
6. $G^{2e} = \{R_0, R_7\}$
7. $G^{4a} = \{R_0, R_3, R_5, R_6\}$
8. $G^{4b} = \{R_0, R_1, R_2, R_3\}$
9. $G^{4c} = \{R_0, R_3, R_4, R_7\}$
10. $G^{8a} = \{R_0, R_1, R_2, R_3, R_4, R_5, R_6, R_7\}$

Irreducible representations of the subgroups

As the internal symmetries (see section 3.4.1) of the basis elements can be classified with respect to the one-dimensional IRs of the subgroups, we give here the character tables of these IRs (see ref. [16]).

The subgroup G_{1a} corresponds to the trivial cyclic group C_1, which has one one-dimensional IR labelled with $j_{1a} = 0$. The character $c^{j_{1a}}$ is trivial.

	1st class: R_0
$j_{1a} = 0$	1

The subgroups $G_{2n}, n = a, b, c, d$ correspond to the cyclic group C_2, which has two one-dimensional IRs labelled with $j_{1n} = 0, 1$. The characters $c^{j_{2n}}$ are:

	1st class: R_0	2nd class
$j_{2n} = 0$	1	1
$j_{2n} = 1$	1	-1

The 2nd class of the subgroups consists of the corresponding second element of the subgroups.

The subgroup G_{4a} corresponds to the cyclic group C_4, which has four one-dimensional IRs labelled with $j_{4a} = 0, 1, 2, 3$. The characters $c^{j_{4a}}$ are:

	1st class: R_0	2nd class: R_3	3rd class: R_5	4th class: R_6
$j_{4a} = 0$	1	1	1	1
$j_{4a} = 1$	1	1	-1	-1
$j_{4a} = 2$	1	-1	i	$-$i
$j_{4a} = 3$	1	-1	$-$i	i

The subgroups $G_{4n}, n = b, c$ correspond to the dihedral group D_2, which has four one-dimensional IRs labelled with $j_{4n} = 0, 1, 2, 3$. The characters $c^{j_{4n}}$ are:

	1st class: R_0	2nd class	3rd class	4th class
$j_{4n} = 0$	1	1	1	1
$j_{4n} = 1$	1	1	-1	-1
$j_{4n} = 2$	1	-1	1	-1
$j_{4n} = 3$	1	-1	-1	1

The 2nd class, 3rd class and 4th class consists of the corresponding second, third and fourth element of the subgroups. The subgroups G_{8a} correspond to the group G_{lr} itself. Table 3.1 gives the corresponding characters.

Multiplicities

As in section 3.2.2 we can use the formula (3.8) to calculate the multiplicities, i.e. how often the IR of a group occurs in the subduced representation of the subgroup. In the following tables we give these multiplicities for the subgroups of G_{lr}.

Multiplicities $m_{J^P}^{j_{1a}}$ for G^{1a}:

	$j_{1a}=0$
$J^P=0^+$	1
$J^P=0^-$	1
$J^P=1^\pm$	2
$J^P=2^+$	1
$J^P=2^-$	1

Multiplicities $m_{J^P}^{j_{2a}}$ for G^{2a} and $m_{J^P}^{j_{2b}}$ for G^{2b}:

	$j_{2a}=0$	$j_{2a}=1$
$J^P=0^+$	1	0
$J^P=0^-$	0	1
$J^P=1^\pm$	1	1
$J^P=2^+$	1	0
$J^P=2^-$	0	1

	$j_{2b}=0$	$j_{2b}=1$
$J^P=0^+$	1	0
$J^P=0^-$	0	1
$J^P=1^\pm$	1	1
$J^P=2^+$	1	0
$J^P=2^-$	0	1

Multiplicities $m_{J^P}^{j_{2c}}$ for G^{2c} and $m_{J^P}^{j_{2d}}$ for G^{2d}:

	$j_{2c}=0$	$j_{2c}=1$
$J^P=0^+$	1	0
$J^P=0^-$	1	0
$J^P=1^\pm$	0	2
$J^P=2^+$	1	0
$J^P=2^-$	1	0

	$j_{2d}=0$	$j_{2d}=1$
$J^P=0^+$	1	0
$J^P=0^-$	0	1
$J^P=1^\pm$	1	1
$J^P=2^+$	0	1
$J^P=2^-$	1	0

Multiplicities $m_{J^P}^{j_{2e}}$ for G^{2e}:

	$j_{2e}=0$	$j_{2e}=1$
$J^P=0^+$	1	0
$J^P=0^-$	0	1
$J^P=1^\pm$	1	1
$J^P=2^+$	0	1
$J^P=2^-$	1	0

Concerning subgroup G^{4a} we do not need to consider the complex valued IRs, as there are no complex phases under rotation and reflections (see section 2.3.4). Thus a basis element $\Pi_C^{\pm}\chi^{\alpha}$ can never be an irreducible basis vector with respect to the IRs of G^{4a} labelled with $j_{4a} = 2, 3$, i.e.

$$T(R)\Pi_C^{\pm}\chi^{\alpha} = D^{j_{4a}=2,3}(R)\Pi_C^{\pm}\chi^{\alpha}$$

never occurs. Thus we only need the following multiplicities $m_{J^P}^{j_{4a}}$ for G^{4a}:

	$j_{4a}=0$	$j_{4a}=1$
$J^P = 0^+$	1	0
$J^P = 0^-$	1	0
$J^P = 1^{\pm}$	0	0
$J^P = 2^+$	0	1
$J^P = 2^-$	0	1

Subgroup G^{4b} was given as an example in section 3.4.1.

Multiplicities $m_{J^P}^{j_{4c}}$ for G^{4c}:

	$j_{4c}=0$	$j_{4c}=1$	$j_{4c}=2$	$j_{4c}=3$
$J^P = 0^+$	1	0	0	0
$J^P = 0^-$	0	1	0	0
$J^P = 1^{\pm}$	0	0	1	1
$J^P = 2^+$	0	1	0	0
$J^P = 2^-$	1	0	0	0

For the internal symmetries we are interested in the one-dimensional IRs only. Consequently we do not consider the two-dimensional IR of $G_{8a} = G_{lr}$ labelled with $j_{8a} = J^P = 1^{\pm}$. Thus we get the following multiplicities $m_{J^P}^{j_{8a}}$ for G^{8a}:

	$j_{8a}=0^+$	$j_{8a}=0^-$	$j_{8a}=2^+$	$j_{8a}=2^-$
$J^P = 0^+$	1	0	0	0
$J^P = 0^-$	0	1	0	0
$J^P = 1^{\pm}$	0	0	0	0
$J^P = 2^+$	0	0	1	0
$J^P = 2^-$	0	0	0	1

C.3 Diagonalisation

We saw in chapter 3 in eq. (3.17), that the basis η

$$\eta^{\alpha}_{J^{PC},\nu\sigma} = \frac{\Pi^0 \Pi^{J^P}_{\nu\sigma} \Pi^{\pm}_C \chi^{\alpha}}{||\Pi^0 \Pi^{J^P}_{\nu\sigma} \Pi^{\pm}_C \chi^{\alpha}||} \tag{C.1}$$

is orthogonal with respect to the quantum numbers J^{PC} and the magnetic number σ:

$$\begin{aligned} & \langle \eta^{\alpha}_{J^{PC},\nu\sigma} | \eta^{\beta}_{J^{PC'},\nu'\sigma'} \rangle \\ = \; & |G_{lt}| \frac{(\dim J^P)}{|G_{lr}|} \sum_{R \in G_{\chi^\beta}} p(R) D^{J^P}_{\nu'\nu}(R^{-1}) \delta_{J^{PC} J^{PC'}} \delta_{\sigma\sigma'} \delta_{\alpha\beta} \begin{cases} 1 \,, & \text{if } T_C \chi^{\alpha} = \chi^{\alpha} \\ \frac{1}{2} \,, & \text{else} \end{cases} . \end{aligned}$$

Concerning the magnetic number ν we have to diagonalise the norm matrix

$$\frac{(\dim J^P)}{|G_{lr}|} \sum_{R \in G_{\chi^\beta}} p(R) D^{J^P}_{\nu'\nu}(R^{-1}) \,,$$

where G_{χ^β} is a possible internal symmetry group of a basis element $\Pi^{\pm}_C \Pi^0 \chi^{\beta}$ and $p(R) = \pm 1$ is the phase this basis element gets under a rotation $R \in G_{\chi^\beta}$.

For the one-dimensional IRs of G_{lr}, labelled with $J^P = 0^+, 0^-, 2^+, 2^-$ this is fulfilled trivially. Therefore for the diagonalisation we only have to consider the two-dimensional IR of G_{lr}, which corresponds to $J^P = 1^{\pm}$ and has the dimension $\dim J^P = 2$.

As we discussed in section 3.4.1 the internal symmetry groups correspond to the one-dimensional IRs of the subgroups of G_{lr}. These will here be considered separately.

We can deduce from the multiplicity tables in the last section, which IRs of subgroups contribute to the angular momentum/parity $J^P = 1^{\pm}$.

Subgroup $G_{\chi^\beta} = G^{1a}$

If the internal symmetry of a basis element corresponds to the subgroup $G_{\chi^\beta} = G^{1a} = \{R_0\}$, the basis element has no symmetry under rotations and reflections. Subgroup G^{1a} has one one-dimensional IR labelled with $j_{1a} = 0$. For the norm matrix we get:

$$\frac{2}{8} \sum_{R \in G_{\chi^\beta}} D^{J^P}_{\nu\nu'}(R^{-1}) = \frac{1}{4} \begin{pmatrix} 1 & 0 \\ 0 & 1 \end{pmatrix} .$$

It is diagonal. Again, we get two orthonormal basis elements labelled with $\nu = 0, 1$:

$$\begin{aligned} \eta^{\beta}_{1^{\pm C},0\sigma} &= 2 \Pi^{1^{\pm}}_{0\sigma} \Pi^{\pm}_C \Pi^0 \chi^{\beta} \\ \eta^{\beta}_{1^{\pm C},1\sigma} &= 2 \Pi^{1^{\pm}}_{1\sigma} \Pi^{\pm}_C \Pi^0 \chi^{\beta} \,. \end{aligned}$$

Subgroup $G_{\chi^\beta} = G^{2a}$

Subgroup $G_{\chi^\beta} = G^{2a} = \{R_0, R_1\}$ has two one-dimensional IRs labelled with $j_{2a} = 0, 1$. For $j_{2a} = 0$ we have the phases $p(R_0) = p(R_1) = 1$ and for the norm matrix we get:

$$\frac{2}{8} \sum_{R \in G_{\chi^\beta}} D^{J^P}_{\nu\nu'}(R^{-1}) = \frac{1}{2} \begin{pmatrix} 0 & 0 \\ 0 & 1 \end{pmatrix} .$$

It is diagonal. Here, we get only one basis element labelled with $\nu = 1$:

$$\eta^\beta_{1^{\pm_C},1_\sigma} = \sqrt{2}\Pi^{1^\pm}_{1_\sigma}\Pi^\pm_C\Pi^0\chi^\beta .$$

For $j_{2a} = 1$ we have the phases $p(R_0) = 1$ and $p(R_1) = -1$ and for the norm matrix we get:

$$\frac{2}{8} \sum_{R \in G_{\chi^\beta}} D^{J^P}_{\nu\nu'}(R^{-1}) = \frac{1}{2} \begin{pmatrix} 1 & 0 \\ 0 & 0 \end{pmatrix} .$$

It is also diagonal. Here, we get only one basis element labelled with $\nu = 0$:

$$\eta^\beta_{1^{\pm_C},0_\sigma} = \sqrt{2}\Pi^{1^\pm}_{0_\sigma}\Pi^\pm_C\Pi^0\chi^\beta .$$

Subgroup $G_{\chi^\beta} = G^{2b}$

Subgroup $G_{\chi^\beta} = G^{2b} = \{R_0, R_2\}$ has also two one-dimensional IRs labelled with $j_{2b} = 0, 1$. For $j_{2b} = 0$ we have the phases $p(R_0) = p(R_2) = 1$ and we get the same norm matrix as for $j_{2a} = 1$ (see subgroup G^{2a} above). Thus it is diagonal and we get only one basis element labelled with $\nu = 0$:

$$\eta^\beta_{1^{\pm_C},0_\sigma} = \sqrt{2}\Pi^{1^\pm}_{0_\sigma}\Pi^\pm_C\Pi^0\chi^\beta .$$

For $j_{2b} = 1$ we have the phases $p(R_0) = 1$ and $p(R_2) = -1$ and we get a norm matrix analogous to the one for $j_{2a} = 0$ (see above). It is also diagonal and we get only one basis element labelled with $\nu = 1$:

$$\eta^\beta_{1^{\pm_C},1_\sigma} = \sqrt{2}\Pi^{1^\pm}_{1_\sigma}\Pi^\pm_C\Pi^0\chi^\beta .$$

Subgroup $G_{\chi^\beta} = G^{2c}$

Subgroup $G_{\chi^\beta} = G^{2c} = \{R_0, R_3\}$ again has two one-dimensional IRs labelled with $j_{2c} = 0, 1$. In the corresponding multiplicity table we see that for $j_{2c} = 0$ we have no contribution to angular momentum/parity $J^P = 1^\pm$. For $j_{2c} = 1$ we have the phases $p(R_0) = 1, p(R_3) = -1$ and for the norm matrix we get:

$$\frac{2}{8} \sum_{R \in G_{\chi^\beta}} D^{J^P}_{\nu\nu'}(R^{-1}) = \frac{1}{2} \begin{pmatrix} 1 & 0 \\ 0 & 1 \end{pmatrix} .$$

It is diagonal and we get two orthonormal basis elements labelled with $\nu = 0, 1$:

$$\eta^\beta_{1^{\pm_C},0_\sigma} = \sqrt{2}\Pi^{1^\pm}_{0_\sigma}\Pi^\pm_C\Pi^0\chi^\beta$$
$$\eta^\beta_{1^{\pm_C},1_\sigma} = \sqrt{2}\Pi^{1^\pm}_{1_\sigma}\Pi^\pm_C\Pi^0\chi^\beta .$$

Subgroup $G_{\chi^\beta} = G^{2d}$

Subgroup $G_{\chi^\beta} = G^{2d} = \{R_0, R_4\}$ has two one-dimensional IRs labelled with $j_{2d} = 0, 1$. For $j_{2d} = 0$ we have the phases $p(R_0) = p(R_1) = 1$ and we get the following norm matrix:

$$\frac{2}{8} \sum_{R \in G_{\chi^\beta}} D^{J^P}_{\nu\nu'}(R^{-1}) = \frac{1}{4} \begin{pmatrix} 1 & 1 \\ 1 & 1 \end{pmatrix} .$$

It can be diagonalised by the matrix $S = \begin{pmatrix} \frac{1}{\sqrt{2}} & \frac{1}{\sqrt{2}} \\ \frac{1}{\sqrt{2}} & \frac{-1}{\sqrt{2}} \end{pmatrix}$ and we get:

$$S^{-1} \frac{1}{4} \begin{pmatrix} 1 & 1 \\ 1 & 1 \end{pmatrix} S = \frac{1}{2} \begin{pmatrix} 1 & 0 \\ 0 & 0 \end{pmatrix} .$$

Thus we have one basis element labelled with $\nu = 0$:

$$\eta^\beta_{1^\pm C, 0\sigma} = \sqrt{2}(\frac{1}{\sqrt{2}} \Pi^{J^P}_{0\sigma} + \frac{1}{\sqrt{2}} \Pi^{J^P}_{1\sigma}) \Pi^\pm_C \Pi^0 \chi^\beta = 2 \Pi^{J^P}_{0\sigma} \Pi^\pm_C \Pi^0 \chi^\beta .$$

We have used that for an element $\Pi^\pm_C \Pi^0 \chi^\beta$, which has an internal symmetry corresponding to this IR, we have:

$$\Pi^{J^P}_{1\sigma} \Pi^\pm_C \Pi^0 \chi^\beta = \Pi^{J^P}_{0\sigma} \Pi^\pm_C \Pi^0 \chi^\beta .$$

For $j_{2d} = 1$ we have the phases $p(R_0) = 1$ and $p(R_1) = -1$ and we get the following norm matrix:

$$\frac{2}{8} \sum_{R \in G_{\chi^\beta}} D^{J^P}_{\nu\nu'}(R^{-1}) = \frac{1}{4} \begin{pmatrix} 1 & -1 \\ -1 & 1 \end{pmatrix} .$$

It can be diagonalised by the same matrix S and we get:

$$S^{-1} \frac{1}{4} \begin{pmatrix} 1 & -1 \\ -1 & 1 \end{pmatrix} S = \frac{1}{2} \begin{pmatrix} 0 & 0 \\ 0 & 1 \end{pmatrix} .$$

Thus we have one basis element labelled with $\nu = 0$:

$$\eta^\beta_{1^\pm C, 0\sigma} = \sqrt{2}(\frac{1}{\sqrt{2}} \Pi^{J^P}_{0\sigma} - \frac{1}{\sqrt{2}} \Pi^{J^P}_{1\sigma}) \Pi^\pm_C \Pi^0 \chi^\beta = 2 \Pi^{J^P}_{0\sigma} \Pi^\pm_C \Pi^0 \chi^\beta .$$

We have used that for an element $\Pi^\pm_C \Pi^0 \chi^\beta$, which has an internal symmetry corresponding to this IR, we have:

$$\Pi^{J^P}_{1\sigma} \Pi^\pm_C \Pi^0 \chi^\beta = -\Pi^{J^P}_{0\sigma} \Pi^\pm_C \Pi^0 \chi^\beta .$$

Subgroup $G_{\chi^\beta} = G^{2e}$

Subgroup $G_{\chi^\beta} = G^{2e} = \{R_0, R_7\}$ again has two one-dimensional IRs labelled with $j_{2e} = 0, 1$, we get the same result for $j_{2e} = 0$ as for the IR of subgroup G^{2d} labelled with $j_{2d} = 1$. Thus we have the following basis element:

$$\eta^\beta_{1^\pm C, 0\sigma} = \sqrt{2}(\frac{1}{\sqrt{2}} \Pi^{J^P}_{0\sigma} - \frac{1}{\sqrt{2}} \Pi^{J^P}_{1\sigma}) \Pi^\pm_C \Pi^0 \chi^\beta = 2 \Pi^{J^P}_{0\sigma} \Pi^\pm_C \Pi^0 \chi^\beta .$$

And for $j_{2e} = 1$ we get the same result as for $j_{2d} = 0$:

$$\eta^\beta_{1^\pm C, 0\sigma} = \sqrt{2}(\frac{1}{\sqrt{2}} \Pi^{J^P}_{0\sigma} + \frac{1}{\sqrt{2}} \Pi^{J^P}_{1\sigma}) \Pi^\pm_C \Pi^0 \chi^\beta = 2 \Pi^{J^P}_{0\sigma} \Pi^\pm_C \Pi^0 \chi^\beta .$$

Subgroup $G_{\chi^\beta} = G^{4a}$

Subgroup G^{4a} has no contribution to angular momentum/parity $J^P = 1^\pm$, as can be deduced from the corresponding multiplicity table in the last section.

Subgroup $G_{\chi^\beta} = G^{4b}$

Subgroup $G_{\chi^\beta} = G^{4b} = \{R_0, R_1, R_2, R_3\}$ has four one-dimensional IRs labelled with $j_{4b} = 0, 1, 2, 3$. For $j_{4a} = 0, 3$ we have no contribution to angular momentum/parity $J^P = 1^\pm$. For $j_{4b} = 1$ we have the phases $p(R_0) = p(R_1) = 1$ and $p(R_2) = p(R_3) = -1$ and we get the following norm matrix:

$$\frac{2}{8} \sum_{R \in G_{\chi^\beta}} D^{J^P}_{\nu\nu'}(R^{-1}) = \begin{pmatrix} 0 & 0 \\ 0 & 1 \end{pmatrix}$$

It is diagonal. Here, we get again only one basis element labelled with $\nu = 1$:

$$\eta^\beta_{1^{\pm C}, 1\sigma} \quad = \quad \Pi^{1^\pm}_{1\sigma} \Pi^\pm_C \Pi^0 \chi^\beta \, .$$

For $j_{4b} = 2$ we have the phases $p(R_0) = p(R_2) = 1$ and $p(R_1) = p(R_3) = -1$ and we get the following norm matrix:

$$\frac{2}{8} \sum_{R \in G_{\chi^\beta}} D^{J^P}_{\nu\nu'}(R^{-1}) = \begin{pmatrix} 1 & 0 \\ 0 & 0 \end{pmatrix}$$

It is also diagonal and we have only one basis element labelled with $\nu = 0$:

$$\eta^\beta_{1^{\pm C}, 0\sigma} \quad = \quad \Pi^{1^\pm}_{0\sigma} \Pi^\pm_C \Pi^0 \chi^\beta \, .$$

Subgroup $G_{\chi^\beta} = G^{4c}$

Subgroup $G_{\chi^\beta} = G^{4c} = \{R_0, R_3, R_4, R_7\}$ has four one-dimensional IRs labelled with $j_{4c} = 0, 1, 2, 3$. The IRs $j_{4c} = 0, 1$ have no contribution to angular momentum/parity $J^P = 1^\pm$. For $j_{4c} = 2$, which has the phases $p(R_0) = p(R_4) = 1$ and $p(R_3) = p(R_7) = -1$, we get the following norm matrix:

$$\frac{2}{8} \sum_{R \in G_{\chi^\beta}} D^{J^P}_{\nu\nu'}(R^{-1}) = \frac{1}{2} \begin{pmatrix} 1 & 1 \\ 1 & 1 \end{pmatrix}$$

For $j_{4c} = 3$, which has the phases $p(R_0) = p(R_7) = 1, p(R_3) = p(R_4) = -1$, we find the norm matrix:

$$\frac{2}{8} \sum_{R \in G_{\chi^\beta}} D^{J^P}_{\nu\nu'}(R^{-1}) = \frac{1}{2} \begin{pmatrix} 1 & -1 \\ -1 & 1 \end{pmatrix}$$

They can be diagonalised with the matrix S we have used for subgroup G^{2d}. With the same arguments we get here for $j_{4c} = 2$ the following basis element

$$\eta^\beta_{1^{\pm C}, 0\sigma} = (\frac{1}{\sqrt{2}} \Pi^{J^P}_{0\sigma} + \frac{1}{\sqrt{2}} \Pi^{J^P}_{1\sigma}) \Pi^\pm_C \Pi^0 \chi^\beta = \sqrt{2} \Pi^{J^P}_{0\sigma} \Pi^\pm_C \Pi^0 \chi^\beta \, ,$$

and for $j_{4c} = 3$:

$$\eta^\beta_{1^{\pm C}, 0\sigma} = (\frac{1}{\sqrt{2}} \Pi^{J^P}_{0\sigma} - \frac{1}{\sqrt{2}} \Pi^{J^P}_{1\sigma}) \Pi^\pm_C \Pi^0 \chi^\beta = \sqrt{2} \Pi^{J^P}_{0\sigma} \Pi^\pm_C \Pi^0 \chi^\beta \, .$$

Subgroup $G_{\chi^\beta} = G^{8a}$

Subgroup $G_{\chi^\beta} = G^{8a} = G_{lr}$ has no contribution to angular momentum and parity $J^P = 1^\pm$.

Concluding remark

In our computer program we do not diagonalise the norm matrix to find these linear independent basis elements, but we use a numerical method described in ref. [64], which leads to the same results.

Bibliography

[1] S. L. Altmann, A. P. Cracknell, *Lattice Harmonics 1. Cubic Groups*, Rev. of Modern Physics, **37**, 1 (1965).

[2] C. Amsler, *Non-Q Qbar Mesons (Rev.)*, Phys. Rev. D **66**, 010001 (2002).

[3] C. Amsler, *Further evidence for a large glue component in the f0(1500) meson*, Phys. Lett. B **541**, 22 (2002) [arXiv:hep-ph/0206104].

[4] H. Arisue, *Variational Study Of The Mass Spectrum In (2+1)-Dimensional SU(2) Lattice Gauge Theory*, Prog. Theor. Phys. **84**, 951 (1990);

[5] H. Arisue, M. Kato and T. Fujiwara, *Variational Study Of Vacuum Wave Function For Lattice Gauge Theory In (2+1)-Dimension*, Prog. Theor. Phys. **70**, 229 (1983).

[6] G. S. Bali, *'Glueballs': Results and perspectives from the lattice*, [arXiv:hep-ph/0110254].

[7] B. Berg and A. Billoire, *Glueball Spectroscopy In Four-Dimensional SU(3) Lattice Gauge Theory. 1*, Nucl. Phys. B **221**, 109 (1983).

[8] V. Bernard, N. Kaiser and U. G. Meissner, *Chiral dynamics in nucleons and nuclei*, Int. J. Mod. Phys. E **4**, 193 (1995) [arXiv:hep-ph/9501384].

[9] J. Carlsson, J. A. McIntosh, B. H. McKellar and L. C. Hollenberg, *An analytic variational study of the mass spectrum in 2+1 dimensional SU(3) Hamiltonian lattice gauge theory*, [arXiv:hep-lat/0207019].

[10] J. Q. Chen, *Group Representation Theory for Physicists*, World Scientific (1989).

[11] Q. Z. Chen, X. Q. Luo, S. H. Guo and X. Y. Fang, *Glueball Masses In QCD In Three-Dimensions*, Phys. Lett. B **348**, 560 (1995) [arXiv:hep-ph/9502235].

[12] F. E. Close and A. Kirk, *Scalar glueball q anti-q mixing above 1-GeV and implications for lattice QCD*, Eur. Phys. J. C **21**, 531 (2001) [arXiv:hep-ph/0103173].

[13] M. Creutz, *Quarks, gluons and lattice*, Cambridge Monographs on Mathematical Physics, Cambridge University Press, Cambridge (1985).

[14] S. Dalley and B. van de Sande, *Precision study of large-N Yang-Mills theory in 2+1 dimensions*, Phys. Rev. D **63**, 076004 (2001) [arXiv:hep-lat/0010082].

[15] E. El Baz and B.Castel, *Graphical Methods of Spin Algebras in Atomic, Nuclear, and Particle Physics*, Marcel Dekker, Inc., New York (1972).

[16] F. Engelke, *Aufbau der Moleküle*, Teubner Studienbücher: Chemie, Stuttgart (1992).

[17] X. Y. Fang, D. Schütte, V. Wethkamp and A. Wichmann, *Coupled cluster expansions for the massive Schwinger model in the lattice Hamiltonian formalism*, Phys. Rev. D **64**, 014501 (2001).

[18] X. Y. Fang, P. Hui, Q. Z. Chen and D. Schütte, *Fourth order approximation of the 0++ glueball mass of (2+1)-dimensional SU(3) lattice gauge theory*, Phys. Rev. D **65**, 114505 (2002).

[19] J. P. Greensite, *Large Scale Vacuum Structure And New Calculational Techniques In Lattice SU(N) Gauge Theory*, Nucl. Phys. B **166**, 113 (1980).

[20] S. Guo, Q. Chen and L. Li, *Analytic calculation of the vacuum wave function for (2+1)-dimensional SU(2) lattice gauge theory*, Phys. Rev. D **49**, 507 (1994).

[21] C. J. Hamer, *Scales Of Euclidean And Hamiltonian Lattice Gauge Theory In Three-Dimensions*, Phys. Rev. D **53**, 7316 (1996).

[22] C. J. Hamer, M. Samaras and R. J. Bursill, *Green's function Monte Carlo study of SU(3) lattice gauge theory in (3+1)D*, Phys. Rev. D **62**, 074506 (2000) [arXiv:hep-lat/0005009]

[23] C. J. Hamer, M. Sheppeard, W. h. Zheng and D. Schütte, *Universality for SU(2) Yang-Mills Theory in (2+1)D*, Phys. Rev. D **54**, 2395 (1996) [arXiv:hep-th/9511179];

[24] C. J. Hamer, J. Oitmaa and W. . Zheng, *Series Analysis Of U(1) And SU(2) Lattice Gauge Theory In (2+1)-Dimensions*, Phys. Rev. D **45**, 4652 (1992).

[25] A. Hart, C. McNeile and C. Michael [UKQCD Collaboration], *Masses of singlet and non-singlet 0++ particles*, [arXiv:hep-lat/0209063].

[26] A. Hart and M. Teper [UKQCD Collaboration], *On the glueball spectrum in O(a)-improved lattice QCD*, Phys. Rev. D **65**, 034502 (2002) [arXiv:hep-lat/0108022].

[27] P. Hui, X. Y. Fang and Q. Z. Chen, *Approximated Fourth Order Calculation Of The Vacuum Wave Function Of (2+1)-Dimensional SU(3) Lattice Gauge Theory*, Phys. Rev. D **62**, 034505 (2000).

[28] R. C. Johnson, *Angular momentum on a lattice*, Phys. Lett. **B114**, 147 (1982).

[29] T. A. Kaeding and H. T. Williams, *Program for generating tables of SU(3) x U(1) coupling coefficients*, Comput. Phys. Commun. **98**, 398 (1996) [arXiv:nucl-th/9511025].

[30] E. Klempt, *On The Existence Of Glueballs*, Acta Phys. Polon. B **31**, 2587 (2000).

[31] E. Klempt, *Meson spectroscopy: Glueballs, hybrids and Q anti-Q mesons*, [arXiv:hep-ex/0101031].

[32] J. Kogut and L. Susskind, *Hamiltonian formulation of Wilson's lattice gauge theories*, Phys. Rev. **D 11**, 395 (1975).

[33] M. Koll, R. Ricken, D. Merten, B. C. Metsch and H. R. Petry, *A relativistic quark model for mesons with an instanton induced interaction*, Eur. Phys. J. A **9**, 73 (2000) [arXiv:hep-ph/0008220].

[34] W. J. Lee and D. Weingarten, *Scalar quarkonium masses and mixing with the lightest scalar glueball*, Phys. Rev. D **61**, 014015 (2000) [arXiv:hep-lat/9910008].

[35] P. Lepage, *Perturbative improvement for lattice QCD: An update*, Nucl. Phys. Proc. Suppl. **60A** (1998) 267 [arXiv:hep-lat/9707026].

[36] N. E. Ligterink, N. R. Walet and R. F. Bishop, *Towards a many-body treatment of Hamiltonian lattice SU(N) gauge theory*, Annals Phys. **284**, 215 (2000) [arXiv:hep-lat/0001028].

[37] J. S. Lomont, *Application of Finite Groups*, Academic Press, New York, London (1959).

[38] U. Loring, B. C. Metsch and H. R. Petry, *The light baryon spectrum in a relativistic quark model with instanton-induced quark forces: The strange baryon spectrum*, Eur. Phys. J. A **10**, 447 (2001) [arXiv:hep-ph/0103290].

[39] U. Loring, B. C. Metsch and H. R. Petry, *The light baryon spectrum in a relativistic quark model with instanton-induced quark forces: The non-strange baryon spectrum and ground-states*, Eur. Phys. J. A **10**, 395 (2001) [arXiv:hep-ph/0103289].

[40] U. Loring, K. Kretzschmar, B. C. Metsch and H. R. Petry, *Relativistic quark models of baryons with instantaneous forces*, Eur. Phys. J. A **10**, 309 (2001) [arXiv:hep-ph/0103287].

[41] C. McNeile, *Lattice predictions for hybrids and glueballs*, Nucl. Phys. A **711**, 303 (2002) [arXiv:hep-lat/0207001].

[42] C. Michael, *Beyond the quark model of hadrons from lattice QCD*, [arXiv:hep-lat/0207017].

[43] P. Minkowski and W. Ochs, *The glueball among the light scalar mesons*, [arXiv:hep-ph/0209225].

[44] I. Montvay, G. Münster, *Quantum Fields on a Lattice*, Cambridge Monograghs in Mathematical Physics, Cambridge University Press, Cambridge (1994).

[45] C. J. Morningstar and M. J. Peardon, *The glueball spectrum from an anisotropic lattice study*, Phys. Rev. D **60**, 034509 (1999) [arXiv:hep-lat/9901004].

[46] G. Münster and M. Walzl, *Lattice gauge theory: A short primer*, [arXiv:hep-lat/0012005].

[47] H. Neff, *Probleme der Gittereichtheorie im Rahmen der Coupled-Cluster Methode*, diploma thesis TK-97-15, ITKP, Bonn (1997).

[48] J. Nitschkowski, *Untersuchungen verschiedener Eichfixierungen am Beispiel einer sphärisch symmetrischen Yang-Mills-Eichtheorie*, Ph. D. thesis, TK-96-31, ITKP, Bonn (1996).

[49] M. F. O'Reilly, *A closed formula for the product of irreducible representations of SU(3)*, J. Math. Phys. **23**, 11 (1982).

[50] R. Ricken, M. Koll, D. Merten, B. C. Metsch and H. R. Petry, *The meson spectrum in a covariant quark model*, Eur. Phys. J. A **9**, 221 (2000) [arXiv:hep-ph/0008221].

[51] D. Robson and D. M. Webber, *Gauge Covariance in Lattice Gauge Theories*, Z. Phys. C **15**, 199 (1982).

[52] H. J. Rothe, *Lattice Gauge Theories*, in World Scientific Lecture Notes in Physics, World Scientific (1992).

[53] S. Samuel, *On the 0++ glueball mass*, Phys. Rev. D **55**, 4189 (1997) [arXiv:hep-ph/9604405].

[54] S. Spanier and N. A. Tornqvist, *Scalar Mesons (Rev.)*, Phys. Rev. D **66**, 010001 (2002).

[55] D. E. Stewart and Z. Leyk, *Meschach Library*, software package (1994), ftp://ftpmaths.anu.edu.au/pub/meschach/README.

[56] D. Schütte, W. Zheng and C. J. Hamer, *The coupled cluster method in Hamiltonian lattice field theory* Phys. Rev. D **55**, 2974 (1997), [hep-lat/9603026].

[57] L. Susskind, *Coarse grained quantum chromodynamics*, in *Interactions éléctromagnétiques et faibles à haute énergie*, S. 206-308, Les Houches, France, Les Houches Summer School (1976).

[58] J. J. de Swart, *The Octet Model and its Clebsch-Gordan Coefficients*, Rev. Mod. Phys. **35**, 4 (1963).

[59] K. Symanzik, *Continuum limit and improved action in lattice theories. 1. Principles and ϕ^4 theory*, Nucl. Phys. B **226**, 187 (1983).

[60] M. J. Teper, *SU(N) gauge theories in 2+1 dimensions*, Phys. Rev. D **59**, 014512 (1999) [arXiv:hep-lat/9804008].

[61] W. K. Tung, *Group theory in Physics*, World Scientific (1985).

[62] D. A.Varshalovich, A. N. Moskalev and V. K. Khersonskii, *Quantum Theory of Angular Momentum*, World Scientific (1989).

[63] C. Weichmann, *Investigations of the Hamiltonian Lattice Theory within the Coupled Cluster Method*, Ph. D. thesis, TK 98-02, ITKP, Bonn (1998).

[64] A. Wichmann, *The Coupled Cluster Methode in Lattice Gauge Theory: SU(2) glueballs*, Ph. D. thesis, TK-01-03, ITKP, Bonn (2001)

A. Wichmann, D. Schütte, B. C. Metsch and V. Wethkamp, *The coupled cluster method in Hamiltonian lattice field theory: SU(2) glueballs*, Phys. Rev. D **65**, 094511 (2002) [arXiv:hep-lat/0112015];

D. Schütte, A. Wichmann and V. Wethkamp, *QCD Glueballs Within A Coupled Cluster Approach*, Int. J. Mod. Phys. B **15** (2001) 1732.

[65] H. T. Williams, *SU3 isoscalar factors*, J. Math. Phys. **37**, 4187 (1996) [arXiv:hep-th/9509167].

[66] H. T. Williams, *Symmetry Properties Of SU(3) Vector Coupling Coefficients*, arXiv:nucl-th/9309023.

[67] K. G. Wilson, *Confinement Of Quarks*, Phys. Rev. D **10**, 2445 (1974).

Danksagung

Bei Herrn Prof. Dr. D. Schütte möchte ich mich für die Möglichkeit bedanken, mich mit dem schönen und interessanten Gebiet der Hamiltonschen Gittereichtheorie beschäftigen zu können. Seine Erfahrungen zu diesem Thema, seine Ideen und Ratschläge haben einen wesentlichen Anteil am Gelingen dieser Arbeit.

Ein besonderer Dank gilt Herrn Priv. Doz. Dr. Bernard C. Metsch für seine freundliche Unterstützung bei zahlreichen inhaltlichen und technischen Fragen, für seine Betreuung und seine immer währende motivierende Diskussionsbereitschaft. Auch danke ich ihm für die aufmerksame Durchsicht des Manuskripts zu dieser Dissertation.

Herrn Prof. Dr. H. Monien danke ich für die freundliche Übernahme des Koreferates.

Bei T. A. Kaeding möchte ich mich für die Bereitstellung des Computerprogramms zu [29] bedanken. Es wurde für Rechnungen in dieser Arbeit genutzt und angepasst.

Ferner möchte ich mich bedanken für die finanzielle Unterstützung in Form eines Stipendiums und die Finanzierung des Besuchs der PSI Zuoz Summer School *Phenomenology of Gauge Interaction* in Zuoz in der Schweiz im Sommer 2000 und der Reisen zu DPG-Jahrestagungen beim Graduiertenkolleg *Die Erforschung subnuklearer Strukturen der Materie* vertreten durch Herrn Prof. Dr. F. Klein.

Andreas Wichmann danke ich für die gute Zusammenarbeit und für das Hinterlassen eines sehr gut dokumentierten Computercodes. Auch für das Korrekturlesen dieser Arbeit danke ich ihm.

Bei allen Mitglieder des Instituts für theoretische Kernphysik bedanke ich mich für die angenehme und freundliche Atmosphäre. Ein besonders herzlicher Dank gilt Matthias Koll, Bernadette Schorn und Isabel Herget für die schöne Zeit im "Mädchenzimmer" Raum 305. Für viele Hilfestellungen und Ermutigungen danke ich Renate Mähler. Dirk Merten danke ich für manchen Hinweis zu computer-technischen Fragen und für die Durchsicht des Manuskripts.

Für das aufmerksame Korrekturlesen meiner Arbeit möchte ich mich auch ganz herzlich bei Jens Nitschkowski, Ralf Ricken, Ines Schneider, Ingrid und Werner Wethkamp, Heinrich Baumbach und Monika Lepszy bedanken.

Ganz herzlich danke ich meinen Eltern, Ingrid und Werner Wethkamp. Neben der Finanzierung meines Studiums waren sie immer für mich da und haben mich liebevoll unterstützt und gefördert. Meiner Schwester Roswitha danke ich für viele ermutigende Gespräche und zusammen mit meinen Brüdern Johannes und Andreas für viele Hilfestellungen. Ein ganz spezieller Dank gilt Ralf.